7-12-2010

Enhanced Zinc Oxide and Graphene Nanostructures for Electronics and Sensing Applications

Ved P. Verma
Florida International University, vverm001@fiu.edu

DOI: 10.25148/etd.FI10080904

FLORIDA INTERNATIONAL UNIVERSITY

Miami, Florida

ENHANCED ZINC OXIDE AND GRAPHENE NANOSTRUCTURES FOR ELECTRONICS AND SENSING APPLICATIONS

A dissertation submitted in partial fulfillment of the

requirements for the degree of

DOCTOR OF PHYLOSOPHY

in

MATERIALS SCIENCE AND ENGINEERING

by

Ved Prakash Verma

2010

To: Dean Amir Mirmiran
College of Engineering and Computing

This dissertation, written by Ved Prakash Verma, and entitled Enhanced Zinc Oxide and Graphene Nanostructures for Electronics and Sensing Applications, having been approved in respect to style and intellectual content, is referred to you for judgment.

We have read this dissertation and recommend that it be approved.

_____
Norman D. H. Munroe

_____
Jiuhua Chen

_____
Joong-ho Moon

_____
Wonbong Choi, Major Professor

Date of Defense: July 12, 2010

The dissertation of Ved Prakash Verma is approved.

_____
Dean Amir Mirmiran
College of Engineering and Computing

_____
Interim Dean Kevin O'Shea
University Graduate School

Florida International University, 2010

ACKNOWLEDGMENTS

I would like to express my sincere gratitude to my committee members, Dr. Wonbong Choi, Dr. Jiuhua Chen, Dr. Norman D. H. Munroe and Dr. Joong-ho Moon for their continuous support and encouragement. My foremost thanks go to my dissertation advisor Dr. Wonbong Choi who led me towards an exciting area of my career with his insights and suggestions that helped to shape my research skills. I am also grateful to Dr. Choi for providing me opportunities during my studies at Florida International University (FIU).

I wish to express my warm and sincere thanks to Dr. Arvind Agarwal, Department of mechanical and materials engineering, FIU who helped me during my fellowship and was always available when I needed him. I am also thankful to Dr. Minhyon Jeon and his student Sookhyun Hwang for collaborating with me for my experiments and research.

Special thanks go to my friends and lab members and staff at Advanced Materials Engineering Research Institute (AMERI) who helped me throughout my research and study at FIU. Many thanks go to Dr. Do Hyun Kim for introducing me to various nanofabrication and electrical measurement techniques during the early stage of my experiments at FIU. I am thankful to Dr. Somenath Roy for his helpful discussion and Mr. Neal Ricks for his teaching and training to use cleanroom facility at AMERI. Many thanks to Dr. Harindra, Dr. Raghu, Dr. Jun, Indranil and Santanu for helping me in my experiments.

I gratefully acknowledge the financial support from Dissertation Year Fellowship program at FIU.

Finally, I want to thank my parents for their endless support, courage and love. Next, I am expressing my gratitude to my brother, sisters and other family members. My brother Jai Prakash is always proud of me and supports all my pursuits. I extend my thanks to my lovely wife Lyci, who has been encouraging me from the background whenever I needed. I want to share every success with her and this dissertation is a present to her.

ABSTRACT OF THE DISSERTATION

ENHANCED ZINC OXIDE AND GRAPHENE NANOSTRUCTURES FOR ELECTRONICS AND SENSING APPLICATIONS

by

Ved Prakash Verma

Florida International University, 2010

Miami, Florida

Professor Wonbong Choi, Major Professor

Zinc oxide and graphene nanostructures are important technological materials because of their unique properties and potential applications in future generation of electronic and sensing devices. This dissertation investigates a brief account of the strategies to grow zinc oxide nanostructures (thin film and nanowire) and graphene, and their applications as enhanced field effect transistors, chemical sensors and transparent flexible electrodes.

Nanostructured zinc oxide (ZnO) and low-gallium doped zinc oxide (GZO) thin films were synthesized by a magnetron sputtering process. Zinc oxide nanowires (ZNWs) were grown by a chemical vapor deposition method. Field effect transistors (FETs) of ZnO and GZO thin films and ZNWs were fabricated by standard photo and electron beam lithography processes. Electrical characteristics of these devices were investigated by nondestructive surface cleaning, ultraviolet irradiation treatment at high temperature and under vacuum. GZO thin film transistors showed a mobility of ~5.7 cm^2/ V·s at low operation voltage of <5 V and a low turn-on voltage of ~0.5 V with a sub threshold swing of ~85 mV/decade. Bottom gated FET fabricated from ZNWs exhibit a very high on-to-

off ratio (~10^6) and mobility (~28 cm^2 /V·s). A bottom gated FET showed large hysteresis of ~5.0 to 8.0 V which was significantly reduced to ~1.0 V by the surface treatment process. The results demonstrate charge transport in ZnO nanostructures strongly depends on its surface environmental conditions and can be explained by formation of depletion layer at the surface by various surface states. A nitric oxide (NO) gas sensor using single ZNW, functionalized with Cr nanoparticles was developed. The sensor exhibited average sensitivity of ~46% and a minimum detection limit of ~1.5 ppm for NO gas. The sensor also is selective towards NO gas as demonstrated by a cross sensitivity test with N_2, CO and CO_2 gases.

Graphene film on copper foil was synthesized by chemical vapor deposition method. A hot press lamination process was developed for transferring graphene film to flexible polymer substrate. The graphene/polymer film exhibited a high quality, flexible transparent conductive structure with unique electrical-mechanical properties; ~88.80 % light transmittance and ~1.1742/sq sheet resistance. The application of a graphene/polymer film as a flexible and transparent electrode for field emission displays was demonstrated.

TABLE OF CONTANTS

LIST OF TABLES

TABLE PAGE

LIST OF FIGURES

FIGURE PAGE

CHAPTER 1

INTRODUCTION

1.1 Overview

Nanostructure materials are the essential building blocks of next generation molecular manufacturing industry. Their unique physical and chemical properties at nanoscale encourage invention of novel devices made from nano-circuits and nano-machines. Materials with at least one of their dimension in the nanoscale range (10^{-9} m) are of great research interest for the scientific community from past couple of decades. Scientific knowledge and findings about these materials have developed at a tremendous rate, pushing it towards the next step for their application in commercial devices, making nanotechnology a success.

Semiconducting nanostructure materials have huge potential in future electronic, optical and sensing devices. In general, all the bulk semiconductors can be synthesized to form a nanoscale structure. Zinc oxide (ZnO) is a wide band gap (Eg = 3.37 eV at room temperature) semiconducting material having high exciton binding energy of 60 meV. Even though research focusing on ZnO dates back many decades, the renewed interest is fueled by the synthesis and the application if its nanostructures in various kind of devices. ZnO thin film and nanowires are two main nanostructures which have been of great research interest in recent years.

Also, nanoscale carbon allotropes ranging from graphene (2D), nanotubes (1D) and fullerenes (0D) are of great interest because of their unique atomic structures which

are built from the same hexagonal array of sp^2 carbon atoms. Recently graphene, a new yet ancient two-dimensional material has sparked an exponentially growing interest in the scientific communities, in particular technologist and material scientist exploring the way to incorporate it into future nano-scale devices. Owing to their remarkable electronic, mechanical and thermal properties, graphene has potential applications in transistors, integrated electronic circuits, ultracapacitors, solar cell and biodevices.

This dissertation focuses on synthesis, characterization and incorporation of ZnO nanostructures (thin film and nanowire) and graphene in electronic and chemical sensor devices for their enhanced performance. ZnO nanostructures and graphene film were synthesized using radio-frequency (rf) magnetron sputtering (physical vapor deposition) and chemical vapor deposition methods, respectively. Various characterization techniques such as scanning electron microscopy (SEM), transmission electron microscopy (TEM), x-ray diffraction pattern (XRD) and atomic force microscopy (AFM) were used to study the structure of these nanomaterials. Devices were fabricated in 1000 and 100 class of clean rooms using, mainly standard photolithography, electron beam lithography and sputtering process.

1.2 Motivation and Goal

This dissertation focuses on growth, surface modification and application of ZnO and graphene nanostructures in electronic and sensing devices. High band gap and high exciton binding energy provide stability of ZnO at high temperature and make it more resistant to radiation. Zinc oxide nanostructures are fast capturing the attention of the

scientific and technical community as an important technological material for future nano-electronics, optoelectronics, chemical and biological sensors.

Zinc oxide has a diverse family of nanostructures, both in terms of structures and properties. In the present work, ZnO thin films and nanowires have been selected for the experimental works. Zinc oxide nanostructures contain a large number of surface defects (missing oxygen and zinc atoms from the lattice). These defects are very unstable and react with other molecules present in its ambient, leading to very unstable electrical properties of ZnO nanostructures. This kind of behavior though makes incorporation of zinc oxide in electronics devices a challenging task, but provide an opportunity to use them in chemical and biological sensors. Our aim is to control or modify the surface properties according to the application requirements.

For successful application of zinc oxide nanostructures in future nano-devices, a detailed understanding of the charge transport mechanism is essential. There have been relatively few attempts to study the electronic transport properties of ZnO nanostructures. This dissertation aims to investigate the role of surface defects in determining the electronic properties of zinc oxide nanostructures based field effect transistors and chemical sensors. ZnO nanostructures have been used to fabricate thin film transistors and field effect transistors and their performance in air, vacuum and ultraviolet radiation were investigated thoroughly. A method for enhanced device performance by non-destructive surface cleaning has been proposed. This type of sensor has the potential of real time monitoring of atmospheric pollutants such as nitric oxide gas. Another application of these sensors is for early detection of inflammatory disease by measuring

nasal nitric oxide gas concentration level. Zinc oxide nanostructures are presented as one of the best candidate materials for this purpose.

Another goal of this dissertation is synthesis of graphene film and its application in transparent and flexible devices such as field emission display. Because of its combinational electrical, optical and mechanical properties, graphene can be used as transparent and flexible electrode in various electronic devices such as liquid crystal displays, flat panel displays, plasma displays, touch panels, electronic ink applications, organic light-emitting diodes and solar cells. At present all these devices contain indium tin oxide (ITO), which is one of the most widely, used transparent conductive electrode material. But, because of its fragility, lack of flexibility and scarcity of indium element, an alternate for this material is being sought. Graphene can be a suitable alternate for ITO in the above mentioned applications. Synthesis of graphene film in large dimensions and its transfer to a flexible substrate have also been carried out as a part of this dissertation.

1.3 Scope of this dissertation

Chapter 2 provides the background of the dissertation and discusses the properties of ZnO and graphene materials. Mainly structural, electrical and optical properties of nanostructured ZnO and graphene are described. The progress of the ZnO nanostructure field effect transistors and chemical sensors are also discussed. A recent development in graphene based transparent and flexible electrodes has also been covered in this chapter. Chapter 3 details the synthesis process of ZnO thin film and nanowires by radio frequency magnetron sputtering and chemical vapor deposition method, respectively. It also includes a brief introduction to the synthesis of graphene by CVD method. Chapter 4

describes fabrication of gallium doped ZnO thin film transistors and their device characteristics. Investigating the stability and reliability of the thin film transistor devices are the main emphasis of this chapter. ZnO nanowire field effect transistor and their enhanced electrical performance by nondestructive surface cleaning are described in the chapter 5. The effect of the ambient conditions on transistor characteristics and application of UV irradiation for desorption of chemical species from the ZnO nanowire surface are investigated in this chapter. Chapter 6 addresses the electrical hysteresis phenomenon in bottom gated field effect transistors and the application of vacuum annealing under UV irradiation for the restoration of intrinsic device characteristics. Chapter 7 shows the novel application of functionalized ZnO nanowire for nitric oxide gas sensing at low-ppm concentration level. Chapter 8 discusses the synthesis of graphene film by chemical vapor deposition method and the transfer of graphene film by hot press lamination and chemical etching process. The application of graphene film for transparent and flexible electrode in field emission device is also demonstrated in this chapter. Chapter 9 provides a summary of the dissertation and proposes for future work.

CHAPTER 2

BACKGROUND AND LITERATURE REVIEW

2.1 Properties of Zinc oxide

This part of the chapter overviews the basic physical and chemical properties of zinc oxide which includes crystal structure, electronic properties and optical properties.

2.1.1 Crystal structure and lattice parameters

Zinc oxide is formed in three types of crystal structures which are hexagonal wurtzite (B4), cubic zinc-blende (B3), and cubic rocksalt (B1) consisting of oxygen and zinc atoms at the anion and cation position respectively. These crystal structures are illustrated in Figure 1.

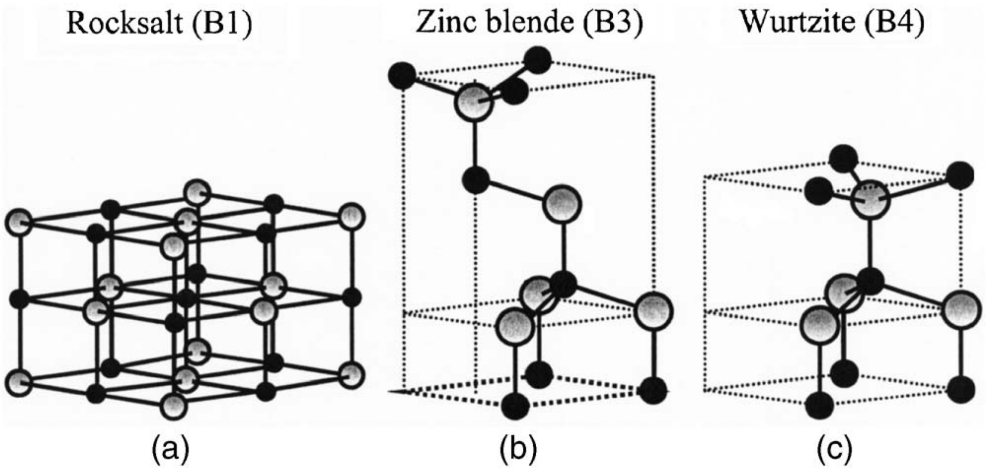

Figure 1. Three different zinc oxide crystal structures (a) rocksalt (b) zinc blende and (c) wurtzite. Gray and black circles represent zinc and oxygen atoms. Figure adapted from Ref. [1].

For wurtzite and zinc-blende crystal structures, each anion is surrounded by four cations at the corners of a tetrahedron, and vice versa. In the case of cubic rocksalt, each of the anion and cation forms a separate interpenetrating face-centered-cubic lattice. Thermodynamically, wurtzite is the most common and stable structure of zinc oxide at ambient condition. This structure has a space group of $P6_3mc$. The c/a ratio for ideal hexagonal wurtzite is 1.633, but in case of zinc oxide the crystal structure deviates from ideal hexagonal wurtzite structure following the relation (1).

$$u = \left(\frac{1}{3}\right)\left(\frac{a^2}{c^2}\right) + \frac{1}{4} \text{ ; where } u = 0.375 \quad \text{.....(1)}$$

In the case of ZnO hexagonal wurtzite crystal structure, Zn and O atoms are separately arranged into a hexagonal crystal structure with interpenetrating lattices. In this structure, every Zn atom is surrounded by four O atoms arranged at the corner of a tetrahedron, and vice versa. The lattice constants for Zinc Oxide, measured by x-ray diffraction method at 18 ℃ are [2]:

a= 3.2426± 0.0001Å

c= 3.2426±0.0003Å

c/a= 1.6020±0.0001

This tetrahedral coordination of anion and cation in ZnO results in a non symmetric crystal structure, which in turn produces piezoelectric and pyroelectric properties in the material. Typical values of piezoelectric and pyroelectric coefficients of ZnO thin film are 11.0 pC/N [3] and -9.4x 10^{-6} C/m²K, respectively. All the ZnO nanostructures synthesized in this work shows hexagonal wurtzite crystal structures.

2.1.2 Electrical and optical properties

Zinc oxide is a group II-IV binary semiconductor compound with direct band gap. It has a relatively large band gap of ~3.37 eV at room temperature [1]. Because of its large band gap which falls near ultraviolet range, pure ZnO is a transparent and colorless material [4]. Also a large band gap means higher breakdown voltages, ability to sustain large electric fields, lower electronic noise, and high-temperature and high-power operation. ZnO possesses a high exciton binding energy of ~60 meV. The electrical and optical properties of bulk ZnO are summarized in Table 1. In general ZnO, is an n-type semiconductor, which can be attributed to its intrinsic defects of zinc interstitial (Zn_i), zinc vacancy (Z_o) and oxygen vacancy (V_o) [1]. The average electron concentration in ZnO film is of approximately 10^{21} cm^{-3} [5].

Table 1. Electrical and optical properties of bulk ZnO, adapted from [6].

Static dielectric constant	8.656
Refractive Index	2.008, 2.029
Energy Gap	3.4 eV
Intrinsic career concentration	$<10^6$ cm^{-3} (max n-type doping$>10^{20}$ cm^{-3} electrons; max p-type doping$>10^{17}$ cm^{-3} holes)
Exciton binding energy	60 meV
Electron effective mass	0.24
Electron Hall mobility at 300 K for low n-type conductivity	200 cm^2/Vs
Hole effective mass	0.59
Hole Hall mobility at 300 K for low p-type conductivity	5-50 cm^2/Vs

Figure 2 shows the energy level of various defects present into the ZnO band gap. In general n-type doping of ZnO can be realized with Group III elements. Al, Ga and In are common n-type doping elements in ZnO. Economical and high quality of ZnO transparent conductive films can be made with n-type doping elements. Transparent

conductive films by Al, Ga and In doping have resistivity in the range of ~10^{-4} Ω cm [7]. The synthesizing p-type ZnO is very difficult because of deep impurity level, low solubility and compensation of dopant in the ZnO. There are several reports for the synthesis of p-type ZnO by doping of group-I and group-V elements in the periodic table such as Li, Na, K, Cu, Ag, N, P and As [1]. As such, a reliable p-type ZnO material that

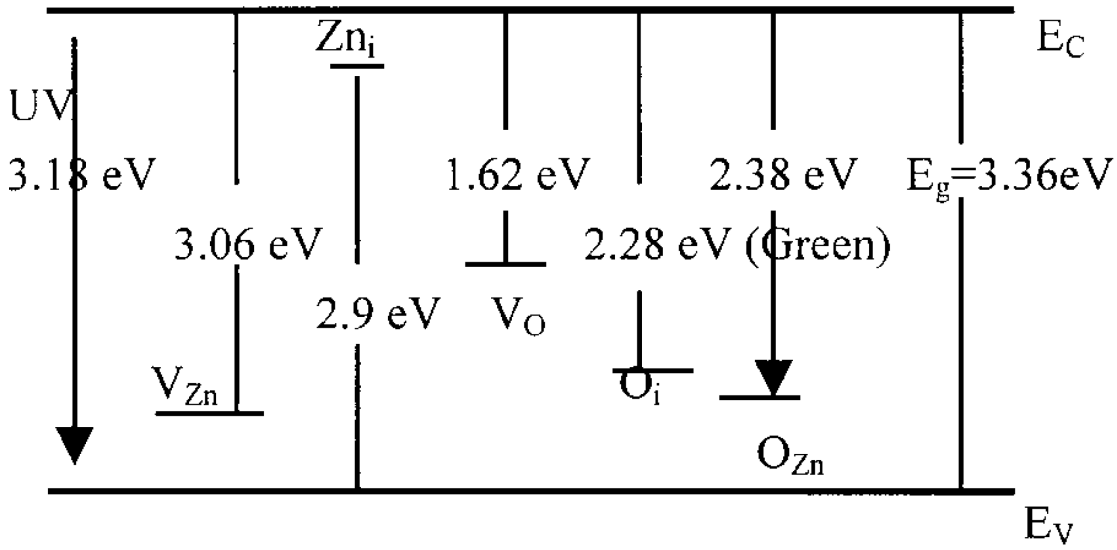

is reproducible has yet to be discovered.

Figure 2. Energy levels of various defects in ZnO, figure adapted from [8].

2.2 Zinc oxide nanostructure field effect transistor

Owing to their wide band, high electron mobility and optical transparency, ZnO thin film transistors are most sought material for display technologies. ZnO thin film transistors are the emerging alternate to amorphous silicon transistors used in flat panel display, printed electronics such as e-books. Table 2 shows ZnO based thin film transistors, their physical and device properties. The first fully transparent thin film

transistor was discovered by Hoffman along with other engineers at Oregon State University in 2003 [9]. Their study showed that ZnO thin film transistor operates in an enhancement-mode with n-channel. On-to-off ratio and mobility of their devices were 10^7 and 0.3 to 2.5 cm^2/Vs, respectively. Also the optical transparencies of devices were more than 75 %. They proposed that the future of these transparent thin film transistors is for elaborate invisible electronics system. Compared with other transparent thin film materials, ZnO thin films are economical and environmental friendly. ZnO thin films are easy to work with, as they can be deposited at low temperature over various substrates. Nomura *et. al.* [10] showed a way for room temperature fabrication of transparent flexible thin film transistors using In-Ga-Zn-O material as an active n-channel.

Table 2. ZnO based thin film transistors and their properties

Channel material	Gate material	Gate structure	Channel width (μm)	Channel Length (μm)	Channel thickness (nm)	$I_{on/off}$	Mobility (cm^2/Vs)	Ref. #
ZnO; rf-sputtered	Aluminum Titanium Oxide (ATO)	Bottom gated	7100	1500	~20–90	N/A	5–50	[11]
ZnO-spin coated	ATO	Bottom gated	200	150	30	10^7	0.20	[12]
ZnO-ion beam	SiO_2 and SiN_x	Bottom gated	2000	50	157	10^6	0.3-2.5	[13]
IGZO; rf-sputtered	Y_2O_3	Top gated	150	10	50	10^8	12	[14]
IZO; dc-sputtering	N_2O/SiH_4	Top gated	1000	100	7–10	10^6	15±3	[15]

The study of semiconducting nanowire based field effect transistors are of great interest because they can be prepared in high yield with reproducible electronic

properties. Compared with conventional lithography and etching method of transistor fabrication, bottom-up synthesis of nanowire and their FETs have several advantages, such as low dimensional, crystalline and smooth surface transistor channel, which are beyond top-down method capabilities. It is believed that this excellent control along with nanoscale channel size could yield device performance exceeding that obtained using top-down techniques.

Various architectures and device designs have been explored for ZnO nanowire field effect transistors. Most of the single nanowire FETs were fabricated depicting a cylinder on plate model with various gate architectures. Goldberger et. al. [16] have demonstrated high performance single ZNW-FET device fabricated on Si/SiO_2 substrate. Their device exhibits very high on-to-off ratio up to ~10^7 and mobility up to ~13 $cm^2\ V^{-1}\ s^{-1}$. Some advanced design concepts show vertical integration of ZNW with surrounded gate [17]. In general, the on-to-off ratio and mobility of ZNW FET varies from 10^3 to 10^7 and 3 to 80 $cm^2\ V^{-1}\ s^{-1}$. Although mobility of ZNW-FET is relatively low, it can be increased by other device modifications such as organic monolayer gate [18] . Electron mobility values of ~ 1175 cm^2/V s [19] have been reported for ZNW-FETs. Several other studies also have been carried out using ZnO nanowires to examine device operation under a variety of conditions, such as the use of different gate dielectrics, surface passivation of the nanowires and gate configuration (Table 3).

Table 3. Zinc oxide nanowire field effect transistors and their properties

Channel material	Gate material	Gate structure	Radius (nm)	Length (μm)	$I_{on/off}$	Mobility ($cm^2 V^{-1} s^{-1}$)	Ref. #
ZnO Nanowire	SiO_2	Back gate	50 to 200	10	10^5 -10^7	13±5	[20]
	SiO_2	Back gate	30-150	14	N/A	3	[21]
	SiO_2	Back gate	~90	n/A	~10^3	20 to 80	[22]
	self-assembled organic monolayers	Back gate	80	5	~10^4	~196	[18]
	Al_2O_3	Omega shaped-Gate	80 to 120	70	10^7	30.2	[23]
	self-assembled organic monolayers	Back gate	120	5	10^7	1175	[19]

2.3 Zinc oxide nanowire sensor devices

Mainly three types of gas sensors based on metal oxide nanowires have been developed, which are conductometric, field effect transistor (FET) and impedometric devices. Owing to their quasi-one-dimensional structure and favorable physical-chemical properties for chemical sensing, ZNWs are the most explored material for conductometry metal oxide gas sensors devices. As shown in Table 4, there are many reports on chemical sensing by ZNW. Wan et. al. [24] introduced ZNW gas sensors fabricated with micro-electro-mechanical system technology. Their sensor consisted of bundles of ZnO nanowire which exhibited high sensitivity and fast response to ethanol gas at 300 °C. They proposed that when a reductive gas at moderate temperature reacts with available surface oxygen species and decreases the surface concentration of O_2^{-2} ion over the ZNW surface. This increases the electron concentration in the ZNW, which eventually reflects an increase in conductivity. Fan et. al. [25] have demonstrated the gas sensitivity by single ZNW towards various gases such as NO_2, NH_3 and CO. They explained that gas

sensing by ZNW is a result of electron transfer between the chemical potential of the gas molecule and the Fermi energy level of the nanowire. They also reported an interesting result that with the decrease of nanowire radius, the sensitivity increases, which can be attributed to the increase in surface to volume ratio of the nanowire.

Table 4. Sensing of various gases by ZNWs

Zinc Oxide	Target Gas	Lowest detection concentration	Response time	Ref. #
Nanorods	H_2	500 ppm (25 °C)	10 min	[26]
	H_2S	50 ppb (RT)	N/A	[27]
	Ethanol	1 ppb (300 °C)	N/A	[28]
	Methanol	50 ppm (300 °C)	N/A	[29]
Single nanowire	H_2	200 ppm (RT)	~30s	[30]
	NO_2	1 ppm (25 °C)	N/A	[25]
	NH_3	1 % Vol	N/A	[25]
	CO	0.5 % Vol	N/A	[25]

The detection of chemicals of low concentration at room temperature is of paramount importance in some industrial and military applications and for disease control. Many strategies and methods have been developed for sensing of chemicals of low concentration by ZNW at room temperature. Fan *et. al.* [31], have demonstrated the gate refreshable ZNW gas sensor for the detection of NO_2 and NH_3 gases at room temperature, using a strong negative field to refresh the sensors by an electro-desorption mechanism. Other techniques for room temperature sensing along with high sensitivity and selectivity involve doping of nanowire with different elements [32] and the decoration of nanowire by catalyst nanoparticles [33, 34]. Wang *et. al.* [26, 35] have

demonstrated that surface modification of ZNW by Pd nanoparticles improves its sensitivity towards hydrogen gas by a factor of 5. In a similar approach, Chang *et. al.* [36-38] have deposited Au and Pd nanoparticles on ZNW by a chemical route for enhanced sensing of acetone, carbon monoxide and ethanol.

2.4 Properties of graphene

This part of the chapter introduces the basic physical properties of graphene material. Atomic structures of graphene film along with its unique electrical, optical and mechanical properties are discussed.

2.4.1 Atomic structure of graphene

Graphene is composed of sp^2 hybridized carbon atoms arranged in a two-dimensional honeycomb lattice[39]. This honeycomb lattice contains two interpenetrating triangular sub-lattices (A and B) as shown in Figure 3a. In this arrangement, atoms of one sub-lattice are at the center of another interpenetrating sub-lattice. The carbon-to-carbon inter-atomic length, $a_{c\text{-}c}$ is 1.42Å. One unit cell of graphene contains two carbon atoms and is invariant under a rotation of 120° around any atom. Graphene shows three in-plane σ bonds/atom and π orbitals perpendicular to the plane as shown in Figure 3b. These in-plane strong σ bonds and perpendicular π orbitals are responsible for its high mechanical and unique electrical properties.

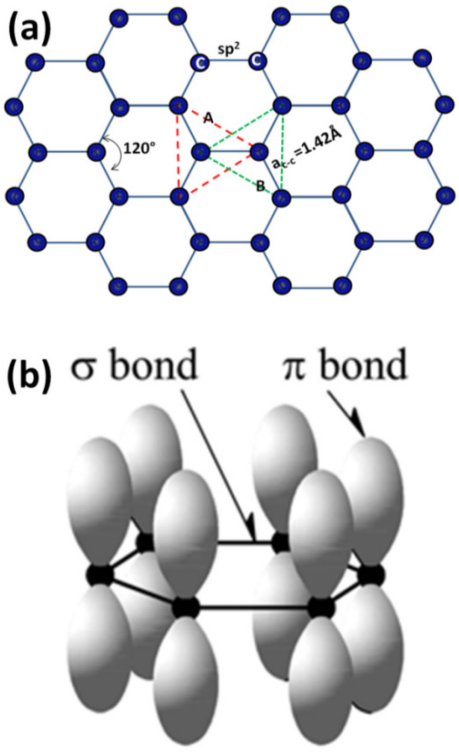

Figure 3. Atomic structure of graphene. (a) Schematic structure of honeycomb lattice structure. (b) Schematic of sp^2 hybrid c-c bond structure containing in plane σ bond and perpendicular π bond. Figure adopted from [39].

There are three common stacking arrangements of honeycomb carbon layers over each other in a few layer graphene film; AA type, AB type and ABC type (Figure 4). AA type stacking is hexagonal, AB is Bernal and ABC has a rhombohedral arrangement [39]. The AB type stacking is most common and abundant in graphite single crystals. This has the lowest energy state arrangement of the three type of graphene stacking. In the AB type stacking, the rotation angle between two interlayer honeycomb lattices, around the z axis is 60°, as shown in figure. The distance between two interlays is C_G = 6.672 Å at 4.2

K and 6.708Å at 297 K [39]. The hexagonal AA type structure doesn't have any rotation between two interlayer of honeycomb structure. The third ABC stacking is the most complex type of arrangement, which can be found in three or more layered graphene structures. ABC stacking can be imagined as a third C layer stacked over the Bernal cell with same orientation relative to the second layer but with a shift of $2a_G/3+ b_G/2$.

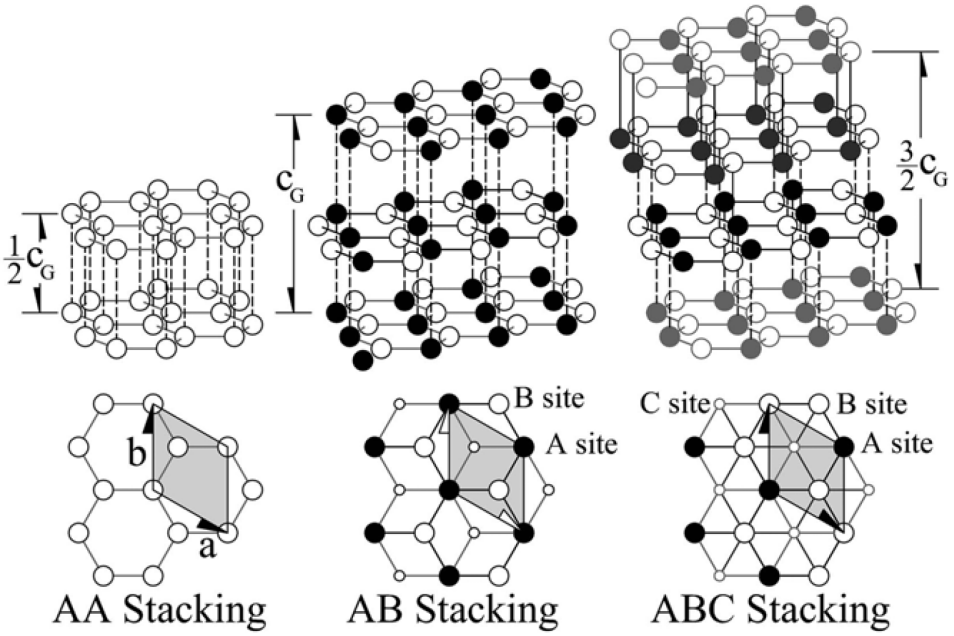

Figure 4. Three common stacking sequences in few layer graphene films; AA type, AB type and ABC type. Figure adopted from [39].

2.4.2 Electronic properties of graphene

Intrinsically, graphene is a semi-metal or zero band gap material. It has very high electron mobility ~15,000 $cm^2/V.s$ at ambient condition [40]. The mobility of graphene is independent of temperature between 10 and 100K, suggesting that the charge scattering is dominated by defects. In their experiment of suspended graphene, Bolotin et. al. [41]

have achieved a record high electron mobility exceeding the value 200,000 $cm^2\ V^{-1}\ s^{-1}$ at electron densities of $\sim 2\times10^{11}\ cm^{-2}$. Estimated mean free path of charge carrier in a suspended graphene film goes upto ~1μm [42]. Under the influence of a gate applied field effect, graphene shows am-bipolar charge characteristics with almost equal electron and hole mobilities [43].

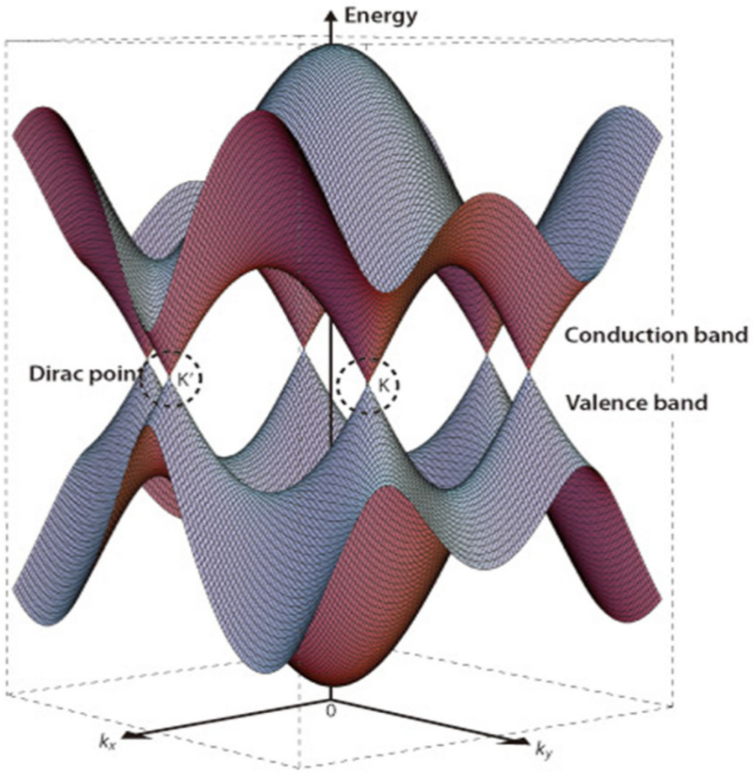

Figure 5. Electronic band structure near Fermi level of single-layer graphene. The conduction and valence bands cross at points K and K'. This point is called Dirac's point. Figure adopted from [44].

Figure 5 shows the electronic band structure near Fermi level of single layer graphene. Energy versus wave vector relation is linear at all the six corners of the

hexagonal Brillion zone. Near these six points, electrons and holes behave as relativistic particles with zero effective mass and they can be described by Dirac's equation for spin half particles. Therefore, the six corners of the Brillion zone are called Dirac points, and the electrons and holes at these points are named fermions [45].

2.4.3 Optical properties of graphene

Graphene monolayer exhibits very high transparency which is related to its low energy and two dimensional gapless electronic structures. One or two layer of suspended graphene film shows white light absorption of 2.3 and 4.6%, respectively with a negligible reflectance, less than 0.1% [46]. Transparency of the graphene layer decreases with the increase of thickness. The band gap of graphene bi-layer FET can be tuned by application of a potential difference and its optical response can be changed with a magnetic field [47].

2.4.4 Mechanical properties of graphene

Graphene is a very strong and rigid form of carbon. Similar to carbon nanotubes in-plane *p* orbitals in graphene honeycomb lattice structure are responsible for its remarkable mechanical properties. The hybridization of in-plane *p* orbitals leads to the formation of strong σ bonds. The rigidity of these bonds defines the mechanical properties of graphene. It is considered as the strongest material ever measured. The measured stiffness of graphene by AFM nanoindentation method is of the order of 300-400 N/m. The defect free graphene shows a breaking strength of 42 N/m and Young's modulus of ~1.0 TP [48]. Mechanical properties of graphene are similar to that of the

diamond and carbon nanotubes, which makes it an ideal reinforcement material and resonators. The comparatively low cost, high conductivity, transparency and chemical and mechanical stability of graphene make it suitable for transparent and flexible electrode.

2.5 Graphene transparent/flexible electrode

Graphene being the thinnest and strongest material is an ideal candidate of transparent and flexible electrodes for foldable and plastic electronics. The potential application of graphene flexible electrodes ranges from printed electronic circuits, photovoltaic cells and LCD screens. Table 5 shows the optical transmittance and sheet resistance of graphene films prepared by different methods. One of the major advances in this area was reported by researchers from Sungkyunkwan University, Korea. In his report Kim et. al. [49] has demonstrated large scale growth of graphene film on Ni substrate and fabrication of patterned graphene films for stretchable transparent electrodes. In his method for transferring graphene film from Ni metal, he used PDMS solution to cure over graphene film and then chemical etching of Ni metal from the bottom. The graphene film over PDMS shows high transmittance (>80%) and electrical conductivity with a strain in up to ~12%. In another example Wang et. al. [50] have fabricated a transparent and flexible electrode by first dip coating the graphene oxide (produced by the Hummers method) flakes solution on quartz substrate and then chemically reducing graphene oxide into a graphene film. This graphene film on quartz had a high conductivity of 550 S/cm and a transparency of more than 70% over 1000-3000 nm. An application of this graphene film has been shown for dye-sensitized solar

cells, in which it replaces the conventional brittle FTO electrodes. In another application, graphene on polymer substrate electrode was used to fabricate transparent and flexible nanogenerator [51]. Similarly, solution processed graphene thin film transparent conductive anodes were used to design organic light-emitting diodes [52]. In most of the above examples, graphene synthesized by CVD or Hummer's process were transferred by scooping, stamping or spin coating methods to non-flexible (glass or quartz) transparent substrates, which limits its application in flexible devices. For successful application of graphene into these devices, a suitable method for fabricating large area graphene film on flexible substrate is required.

Table 5. Transmittance and sheet resistance of graphene films.

Substrate	Synthesis method	Transmittance (%)	Sheet resistance (Ω/sq)	Ref#
Graphene on glass	CVD growth on Ni	90	850	[53]
Graphene on quartz	CVD growth on Ni	80	280	[49]
Graphene on quartz	Hummers method	82	800	[52]
Graphene on quartz	Hummers method	>80	5K-1M	[54]
Graphene on glass	CVD growth on Cu	90	2.1K	[55]
Graphene on quartz	Hummers method	80.80	1.8 - 0.08	[56]

CHAPTER 3

SYNTHESIS OF ZINC OXIDE AND GRAPHENE NANOSTRUCTURES

3.1 Zinc oxide nanostructures

Zinc oxide can be grown in various nanostructure morphologies such as thin film, nanowire, nanotubes, nanobelts, nanocombs, nanosprings, nanopolyhedrals and nanodisks. Some of the ZnO nanostructures grown in our lab by simple thermal evaporation techniques are shown in Figure 6. Different growth kinetics during synthesis process result in the formation of various morphologies of ZnO [57]. The morphology of the nanostructure can be influenced by different growth parameters, such as temperature, distance between source and substrate, pressure and carrier gas flow rate.

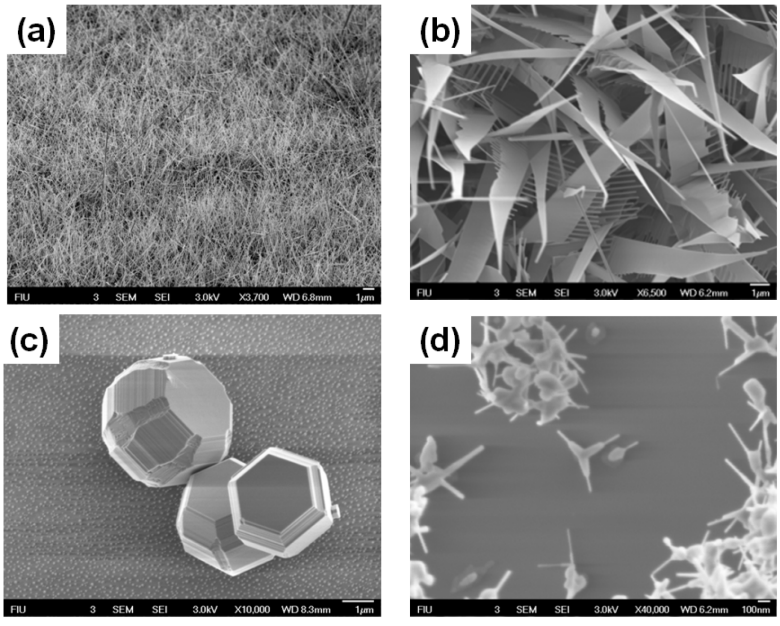

Figure 6. Various ZnO nanostructures grown by vapor deposition technique. (a) SEM images of Zinc oxide nanowires, (b) nanobelts, (c) polyhedron and (d) tripod.

In general nanostructure growth methods including a chemical vapor deposition (CVD), vapor–liquid–solid (VLS) growth mechanism at high temperature and a chemical bath deposition (CBD) at low temperature are applied to synthesize the zinc oxide nanostructures. We have used VLS techniques to synthesize the ZNWs by low pressure chemical vapor deposition system. GZO and ZnO thin films were grown by radiofrequency (rf) magnetron sputtering process. Details of these two growth techniques have been disused in the next section. Figure 7 shows SEM images of ZnO thin film grown by rf magnetron sputtering.

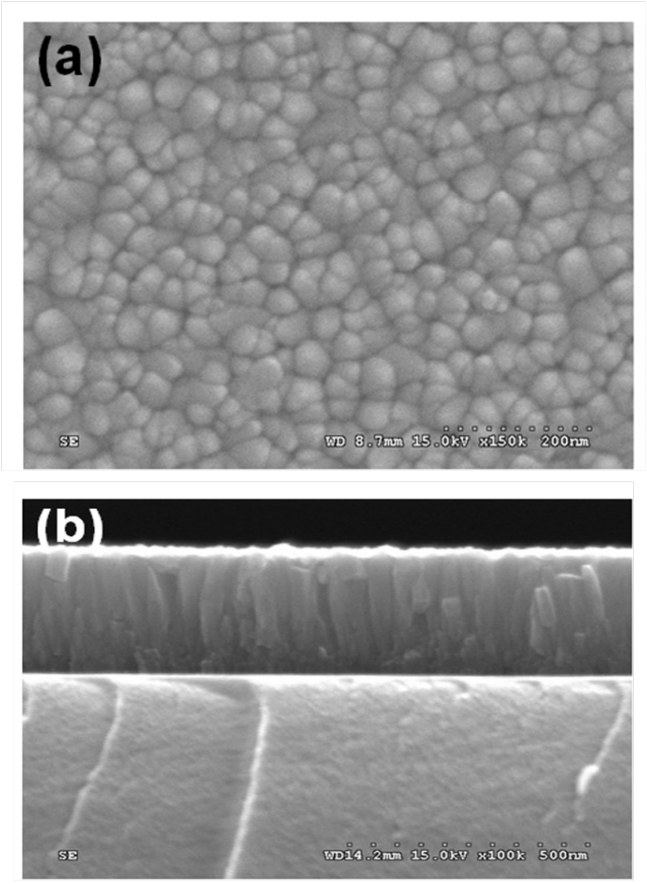

Figure 7. SEM images of ZnO thin film (a) top view and (b) cross section, synthesized by RF magnetron sputtering method.

3.2 Zinc oxide thin film growth

Several techniques have been used to prepare ZnO films such as pulsed laser deposition (PLD), molecular beam epitaxy (MBE), magnetron sputtering, metal organic chemical vapour deposition (MOCVD), spray pyrolysis, hybrid beam deposition (HBD) [58] and Sol-Gel technique. We have used RF magnetron sputtering system to deposit thin films of ZnO and GZO films on various substrates.

3.2.1 Magnetron sputtering process

Magnetron sputtering is a very efficient and versatile technique for the thin film deposition of a wide range of materials, which overcomes the limitation of a conventional sputtering process by increased low deposition rate, low ionization efficiencies in the plasma, and high substrate heating effect [59]. Magnetron sputtering is the most commercially available technique for the coating of high quality films of metal, ceramics, oxides and alloys over a substrate under vacuum. The basic principle of the sputtering process is the physical vapor deposition of a material by its ejection from a source and followed by its deposition on a substrate. In the magnetron sputtering process, the sputtering source or gun is usually a magnetron that utilizes strong electric and magnetic fields to trap electrons close to the surface of the magnetron, which is known as the target. The electrons follow helical paths around the magnetic field lines undergoing more ionizing collisions with gaseous neutrals near the target surface than would otherwise occur. In general, the whole process of ignition of sputtering and deposition of material on the substrate is conducted under vacuum with Ar gas atmosphere. Figure 8 shows a simple schematic of the magnetron sputtering system. The main part of the

sputtering system is the high vacuum chamber, where the sputtering gun serves as a cathode and the substrate holder serves as anode.

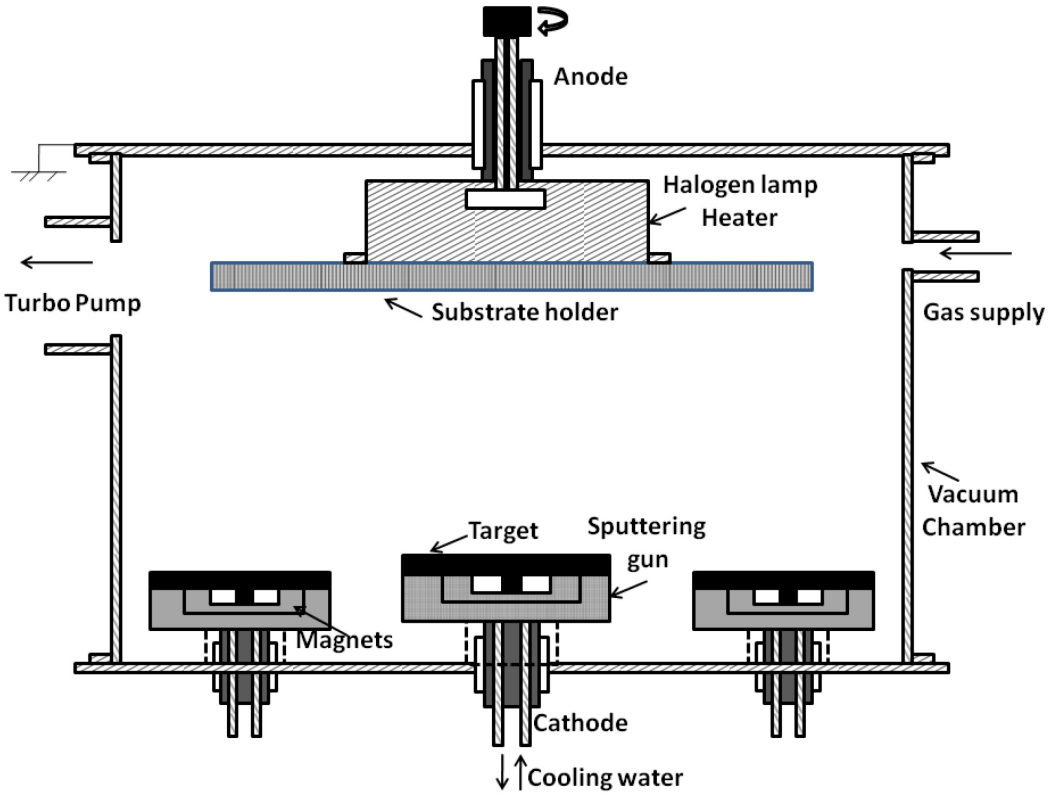

Figure 8. Schematic diagram of a simple magnetron sputtering system.

The three magnetron sputtering guns are installed at the bottom of the cylindrical chamber, where the substrate holder and heater assembly are mounted under the top lid of the chamber. The substrate holder is mounted with a motor, which rotates the holder and substrate along with it at a constant speed facilitating the homogeneous growth of the thin film. A constant pressure of process gases (Ar and or other gases) can be maintained within the chamber with mass flow controllers and turbo gate valve. Deposition of metals by magnetron sputtering is a relatively simple process compared with oxides and

insulating materials where a charge build-up develops hindering the efficiency of the sputtering process. This charge build-up can be avoided by utilizing radio frequency sputtering, where the sign of the anode-cathode bias is varied at a high rate. ZnO and GZO thin films in this study were grown by using the RF magnetron sputtering system shown in Figure 9. Disk shaped sputtering targets of ZnO and GZO, two inch in diameter and 0.25 inch in thickness having high purity ~5N were used.

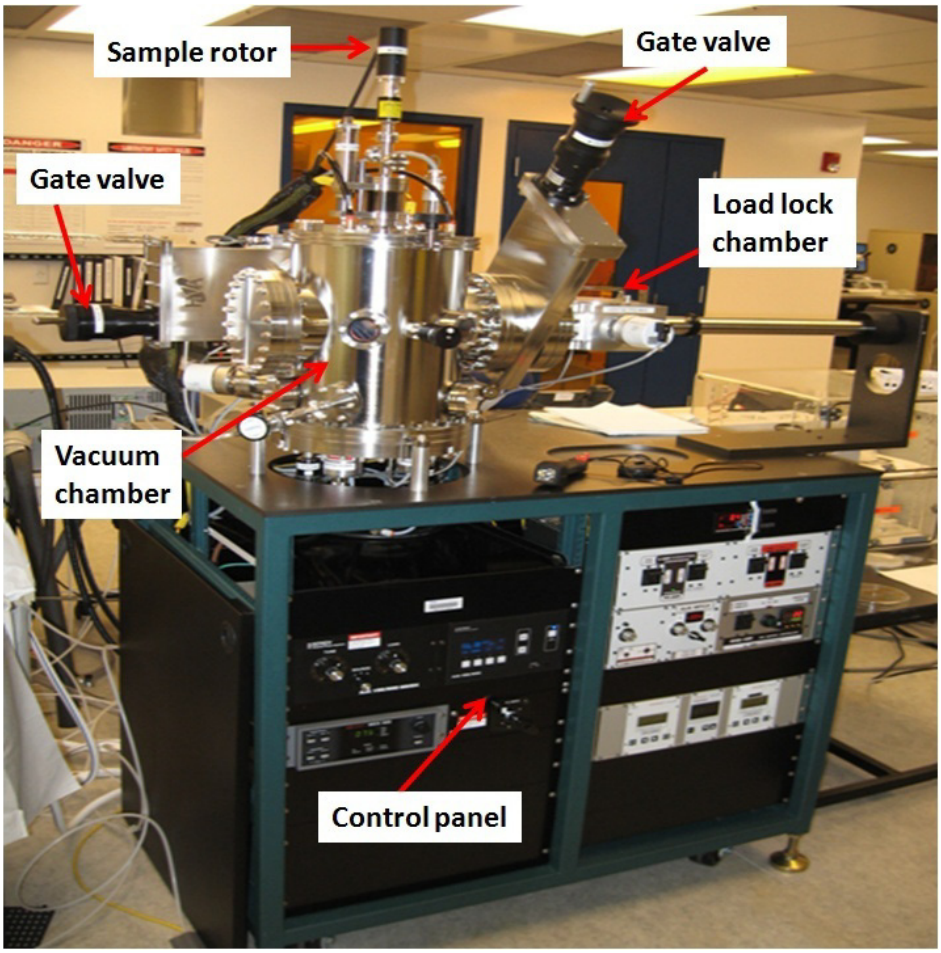

Figure 9. A three gun magnetron sputtering system (AJA International), used to synthesized thin films.

For the sputtering process, first the targets were installed over the sputtering gun inside the vacuum chamber. Sputtering chamber was pumped to the base pressure of $\sim 1\times10^{-7}$ Torr with the help of attached turbo molecular and roughing pump. Substrates were mounted over disk sample holder, which was later transferred into the sputtering chamber through a load lock system. Sample holder with substrates facing down towards the sputtering gun was locked into the anode and was set into rotation mode at constant speed. A continuous flow 10 sccm of Ar gas into the vacuum chamber was maintained with the help of mass flow controller. For generating the plasma or ignition of sputtering gun, chamber pressure was raised to ~25 mTorr with the help of manual gate valve mounted between turbo molecular pump and vacuum chamber. This helps to increase the Ar gas concentration near the target. A sputtering power of ~75 Watt was applied to magnetron gun. High concentration of Ar gas and ~75 Watt of power can easily start the plasma. After generating plasma the pressure was lowered to ~5 mTorr which was the deposition pressure. Reflection power of the sputtering gun was lowered to zero value using tuning of matching circuit. Finally the shutter over the gun is opened for starting the deposition on the substrate. After deposition of thin film for desired time line, sputtering power and gas flow is turned off and sample holder is removed through load lock system. Table 6 shows the standard process condition used for ZnO and GZO thin film deposition. After deposition the film thickness was measured by Tencor Alfa step profilometer. Characterization of the film was performed by SEM, XRD, AFM and Photoluminescence spectroscopy.

Table 6. Standard process conditions used for ZnO and GZO thin film deposition.

Target	ZnO, GZO, Au and Ti (5N purity)
Substrate	silicon, polymer, glass, sapphire and alumina
Substrate to target distance	25-30 cm
Temperature	Room temperature
Base pressure	~10^{-7} Torr range
Process pressure	5 m Torr
Gas used	Ar or Ar/O_2
Gas flow rate	10 sccm
RF power	~75 Watt
Reflection power	<3 Watt

3.3 Zinc oxide nanowire synthesis

Currently there are many techniques available for zinc oxide nanowires synthesis such as thermal evaporation, chemical vapor deposition (CVD), metal organic vapor phase epitaxy (MOVPE) and hydrothermal processing [60]. We have synthesized ZNW in our laboratory by thermal evaporation method using low pressure chemical vapor deposition system.

3.3.1 Low pressure chemical vapor deposition system

Low pressure chemical vapor deposition system consists of a horizontal tube furnace, an alumina tube, a rotary pump system and gas supply and control system shown in Figure 10a. We have Atomate™ low pressure chemical vapor deposition system in our lab (see Figure 10b) which has three-zone horizontal furnace and a 75 cm alumina tube with 2 inch diameter. One side of the tube is connected to gas inlet and other side of the tube is connected to rotary pump. LPCVD system is connected to the gas cylinders which are kept into the support room. The gas delivery system is consisting of MKS gas

controller and mass flow controller. Five mass flow controllers with different flow range are used to flow various gases into the alumina tube. The source and sample loading system consist of two alumina boats and long alumina rods extending to the center of the alumina tube. The two alumina boats are used for holding the source and substrate for the deposition. The LPCVD system can operate at up to 1000 °C and a pressure range of 0.4-760 Torr. The pressure, temperature and gas flow rate can be controlled automatically by Atomate™ workbench software system.

3.3.2 Nanowire synthesis process

Zinc oxide nanowires were grown in our lab by simple carbon-thermal decomposition process. ZnO and graphite in powder forms were mixed together in 1:1 molar ratio into an alcohol medium with a mortar and pestle. This mixture was used as a source material for the ZNW growth. Zinc oxide nanowires are grown on various substrates such as single crystal silicon, quartz and sapphire wafers. Gold nanoparticles of ~2-10 nm (Sigma Aldrich) and thin films (sputtered by 5N pure gold target purchased from Kamis Incorporated) were used as catalyst for the vapor-liquid-solid growth of nanowires. Figure 11 shows schematics of the vapor liquid process for ZnO growth. To grow ZNW, first gold nanoparticles (Sigma Aldrich) (10 nm) suspended in deionized (DI) water were dispersed by ultra-sonicated for 1 hr and then drop-casted on the desired substrate.

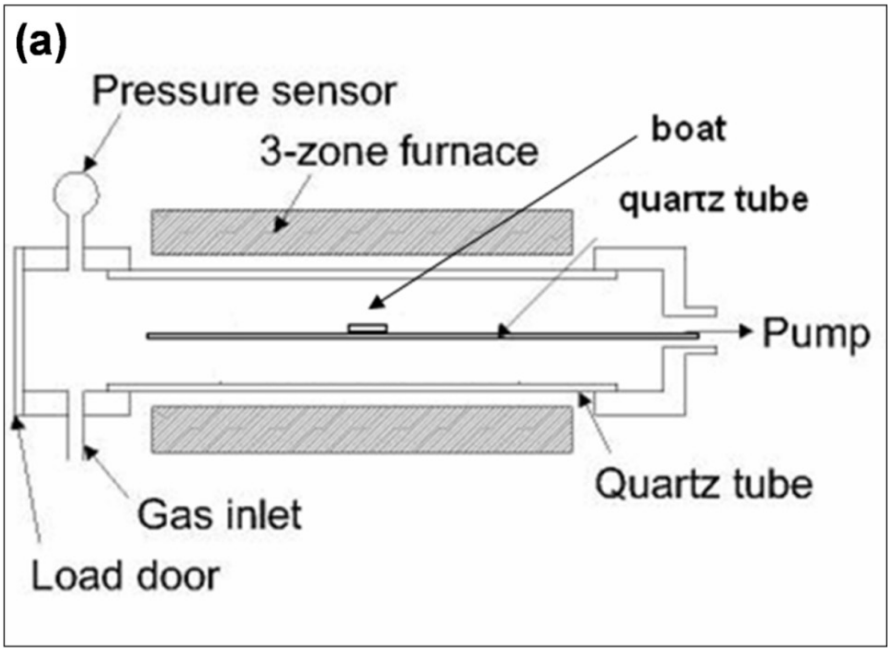

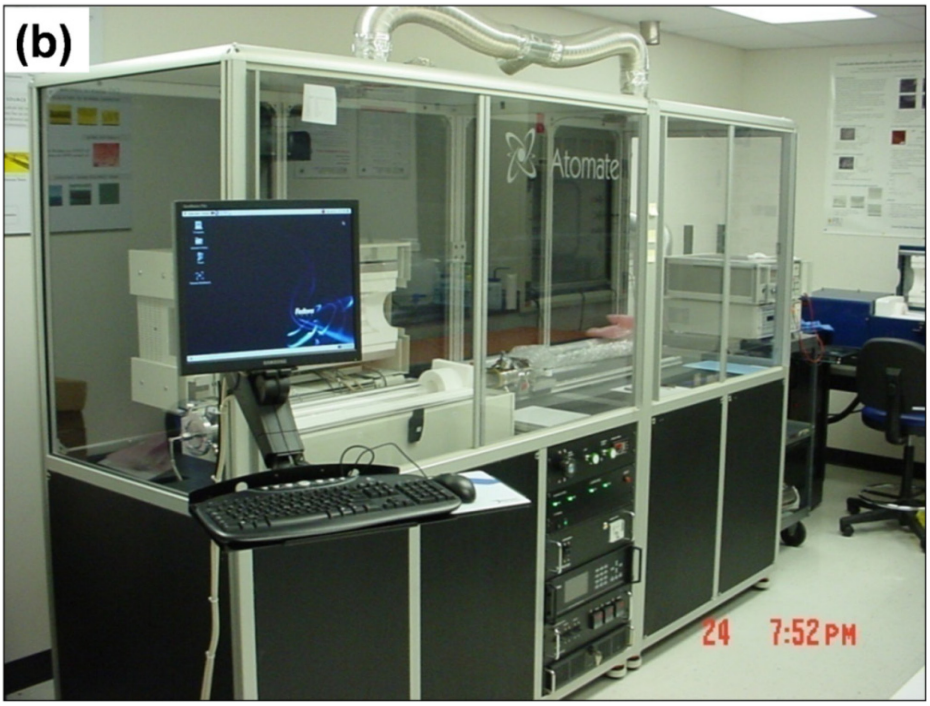

Figure 10. (a) Schematic diagram of LPCVD system (b) Atomate™ LPCVD system.

Figure 12a shows the AFM image of homogeneously dispersed Au nanoparticles on quartz substrate. The particle sizes of the Au nano-dots were in the range of 5 to 10 nm. Two alumina boats were placed over the loading alumina rods at a fixed distance of 4 inch such that the first boat reaches to the center of the furnace. The first boat was filled with source material (mixture of ZnO and graphite powder) while the substrate was placed on second alumina boat. Loading rods along with boats were inserted into the furnace through one end of the alumina tube. Tube was vacuum sealed using a polymer gasket and quick flange assembly. The alumina tube was purged by Ar gas for 30 min at 100 Torr pressure to avoid air and moisture during the growth process. A typical recipe shown in Table 7 was applied for the ZNW synthesis. Initially, the temperature was raised to 970 °C at ramp speed of 100°C /min and was held at 970 °C for an hour, which is the actual time required for the ZNW growth. After that, the furnace was allowed to cool down to room temperature. Throughout the whole synthesis process, 200 sccm of Ar gas was passed through the alumina tube at 100 Torr pressure. Finally, a white colored thin layer of ZNWs was observed on the quartz substrate.

Table 7. Typical process recipe for ZNW growth.

Step	Time (min)	Temperature (°C)	Ar gas flow (sccm)
1. Purging	30	25	200
2. Ramping	9.7	970	200
3. Hold	60	970	200
4. Cooling	45	25	200

The growth reactions of the ZNW are described into equations (1-4). At high temperature the carbon-thermal reduction of ZnO takes place which produces Zn vapor

and carbon monoxide gas (Eq. 1). Zn vapor is then transported over the substrate by Ar carrier gas where at low temperature and presence of Au catalyst Zn vapor react back to CO and residual O_2 gases to form solid ZnO (Eq. 2 and 3).

$ZnO_{(solid)} + C_{(solid)} = Zn_{(vapor)} + CO_{(gas)}$ (T>970 ℃)…..…..…. (1)

$Zn_{(vapor)} + CO_{(gas)} = ZnO + C$…….…..... (2)

$2Zn+O_2 = 2ZnO$……..... (3)

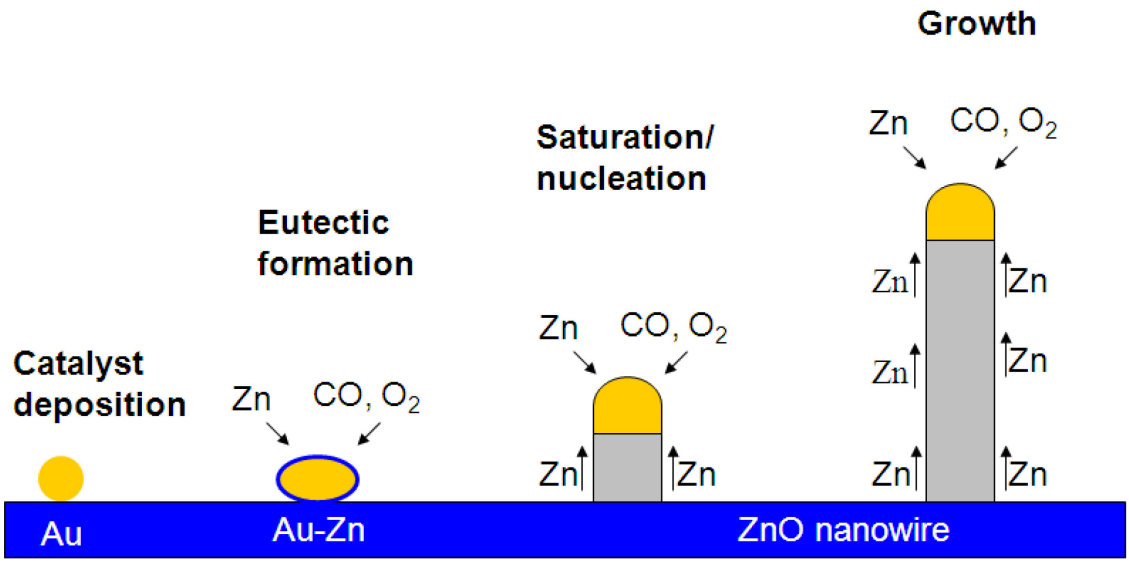

Figure 11. Schematic diagram showing simple vapor liquid solid process for ZnO nanowire growth.

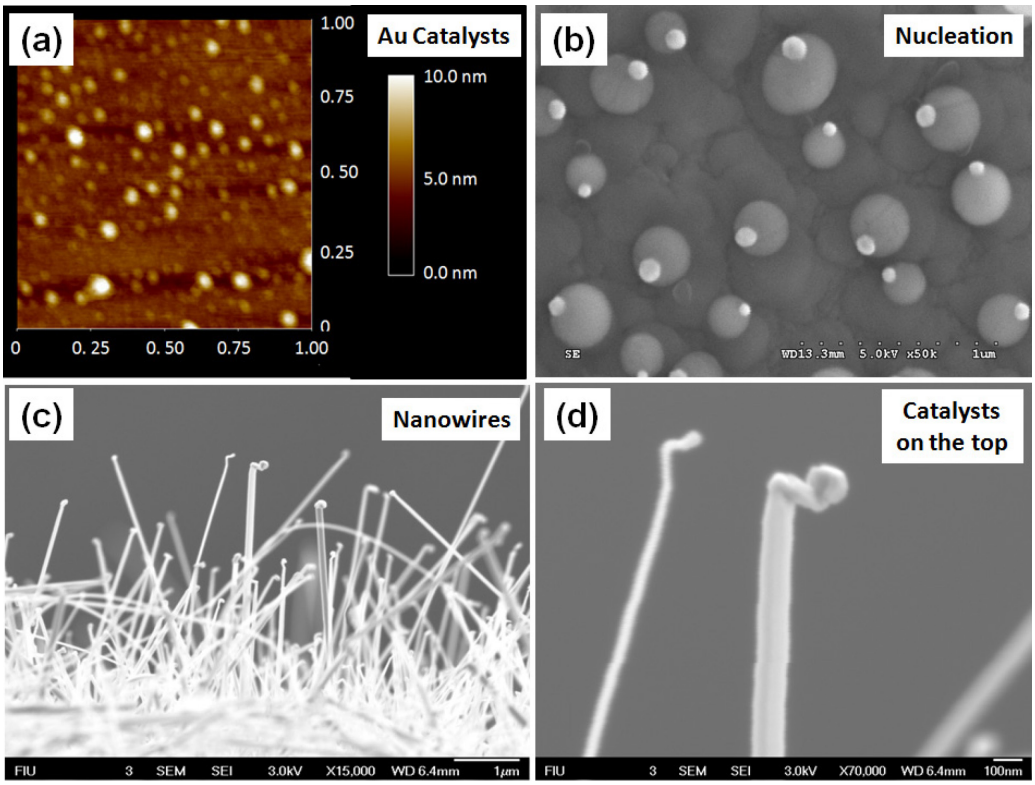

Figure 12. (a) AFM image of Au nanoparticles deposited on quartz substrate. (b) SEM image showing initial stage of nucleation of ZnO crystal; white dots show Au catalyst over ZnO seeds. (c) SEM image of ZNW grown on sapphire substrate; lengths of ZNWs were in range of 1-3 micro meter. (d) SEM image showing catalyst on the top of ZNW.

Zn vapor and Au catalyst forms an Au-Zn eutectic at high temperature and when Zn becomes supersaturated and is oxidized to precipitate ZnO below the catalyst particle. After an initial period of nucleation, ZnO crystal grows into the preferred morphology, which is determined by relative surface activities of various growth facets under given conditions. In the case of ZnO nanowire, the preferred growth direction of crystal is [0001] where for nanobelts the morphology is defined by other available polar surfaces

[61]. Figure 12 shows different stages of ZNW growth. Figure 12a is an AFM image of Au nanodots. The particle size of catalyst nanoparticles were in the range of 2 to 10 nm. Initial growth and nucleation of nanoparticles were shown into Figure 12b. White color catalyst nanoparticles were observed over the ZnO nucleated sites. After complete synthesis process, 1 to 3 μm length of ZNW were grown over the quartz substrate (Figure 12c). Catalyst nanoparticles were observed at the end of nanowires suggesting tip growth mechanism during vapor liquid solid process (Figure 12d).

3.4 Graphene synthesis by chemical vapor deposition process

Numerous metals (Co, Ru, Ir, Ni, and Cu) substrate have been study for graphene growth by chemical vapor deposition process. In our lab graphene films were synthesized by CVD method on thin Cu foils. Cu serves as best metal substrate for graphene growth because of its low cost, wide availability, easy chemical etching and ability to grow in large grain size. Commercial grade of Cu foils were purchased from Nimrod Copper Foil Company. Cu foils were cut into pieces in required dimensions and were annealed for 1 hrs, at 1000 °C and under H_2 + Ar atmosphere at 1 atm pressure. After 1 hrs of annealing the grain size of Cu increases upto 500-1000 μm. After annealing Cu foil was subjected to chemical etching by acetic acid. This process is important to remove any oxide film generated over Cu foil during prolonged annealing. Cu foils were washed with DI water to remove acid trace from the surface. For graphene growth, Cu foils were inserted at center of quartz tube in the LPCVD system. Initially quartz tube was flushed with Ar (500 sccm) gas for 30 min to remove air from the quartz tube. Temperature of quartz tube was raised upto 1000 °C at a rate of 100 °C/min under Ar (500 sccm) and H_2 (50-100

sccm) atmosphere. At 1000 °C, CH_4 (10-25 sccm) along with H_2 (50-100 sccm) gas was introduce into the quartz tube for graphene growth. After 5 to 10 min of growth time furnace was cooled to room temperature under 500 sccm of Ar atmosphere. Whole process was done at 1 atm pressure. Luster of Cu metal foil was changed to little grey after graphene growth over it (Figure 13).

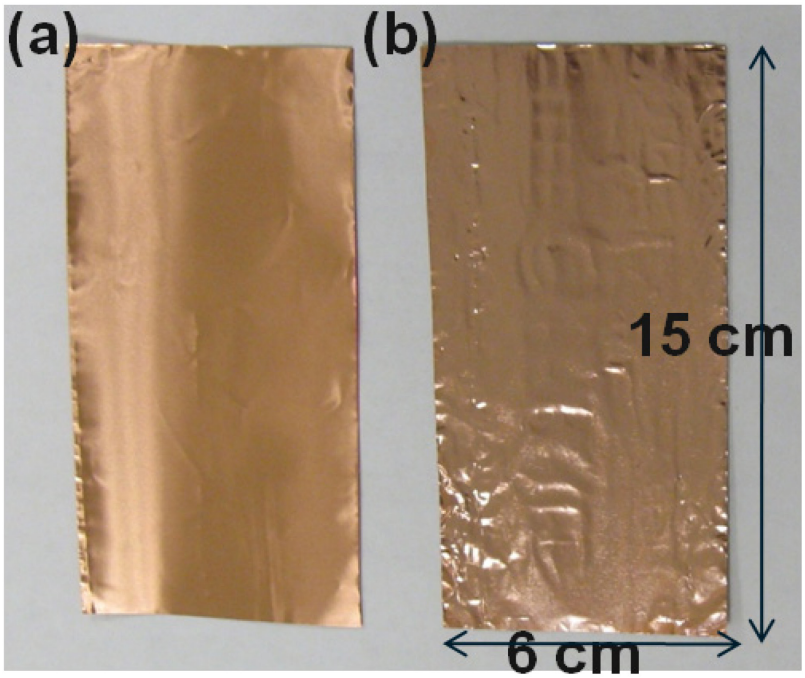

Figure 13. Images of Cu foil (a) before and (b) after graphene growth. After graphene growth, luster of Cu metal changes to grayish.

Characterization of graphene films were done by Raman spectroscopy and HRTEM. Figure 14 a and b show Raman spectrum and HRTEM images of graphene film over Cu substrate, respectively. Raman spectroscopy is a very effective nondestructive

technique to characterize graphene film. This technique is very well known for characterization of graphitic materials (graphite, nanotubes and graphene). The major Raman features for graphite material are defect or D band, graphite or G band (~1580 cm^{-1}) and second order 2D (~2670 cm^{-1}) band. D band originates from defect; G band gives information about in-plane vibration of sp^2 carbon atoms and 2D band represents stacking orders in graphite material [62]. 2D band in graphene is used to identify the number of graphene layers by their symmetry, sharpness and ratio with D band. The obvious difference between the Raman spectra of single layer graphene and graphite is the 2D band which results in sharp and symmetric peak in the former case while that of graphite is very broad. As the graphene thickness increases, the 2D band becomes broader and it is blueshifted for multilayer graphene. Electronic band structure of multi layer graphene cause splitting or overlapping in 2D bands. Depending on the defect (electron or hole) of in the graphene, their charge transfer effect and hence lattice parameters differ resulting in change of 2D band frequency. Electron doping gives a larger Raman frequency shift (blue shift) where as hole doping result in lower Raman shift (red shift) [63]. Raman spectroscopic studies also can be used to find the influence of substrate on mono/multilayer graphene properties and also the effect of folding and insulator deposition on the top layer [64, 65].

HRTEM is another powerful tool for graphene imaging and analysis. Figure 14b shows cross section image of graphene grown over Cu foil. For sample preparation and easy handling process, graphene over on Cu foil was sandwiched with Ag layer. Image shows 3-4 layers of graphene films stacked over Cu foil. Inset shows corresponding diffraction pattern of the interface depicting its crystalline nature.

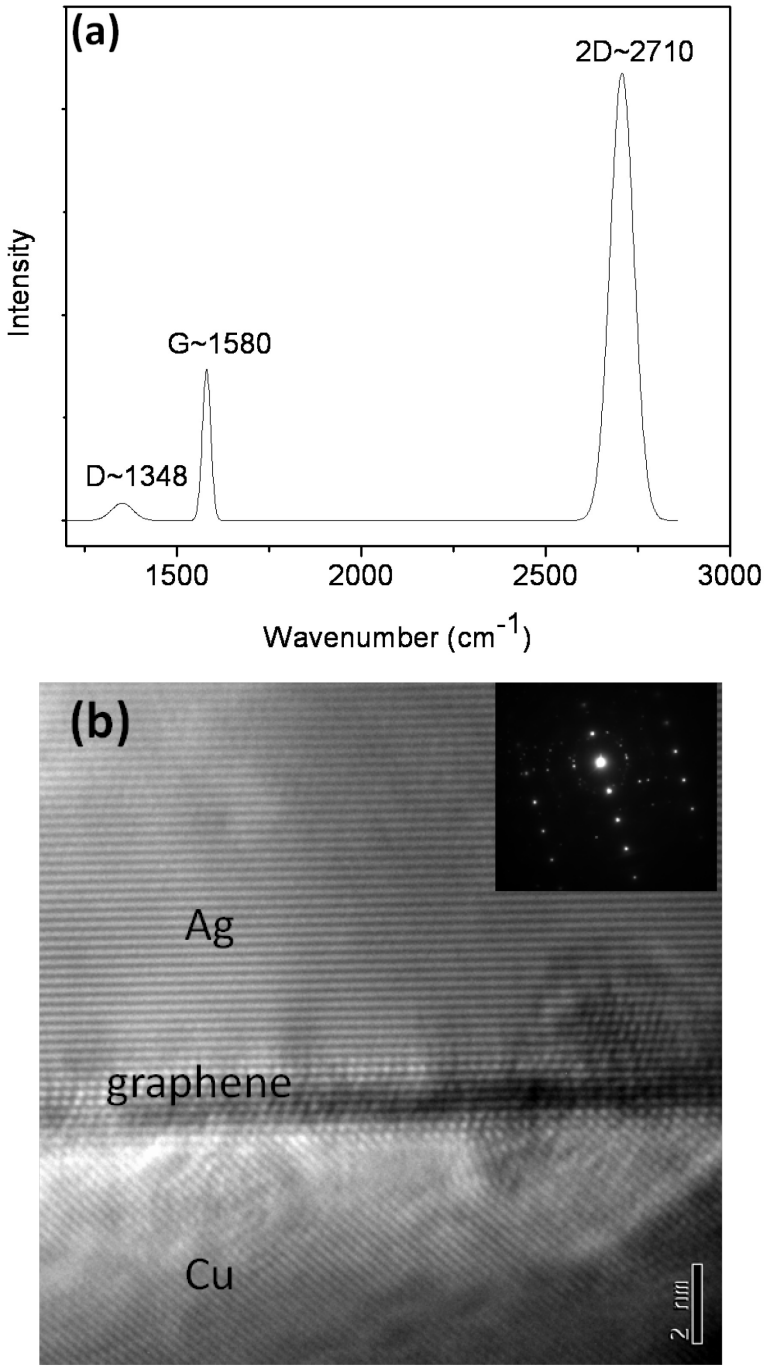

Figure 14. A typical Raman spectrum (fitted) from graphene film over Cu foil. (b) HRTEM image of graphene film between Cu and Ag layer. Inset shows electron diffraction pattern from the interface region.

CHAPTER 4

GALLIUM DOPED ZINC OXIDE THIN FILM TRANSISTORS

4.1 Introduction

Zinc oxide is a transparent and wide band gap (~3.36 eV) semiconducting material that has been extensively studied due to its multi-functionality such as optoelectronic, piezoelectric and pyroelectric with high exciton binding energy of ~60 meV [9, 10, 66]. The potential applications include ultraviolet lasers, light emitting devices, transparent conductors and thin film transistors. The intrinsic oxygen defects and Zn interstitials enable good electrical conductivity of ZnO thin films.

However, the conductivity of ZnO can be further improved by doping with several elements such as As, In, Ga, Fe, Sb, Al and Li. The minimal resistivity of ZnO achieved by doping was about 4-10 Ωcm [67-70]. Of all the elements considered Ga is the best n-type doping element because of its good lattice match with ZnO lattice; the bond lengths of Ga–O and Zn–O are 1.92 Å and 1.97 Å, respectively [71]. Also the Ga atom replaces the zinc ions and acts as substitutional impurity, releasing a free electron in the conduction band at room temperature. High gallium doped zinc oxide material has been used for contact electrodes in transparent oxide thin film transistors due to its high conductivity and transparency [72]. Recently, ZnO films with low resistance and high transparency have been obtained with Ga doping concentration range of 2.0–4.0 at.% [73, 74]. ZnO with different concentration of gallium has been studied for high mobility and crystalline thin films. Carrier concentration of GZO increases linearly with increase in Ga

concentration [75]. An improved high carrier concentration of ~10^{21}/cm^3 can be achieved by Ga doping compared to un-doped zinc oxide thin film which has typical carrier concentration of ~10^{17}/cm^3 [71, 75, 76]. Recent reports demonstrated that low Ga-doped ZnO down to ~1 wt.% can be grown in single crystal by radio frequency magnetron sputtering [77]. This material has potential in optoelectronic devices because it can be grown as a transparent single crystal thin film at room temperature and has a wide band gap of ~3.76 eV [74, 78].

Since the electrical properties of ZnO surface are affected by gaseous molecules present in the ambient, many researchers have studied the effect of annealing on ZnO film at different ambient conditions [77, 79]. However, the choice of annealing atmosphere, temperature and pressure still remains controversial. There is also lack of information about the environmental effects on ZnO thin film grown by rf-magnetron sputtering. This chapter deals with the electrical characteristics of low Ga-doped (1 wt.%) ZnO thin film transistor fabricated at room temperature. Device characteristics with different ambient conditions are studied and the corresponding mechanism is discussed. This work demonstrates our effort to develop a thin film transistor fabricated at room temperature with low Ga-doped (1 wt.%) ZnO, and its environmental effect.

4.2 Results and Discussion

4.2.1 Thin film transistor fabrication and characterization method

GZO-TFTs were fabricated with the use of a thermally grown SiO_2 thin film on Si substrate. Figure 10b shows the schematic of TFT fabricated on Si/SiO_2 substrate. Steps

for device fabrication have been illustrated in Figure 15a. The alignment marks and patterns were generated by standard electron beam lithography process.

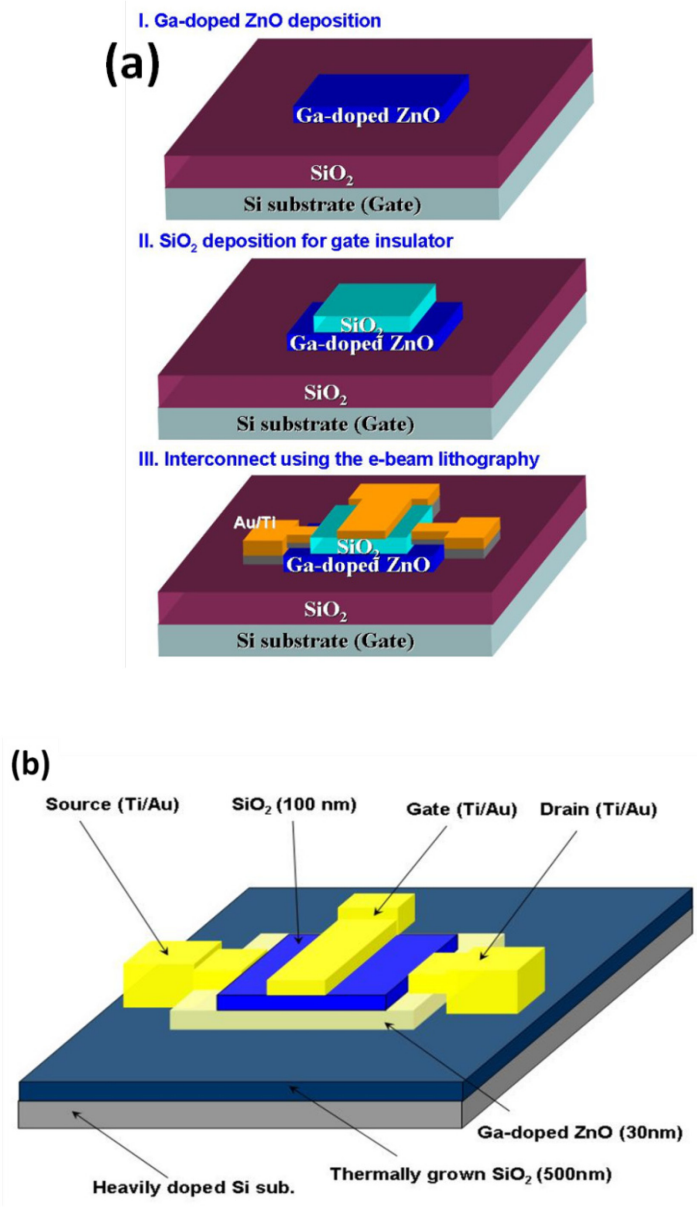

Figure 15. (a) Schematic of steps for fabricating top gated GZO TFT. (b) Side view of top-gate TFT.

A 35 nm of GZO thin film was deposited with a growth rate of 3.5 nm/min at room temperature by rf-magnetron sputtering system using (1 wt.%) gallium doped GZO target. The deposition of active channel was done in Ar ambient at 75 W of rf power, 0.67 Pa pressure and room temperature. Gate insulator of SiO_2 (100 nm) and Ti (10 nm)/Au (70 nm) electrodes were also deposited by same method and conditions. The channel length and gate width were 1 μm and 5 μm, respectively, corresponding to a width-to-length ratio of 0.2. Device image (Figure 16) was taken by field-emission scanning electron microscopy (FE-SEM; JEOL-JSM-7000F) operated at 3 kV.

Structural characterization of the thin film was investigated by high resolution X-ray diffractometry (HRXRD) using Panalytical X' Pert PRO diffractometer equipped with monochromatic copper anode (CuKα 1.54056Å), operated at 40 kV and 30 mA in θ/2θ mode. Atomic force microscopy (AFM) (PSIA XE-100) in contact mode was used to analyze the surface features and surface roughness of the thin film. An etched Si tip (length 130 μm, width 35 μm) with the resonance frequency of 75 kHz and force constant of 0.60 N/m was used for the measurement under ambient condition. The films were analyzed using TEM (Jem2010, JEOL) operating at 200 kV to examine the crystal structure and energy dispersive spectroscopy (EDS) to examine the gallium content in ZnO films. Photoluminescence (PL) and transmittance of thin film was measured at room temperature using 325 nm line of a He–Cd laser at various excitation powers and optical spectrometer (VARIAN CARY 5000) in the range of 200 to 1600 nm, respectively.

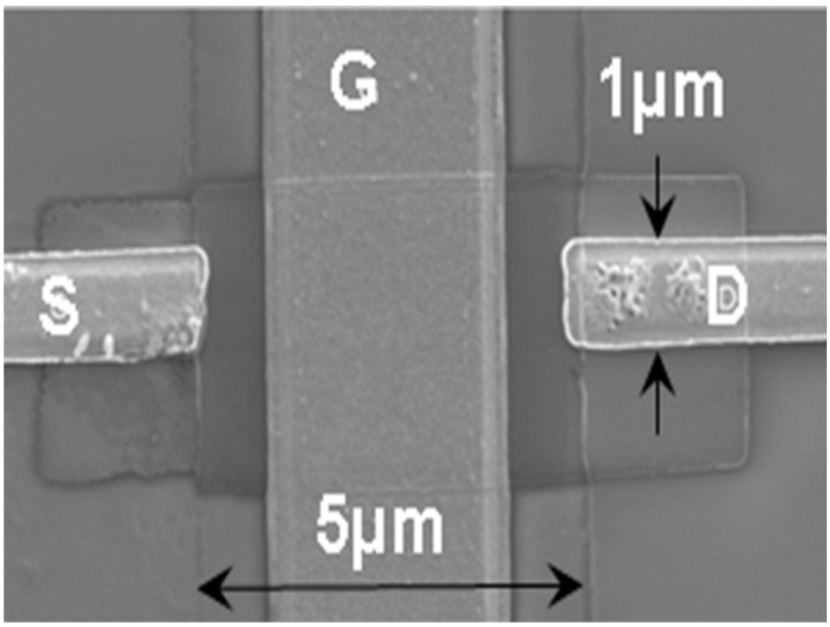

Figure 16. FE-SEM image of top-gate TFT fabricated on SiO2/Si substrate. Length and width of GZO channel were 5 µm and 1 µm. A gate oxide of SiO2 (100 nm) was deposited over GZO thin film. Metal electrodes of (Ti/Au) were deposited for source (S), drain (D) and gate (G).

The structural quality of GZO thin film was investigated by HRXRD scan in θ/2θ mode (Figure 17a). Diffraction pattern revels that the film is strongly oriented in c-plane. A relatively broad peak, full width half maximum of 0.5019, from (0002) plane at 2θ = 34.21° was observed in HRXRD measurement. The broadening of the peak is attributed to the high mosaicity of the sample. The lower diffraction angle compared to ZnO (with reference to JCPDS file number 89-1397 of ZnO powder) suggested that the incorporated Ga atoms result in expansion of wurtzite ZnO lattice [80]. Figure 17b represents the surface morphology of thin film investigated by the AFM.

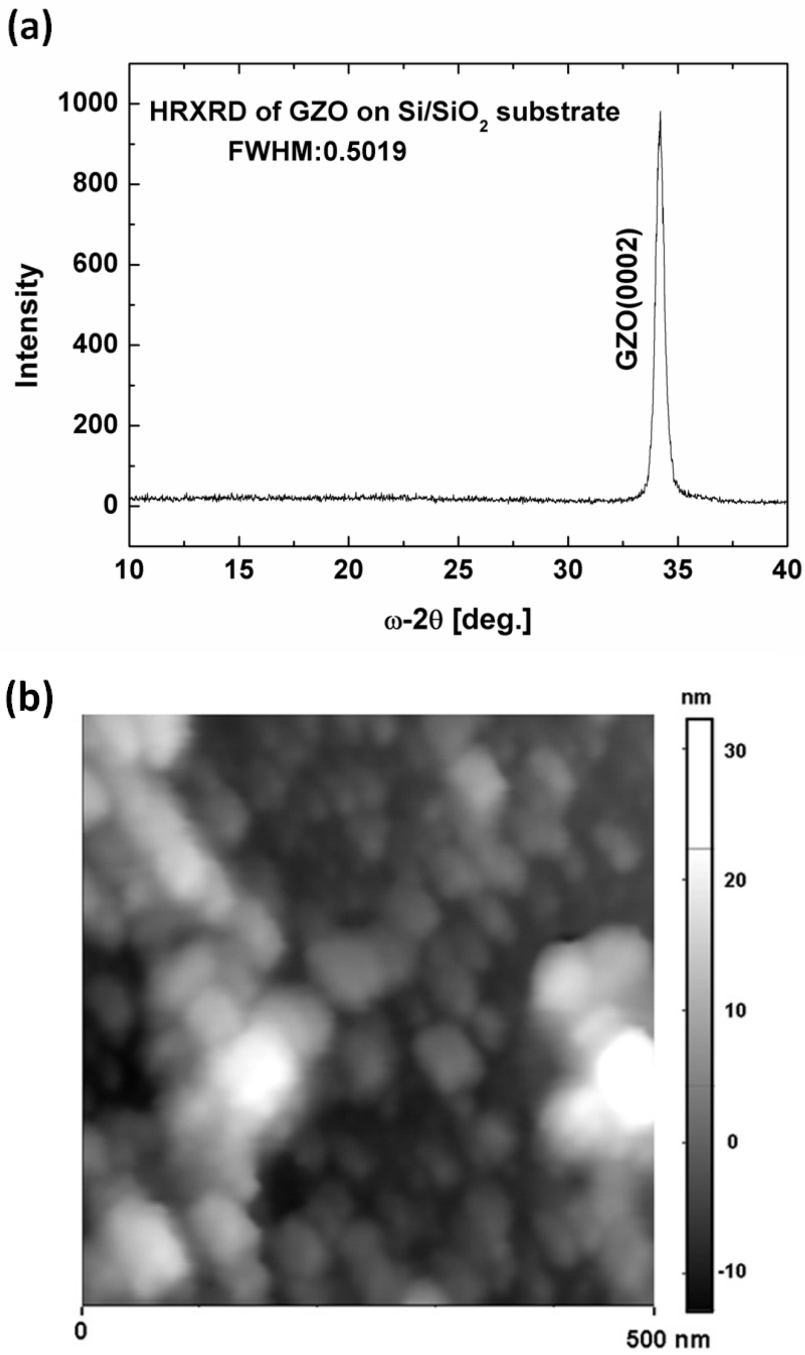

Figure 17. (a) High resolution X-ray diffraction spectrum (Cu Kα radiation) of GZO thin film and (b) AFM image of GZO thin film as-deposited on SiO_2/Si substrate shows a roughness of 5 nm and grain size of 30 nm (root mean square).

The thin film grown at 75 Watt power in Ar (10 sccm) shows high crystalline and smooth surface structure. Surface morphology in a scan area of the 500 nm×500 nm of the thin film shows a roughness of 5 nm and grain size of 30 nm (root mean square). A considerable roughness features a typical three dimensional growth mode of film at room temperature [81]. As the field effect characteristics depend on grain boundary conduction and hence grain size, the results indicate that structural and surface morphology of thin film grown by magnetron sputtering produces high quality thin film for device fabrication at room temperature. Further, TEM cross-sectional investigations were carried out, to investigate interface between substrate and thin film and structure of the film with thickness.

Figure 18a presents the TEM planer bright field image and corresponding selected area diffraction pattern (SADP) (Figure 18b) of 300 nm thick GZO films. A thin film with polynanocrystalline grain structure was observed. The grains were irregularly shaped, and their sizes varied from 10 to 50 nm. The typical column size ranged from 10 to 20 nm, which was in good agreement with the AFM measurements shown in Figure 17b. An interesting film evolution during growth was revered by cross sectional TEM study. At the film/substrate interface, a transition layer of ~50 nm was observed, which consist of a fine crystalline structure with a crystal size of about 10 nm. The diffraction patterns in Figure 18b exhibited a series of diffraction rings confirming the hexagonal crystal structure of GZO film. Figure 18c shows the EDS spectrum of Ga-doped ZnO thin fillm on Si substrate. The peaks in the pattern agreed with those of Zn, Ga, and O. In addition, the EDS measurement of the GZO film implied that the Ga atoms replaced Zn atoms in the hexagonal lattice.

Optical properties of the thin film were investigated by percentage transmittance. A transmission pattern of GZO thin films grown on the glass substrate is shown in Figure 19a. The thin films exhibit a high optical transmittance (above 80%), referred to air in the 310 nm to 1200 nm region. Emission characteristics of the GZO thin film were investigated by PL spectroscopy.

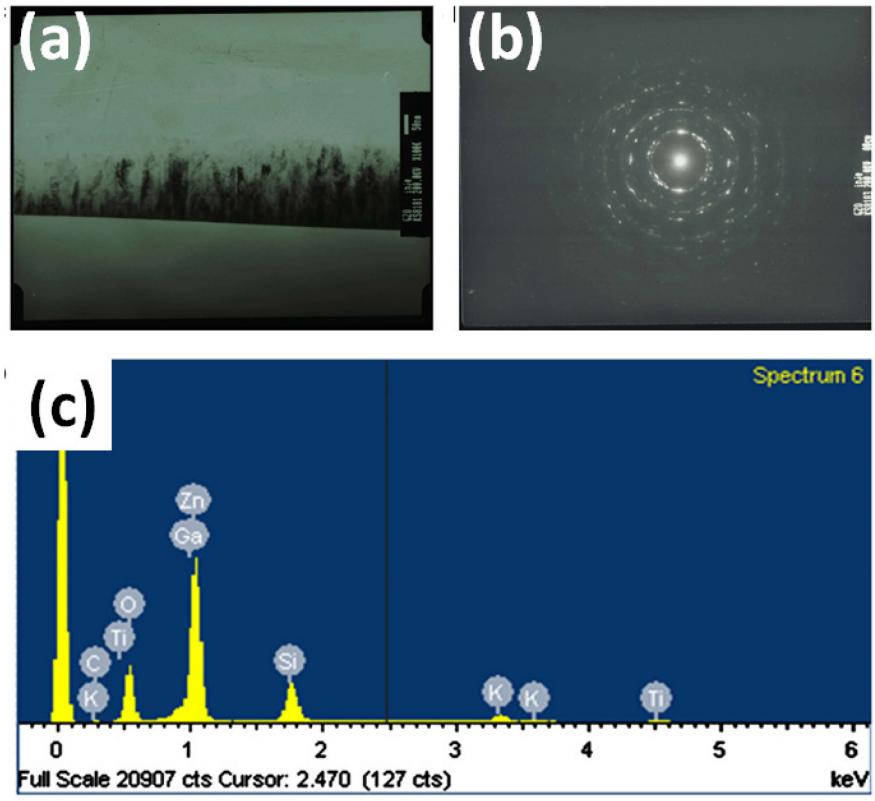

Figure 18. (a) Plane-view TEM images along with the (b) corresponding selected area diffraction pattern (SADP): 300 nm thick GZO films on the substrate. (c) EDS spectra of GZO film. The presence of Ga peaks indicated the incorporation of Ga into the ZnO film.

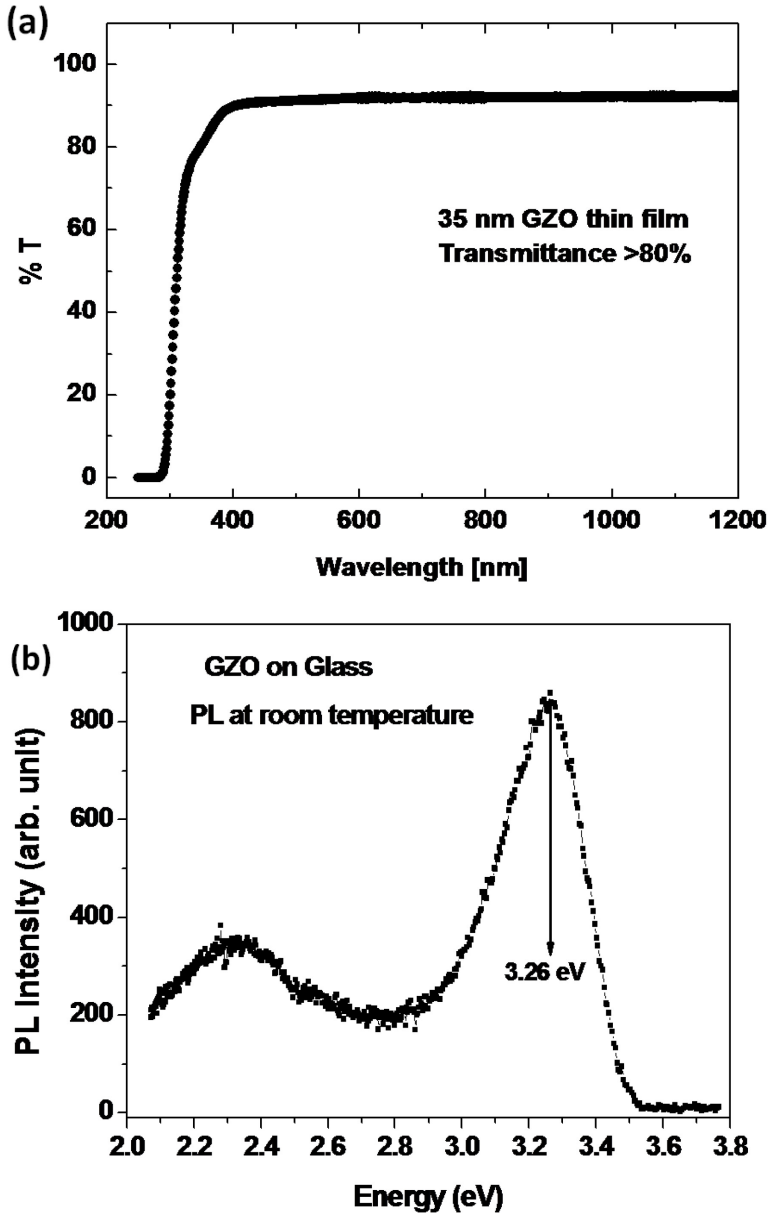

Figure 19. (a) Transmittance spectra of GZO thin film at visible and infrared wavelengths and (b) Room temperature PL pattern measured from the GZO thin film on glass substrate shows a strong emission near ultraviolet region and a defect-related emission near visible region.

Figure 19b shows the room temperature PL pattern of GZO thin films grown on glass substrate. This pattern is featured by a strong PL near the ultraviolet region and a defect-related emission in the visible region. The UV emission peak around 3.26 eV is due to the exciton related recombination contributed by both Zn and Ga atoms [82]. A relatively broad UV emission can be attributed to the presence of the large amount of Ga impurities in the film [77, 83]. A defect related emission near visible region entails the impurities and point defects such as Zn interstitial and/or oxygen vacancies in the film [81].

4.2.2 Device characterization

Electrical measurements for the device characteristics were performed by using four-probe system and precision semiconductor parameter analyzer (HP 4156C). The bottom-gated field effect transistors (FETs) were vacuum annealed at 475 K under vacuum (~3.3×10^{-3} Pa) to investigate the environmental effect on the device characteristics. Several current–voltage measurements with different ambient conditions were performed to investigate the role of absorbed gaseous molecules in the thin film and the stability of device performance. The electrical characteristics of the top-gated GZO-TFTs are depicted in Figure 20a. These devices show n-type FET characteristics with good gate controllability. The drain current gets saturated at relatively small drain bias of 5 V, compared to other results which are in the range of 20 V or higher [84].

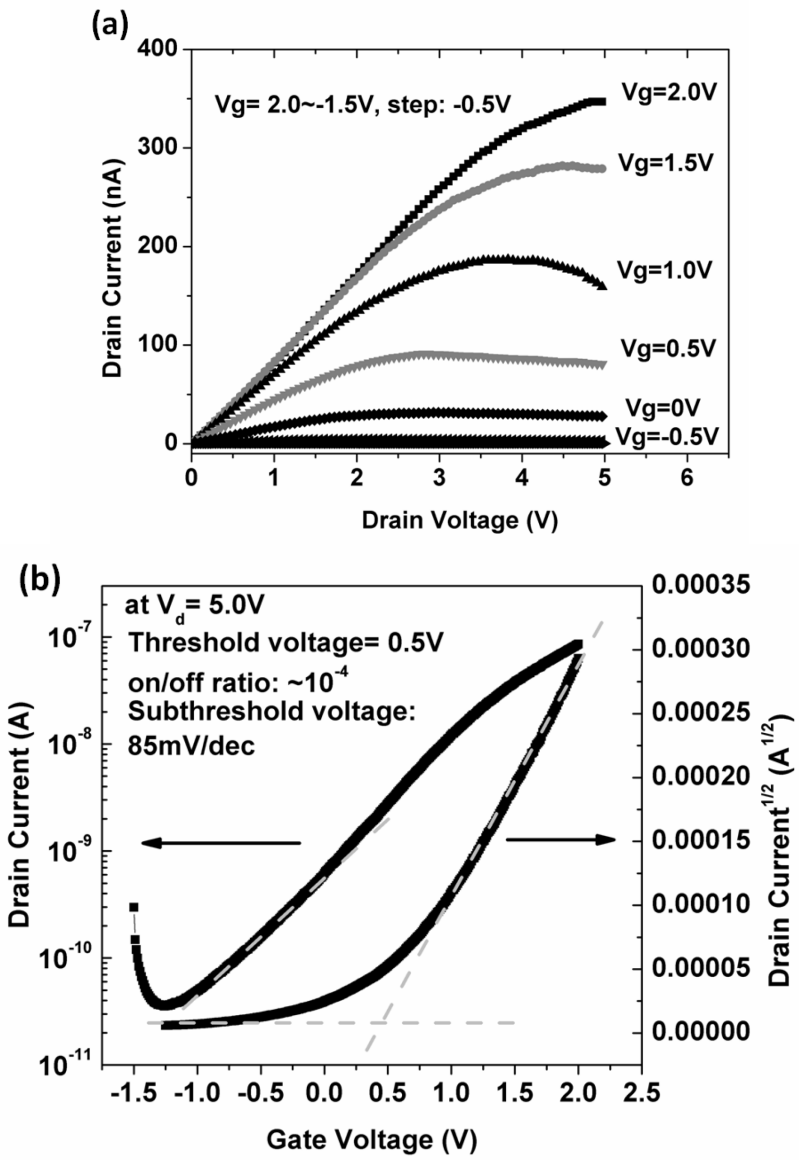

Figure 20. (a) Gate dependent I_d–V_d and (b) I_d–V_g characteristics at V_d =5.0 V for GZO-TFTs.

A number of key transistor parameters, including transconductance, mobility (μ_e), on–off ($I_{on/off}$) ratio, threshold voltage (V_{th}), subthreshold swing (S) and off-state current were calculated for topgated TFTs. The threshold voltage (V_{th}), defined as the gate

voltage at which the device turns on, is approximately 0.5 V. The threshold voltage is derived from linear extrapolation of the $I_{ds}^{-1/2}$–V_{gs} relation at constant drain voltage. Where I_{ds} is drain-source current and V_{gs} is voltage between gate and source. Modulation of ZnO Fermi level by gate voltage is normally described by the subthreshold swing, $S = -[dV_{gs}/d(\log I_{ds})]$, defined as the voltage required to increase the drain current by a factor of 10. A subthreshold swing of 5 mV/decade was obtained for Ga-doped ZnO TFTs, which is lower than that of organic or amorphous silicon TFTs that typically range from one to several volts per decade [85]. We measured an $I_{on/off}$ ratio of 10^4 and off-state leakage current of $\sim 10^{-11}$ A, which are related to power consumption and device performance. A high off-state leakage current and low $I_{on/off}$ ratio can be related to large number of interfacial floating charges trapped at the GZO/SiO_2 interface [86]. To estimate the carrier mobility, the device was modeled using standard equations of TFT. $I_{ds} = (WC_i\mu_{sat}/2L)(V_{gs}-V_{th})^2$, can be calculated from the slope of the plot of $|I_{ds}|^{1/2}$ vs V_{gs} in the saturation region (V_{gs}=2 V), where L is the effective channel length, W is effective channel width and C_i is the capacitance per unit area of the gate insulator. Under appropriate biasing conditions, the device exhibits effective electron mobility of $\mu_e \sim 5.7$ cm^2/Vs at very low operation voltage of 5 V. GZO-TFTs show a higher mobility of ~5.7 cm^2/Vs compared to ZnO FETs, which have mobility of ~0.024 cm^2/Vs [87].

Figure 21 shows the environmental effects on the bottom-gated GZO FETs. To determine the reliability of the device, electrical measurements were performed again after 10 days of device storage. Source-drain current shows a significant decrease from 10^{-6} A to 10^{-8} A in a voltage range of 15 V (curve #2). We attribute this effect to the atmospheric exposed active layer in bottom-gated FET. Intrinsically, ZnO contains

surface and volume defects like oxygen vacancy, oxygen antisite, zinc vacancy and interstitial zinc. Oxygen vacancies and zinc dangling bonds at the surface act as active sites for the absorption of oxygen molecules present in the atmosphere [88-91]. The surface state model presented by Morrison [92] treats the oxygen interaction with metal oxide surface as a two step process. In first step, rapid physisorption of oxygen takes place on the surface which leads to weakly bonded molecules and in second step these molecules capture the electrons from the material and form into strongly bonded chemisorbed species. Effect of these adsorbed gaseous molecules on the surface charge conductance of ZnO thin film has been widely studied [31, 93]. At normal temperature and pressure, the adsorption of oxygen on ZnO film can be treated as an electronic process in which the charge transfer takes place from thin film surface to absorbed oxygen molecules [94]. In case of adsorption of oxygen on the surface, a depletion layer is formed in the thin film channel and overall performance of device decreases. Further increase in vacuum up to 3.3×10^{-2} Pa doesn't increase the current values (curve #3). After that devices were annealed at 400 K (curve #4) and 475 K (curve #5) under vacuum 3.3×10^{-3} Pa. These annealing treatments at high vacuum of 3.3×10^{-3} Pa improve the device performance by removing the oxygen species from the surface which results in increase of source-drain current up to 10−6 A (curve #6).

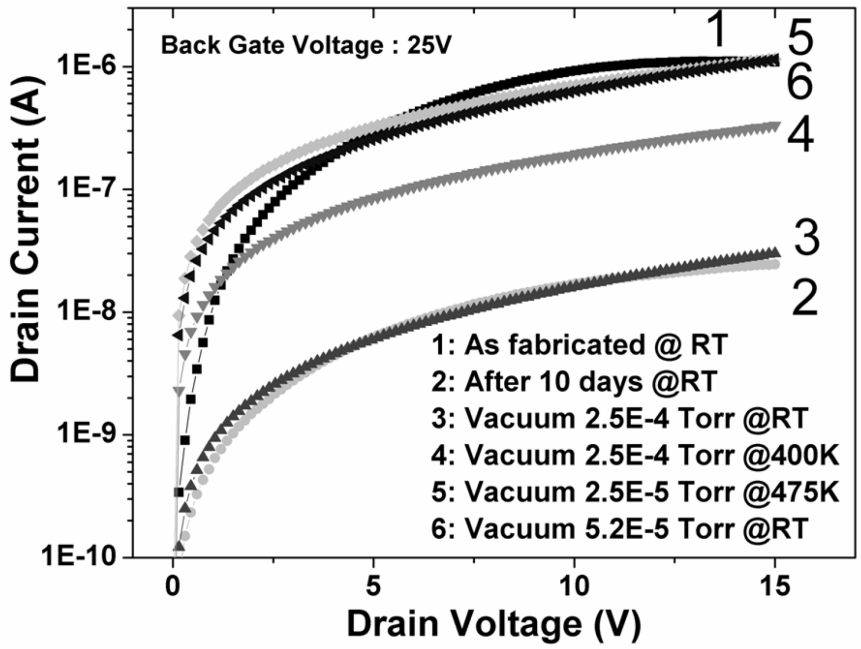

Figure 21. Effect of annealing at high vacuum on device characteristics. Source-drain current value decreases after 10 days of device storage. High vacuum and annealing treatments increase the current values up to ~1 μA at 15 V of bias.

4.3 Conclusion

In summary, transparent GZO (1 wt.% Ga) thin film on Si/SiO_2 and glass substrates were deposited at room temperature by rf-magnetron sputtering. Thin film transistors fabricated with this GZO as an active channel operate at low voltage (<5 V). Current–voltage measurements indicate an n-channel TFT operation which has a drain current saturation and field effect mobility of 5.7 cm^2/Vs at V_{ds} =5 V. Threshold voltage, sub threshold swing and on–off current ratio were 0.5 V, 85 mV/dec and 10^4, respectively. Low reliability and reduction in current density by two orders of magnitude

for bottom-gated GZO-TFTs can be attributed to the adsorption of oxygen on the ZnO thin film surface. The initial device characteristics can be recovered by vacuum-thermal treatment. The results indicated in this letter identify low doped GZO as potential TFT channel materials for future transparent oxide electronics.

CHAPTER 5

ENHANCED ELECTRICAL CONDUCTANCE OF ZINC OXIDE NANOWIRE FET BY NONDESTRUCTIVE SURFACE CLEANING

5.1 Introduction

Semiconducting zinc oxide nanowires are very promising materials for high-power/high-temperature electronics due to their remarkable physical properties like wide band gap of ~3.4 eV and high exciton binding energy of~60 meV [95-98]. FETs with ZNW as an active channel may enable promising applications for flexible and transparent electronics and chemical sensors [99-101]. It is well known that zinc oxide contains a high density of surface defects and dangling bonds that act as absorption sites for gaseous molecules, mainly oxygen species present in the ambient [102, 103]. The surface state model presented by Morrison [104] treats the oxygen interaction with semiconductor surface as a two-step process. Initially, rapid physisorption of oxygen takes place on the surface leading to weakly bonded molecules, which then capture the electrons from material and form into strongly bonded chemisorbed species. Due to high surface to volume ratio in nanoscale materials, these surface states dominate which affects their electron transport properties and catalytic reactions occurring at the surface [105]. In case of metal oxide nanostructures, these surface states defoliate the electronic properties of the materials by scattering and trapping of charge carriers that significantly hinders their application to the high-density and high-speed nanoelectronic circuits [106-108]. Several efforts have been made to passivate these surface states and improve the electrical per-

formance of ZNWs and thin films [109]. Park *et al.* reported the fabrication of high-mobility (~1000 cm^2/V.s) zinc oxide FETs by coating of polyimide layer on the nanorod surface [110]. Also, Keem *et al.* demonstrated omega-shaped-gate ZNW-FETs with Al_2O_3-coated zinc oxide nanowires for high device performance [111]. However, no direct investigation has been done for adsorption and desorption of these gaseous molecules on zinc oxide nanostructures. The aim of this chapter to study the effect of ultraviolet irradiation at elevated temperature and vacuum conditions on electronic properties of ZNW-FETs. This nondestructive cleaning process removes the surface states present on the ZNWin the form of absorbed oxygen species and enhances the device performance of the FET.

5.2 Results and discussion

5.2.1 Fabrication of nanowire field effect transistor and characterization method

As detailed in chapter 3, ZNWs were grown by vapor–liquid–solid process in a high-temperature and low-pressure horizontal chemical-vapor deposition (CVD) system. In order to make ZNW-FET (schematic shown in Figure 22a), the ZNWs were stripped from the substrate and dispersed in isopropanol solution by ultrasonication. ZNWs dissolved in solution were randomly dispersed on a heavily doped p-Si/SiO_2 substrate that had patterned metal electrodes and align marks fabricated by photolithography. Source and drain electrode patterning at the edges of single nanowires was done by electron beam lithography followed by Ti (80 nm)/Au (150 nm) metal deposition. Thermally grown SiO_2 (100 nm) and heavily doped Si (*p*+) substrate under the nanowire

were used as gate oxide and back gate electrode, respectively. An SEM image of single ZNW FET has been shown in Figure 22b.

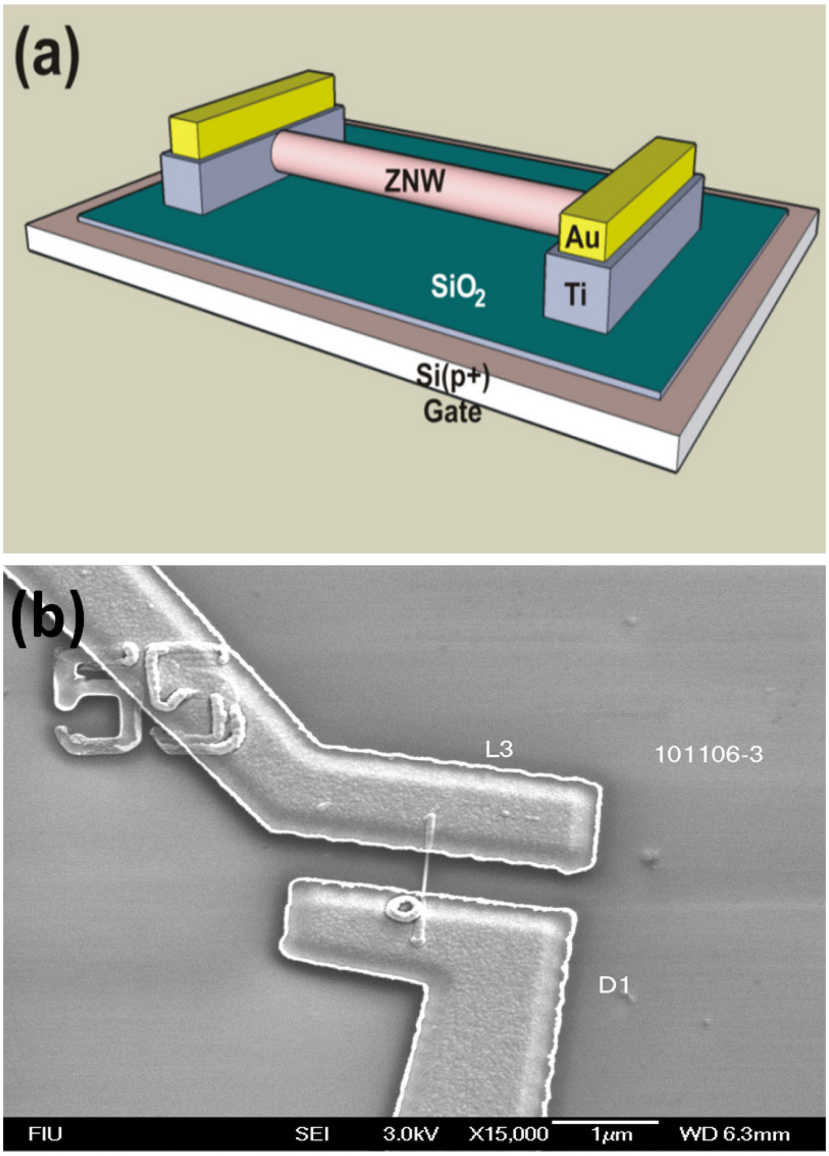

Figure 22. (a) 3D drawing view of single ZNW FET device. (b) SEM image of a single ZNW FET device fabricated on Si/SiO_2 substrate.

Figure 23 shows the scanning electron microscopy image of ZNWs grown on quartz substrate. Typical length and diameter of the nanowires were 2–3 μm and 20–50 nm, respectively. Side view shows that most of the nanowires were vertically aligned with quartz substrate. Catalyst at the end of the nanowires depicts its tip growth mechanism during VLS process. Figure 24 shows the high resolution transmission electron microscopy images of nanowire. Figure 24a shows the image taken at the middle of the nanowire. ZNW shows a very high crystalline structure at the middle of the nanowire, with no visible line or planar defects. HRTEM taken at the tip of a nanowire (Figure 24b) exhibits multigrain structures that are separated by low-angle grain boundary and have a lattice parameter of ~0.510 nm [112]. As shown in inset of the images, SAED pattern of a nanowire depicts its hexagonal crystalline structure and growth direction of [0001]. The d-spacing along the growth direction are indicated by parallel lines, which corresponds to the distance between the (0001) planes, and it is in good agreement with the analytical results of selected area diffraction pattern (SAED), shown in insets. Figure 25a shows the energy-dispersive X-ray spectroscopy (EDX) of zinc oxide nanowires. Very strong peaks for Zn and O from zinc oxide nanowires, Au peak from catalyst and Si peak from substrate are evident in the spectrum. Figure 25b, HRXRD pattern of the zinc oxide nanowire shows that most of the nanowires were oriented into (002) crystal direction.

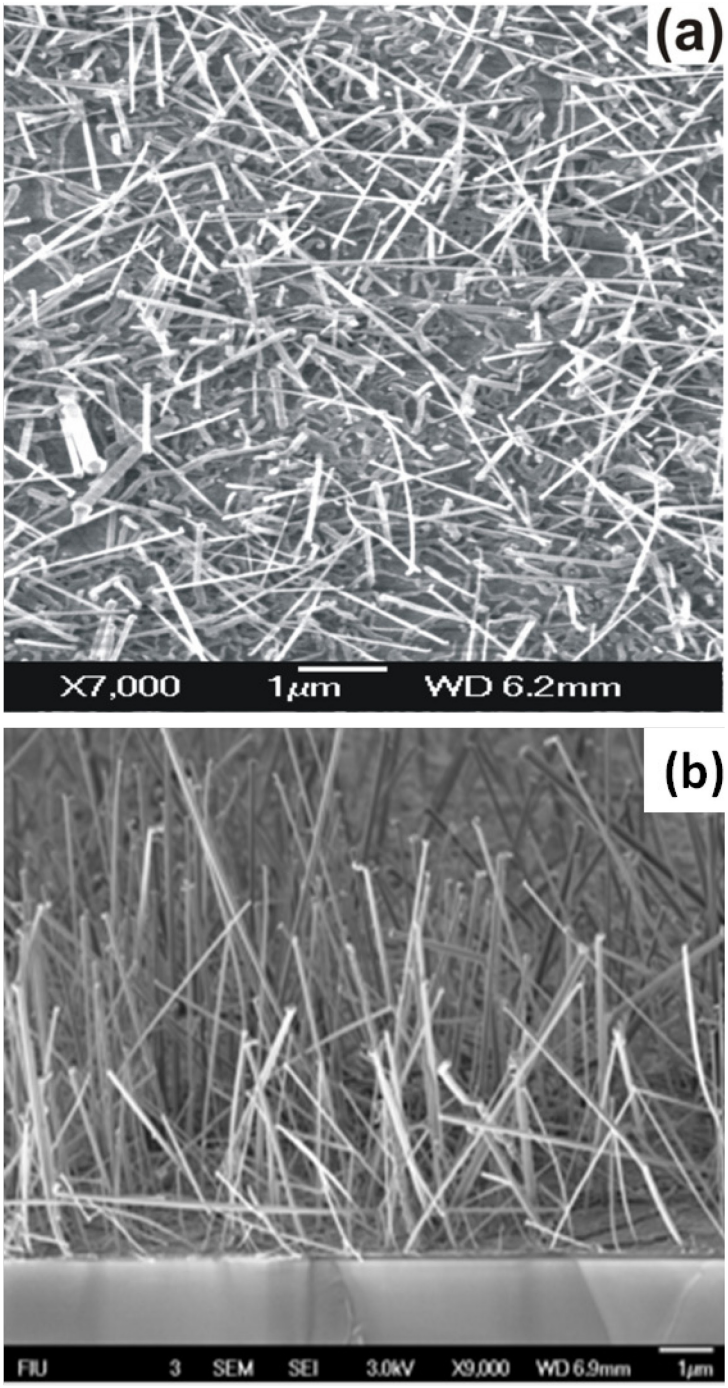

Figure 23. (a) SEM micrograph of ZnO nanowires on a quartz substrate. (b) Side view shows that average length of nanowires were ~5μm.

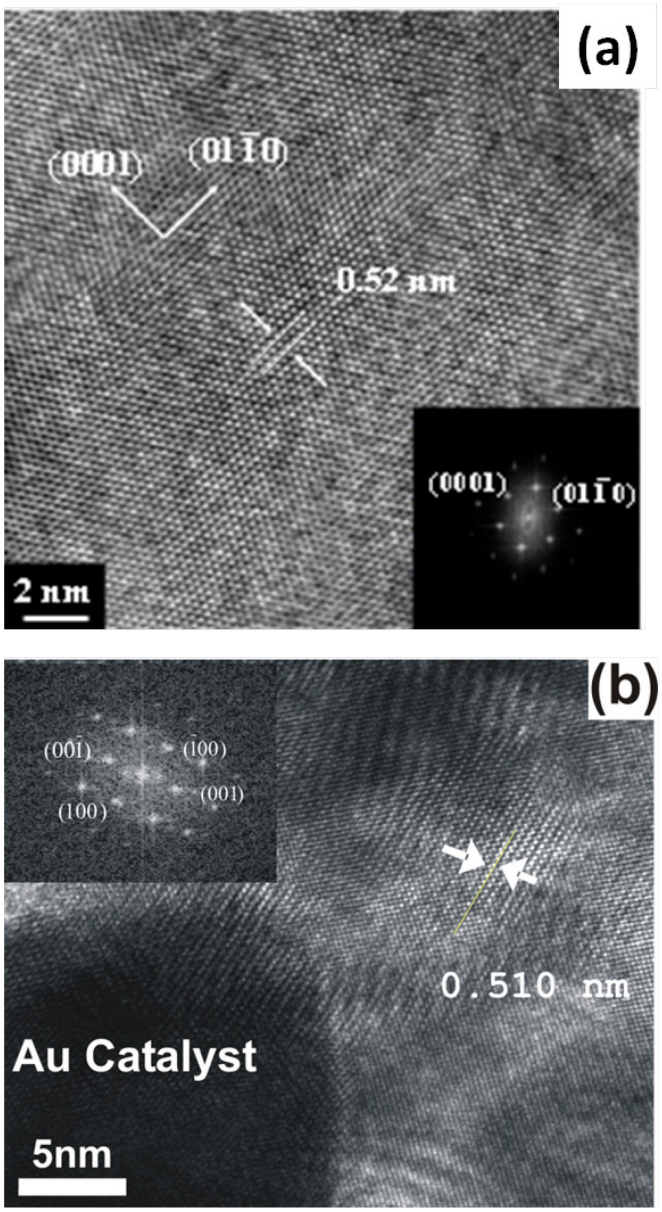

Figure 24. (a) HRTEM image taken from the middle part of nanowire showing single crystal lattice structure and (b) HRTEM image taken at the tip of nanowire, near the Au catalyst showing multigrain structure of an individual nanowire. Inset of each image shows corresponding selected area diffraction pattern of the nanowire. The growth direction of the nanowire is [0001].

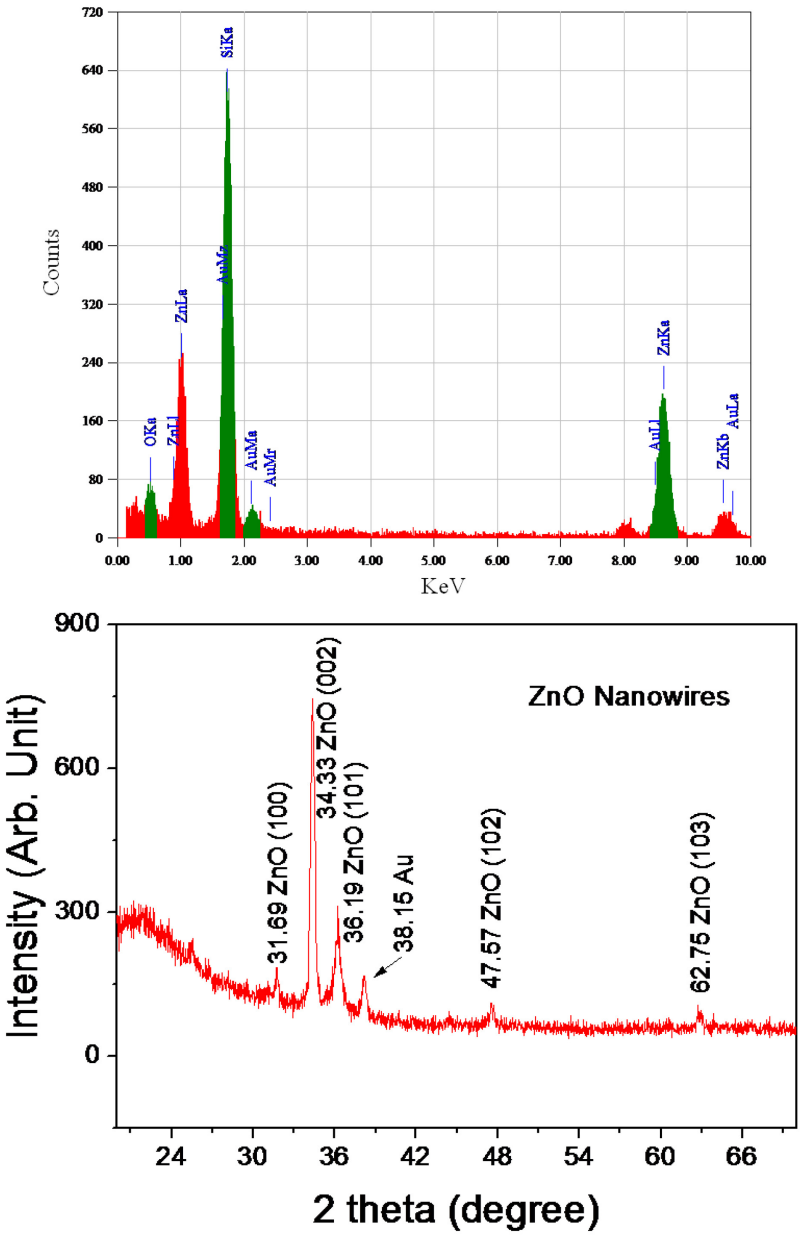

Figure 25. (a) EDX spectrum of zinc oxide nanowire recorded across Si substrate, nanowire and Au catalyst. Spectrum reveals that the nanowires are composed of Zn and O elements. (b) HRXRD shows that majority of nanowires were oriented into (002) direction.

5.2.2 Device characterization

Electrical characterization of the ZNW-FETs was done at room temperature and in dark environment using a four-probe station equipped with a semiconductor parameter analyzer (Agilent 4156 C). Figure 26a shows the four-probe chamber with device inside, to test the effect of various ambient conditions. Figure 26b shows Si/SiO_2 chip base for ZNW-FET device fabrication. Figure 26c shows SEM image of single ZNW-FET. ZNW devices were treated in various ambient conditions of vacuum (air pressure $\sim 4.0 \times 10^{-4}$ torr), elevated temperature (400 K), and ultraviolet (UV) irradiation at 340–390 nm wavelength range and 1.4 $mWcm^{-2}$ intensity.

Figure 27 shows the effect of various surface treatments like vacuum, annealing, and UV irradiation on the electrical characteristics of the nanowire. Earlier reports [113, 114] on UV irradiation effect on ZNW focused on photo induced current measurements, whereas in this work we investigate the effect of UV irradiation on adsorption and desorption of oxygen species on ZNW surface, and therefore, the electrical characterization of ZNW-FETs was done after some time of UV irradiation treatment. Device characteristics were measured at room temperature and dark environment after each surface treatment. As fabricated ZNW-FETs show a nonlinear I_{ds}–V_{ds} characteristic with a current range of 400–500 nA at zero gate voltage (V_{gs}) and bias voltage (V_{ds}) of 3 V. Current values at room temperature increase by factor of ~8 after devices were kept in high vacuum (air pressure $\sim 4.0 \times 10^{-4}$ torr) at an elevated temperature of 400 K for 1 h. After that, annealing under vacuum and UV irradiation further increases the current values by one order of magnitude which is $\sim 6\ \mu A$. Second (II) and third (III) parts of the figure demonstrate the decrease in current in two steps, after decreasing vacuum level

down to 760 torr by air. Just after breaking the vacuum, a sharp decrease in current from ~6 to ~2.5 μA is observed while further decreases in current down to ~700 nA takes several hours.

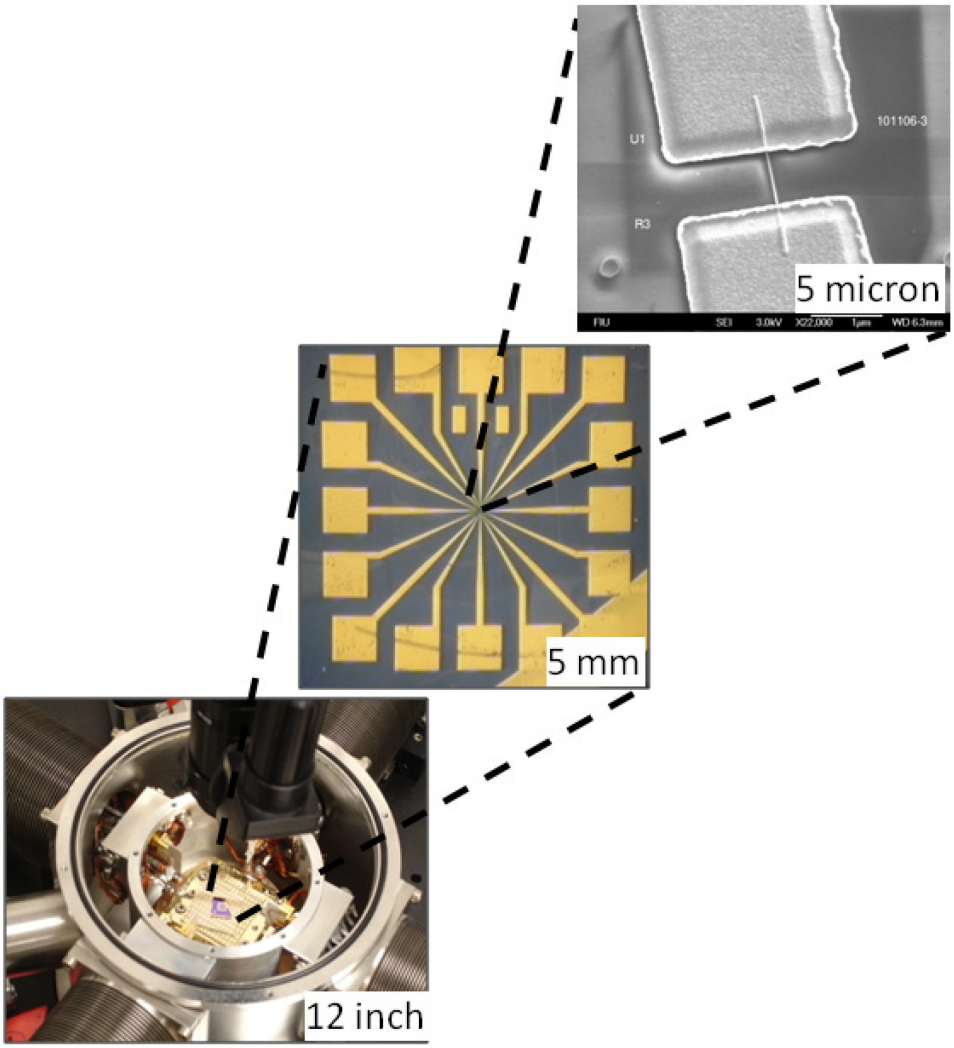

Figure 26. shows (a) Four-probe chamber with device inside, to test the effect of various ambient conditions. (b) Si chip base for ZNW-FET device fabrication. (c) SEM image of single ZNW-FET.

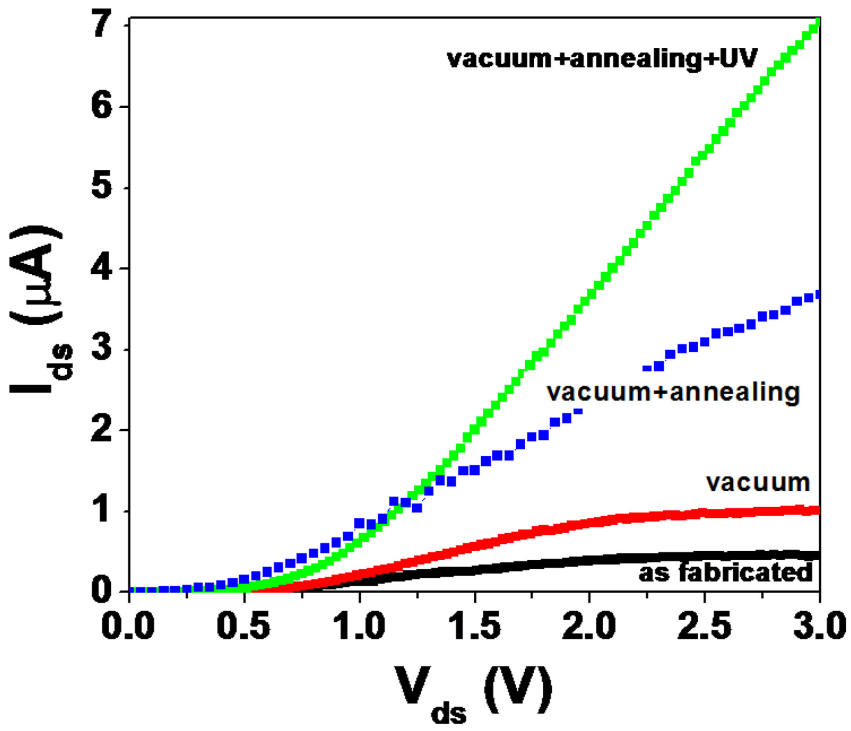

Figure 27. I_{ds} $-V_{ds}$ characteristics of ZNW-FET with various environmental conditions. Dark current at room temperature was measured after following treatments: In ambient, annealing at 400 K under vacuum (~4.0 × 10^{-4} torr), and UV irradiation at high temperature (400 K) and vacuum (~4.0 × 10^{-4} torr). Inset shows the AFM image of ZNW-FET; a nanowire is connected to Ti/Au electrodes at ends.

In general, ZNWs absorb oxygen molecules from atmosphere to form O^{-} and O^{-2} at high temperature (>450 K) and O^{2-} at room temperature by capturing electrons from the conduction band [94]. Due to the high surface-to-volume ratio, ZNWs contain large number of surface oxygen sites, of the order of 10^{20} surface oxygen sites per cubic centimeter of the material [115]. Absorption of these oxygen molecules on surface of

ZNW depletes the surface electron states, and consequently, reduces the channel conductivity [116]. High vacuum and temperature treatment can decrease the density of parasitic gaseous molecules, mainly oxygen species (O^{-}, O^{-2}, and O^{2-}) attached to the dangling bond on the zinc oxide surface that causes decrease in depletion layer thickness and increase in conductive channel diameter into the nanowire [117, 118].

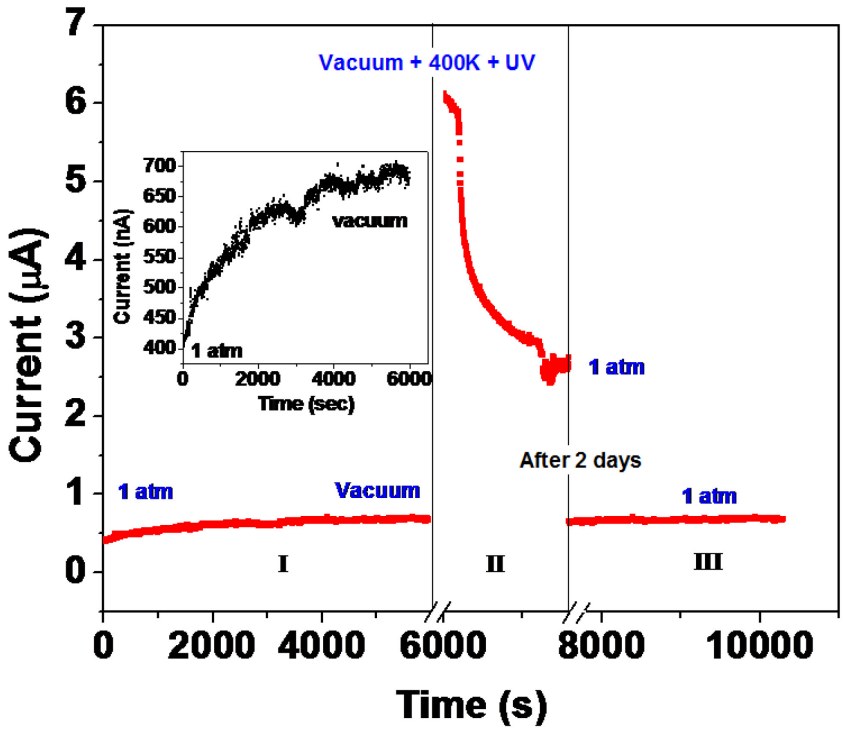

Figure 28. Effect of vacuum, annealing, and UV radiation on ZNW conductivity. Conductivity increases with increase in vacuum. Further vacuum, annealing, and UV radiation together increase the conductivity. The conductivity decreases drastically just after breaking the vacuum. Current values decrease more when the device is kept in air for long time.

Among the oxygen species attached to the surface, O^{-} and O^{-2} are weakly bonded with the zinc dangling bond and can be easily removed by annealing under high vacuum condition [119]. A significant increase in current by UV irradiation added with annealing and high vacuum treatment suggests that UV radiation helps in breaking the bonds of tightly bonded oxygen species to the ZNW surface. A high-energy UV irradiation (>3.2 eV) can easily break the oxygen bond to the surface as the heat of chemisorption of oxygen on the oxides is only of the order of magnitude of 1.0 eV [120]. Also, UV radiation is known to generate electron–hole pairs in semiconducting nanowires. These generated holes migrate toward the surface to react with negatively charged oxygen molecules and escape them from the nanowire surface while the extra electron generated helps in increasing the conductivity of the nanowire [121]. After detaching from the ZNW surface, these gaseous molecules escape from the chamber due to high vacuum and reduce the surface adsorption states and lower the surface band bending. Generally, adsorbed oxygen species on the zinc oxide surface can be categorized into two forms; first, is a rapid physisorbed oxygen species that can be easily desorbed by applying high temperature and vacuum and second is a slow chemisorbed oxygen species that can only be desorbed by added higher energy exposure of UV radiation. Therefore, the conductance enhancement in ZNW by UV irradiation at high temperature and vacuum can be attributed to the desorbing of chemisorbed oxygen species. An improved device characteristic and significant gate control can be achieved after UV irradiation at high vacuum and temperature (Figure 28).

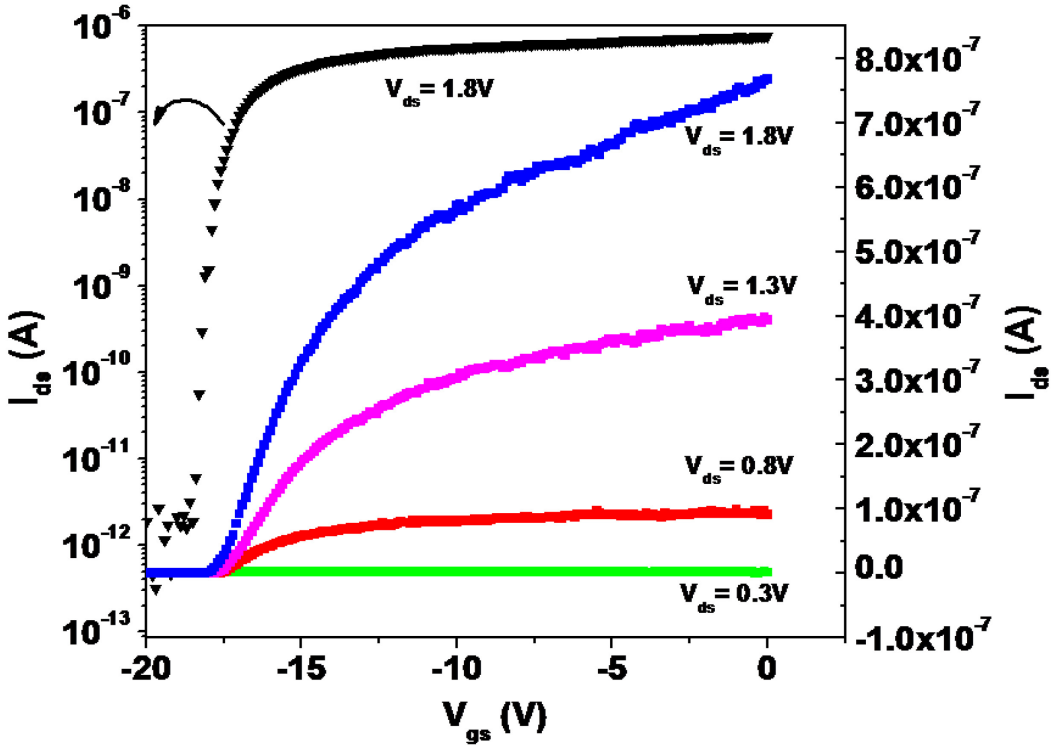

Figure 29. (a) Schematic of a single ZNW-FET. (b) An enhanced linear scale I_{ds} –V_{gs} characteristics of ZnO nanowire FET after UV-assisted surface cleaning. Another log scale plot (▼) of I_{ds} –V_{gs} (at V_{ds} = 1.8 V) shows a high I_{ON}/I_{OFF} ratio and threshold voltage of 10^6 and ∼ −17.5 V, respectively.

Figure 29 shows I_{ds}–V_{gs} characteristics of ZNW-FET. The I_{ds}–V_{gs} curve shows that the devices operate in an n-channel depletion mode of MOSFET. Transconductance $g_m = \frac{dI_{ds}}{dV_{gs}}$ in the linear region (−17 V to −15 V) of the I_{ds}–V_{gs} curve is about 0.16 μS. The measured I_{ON}/I_{OFF} ratio and threshold voltage of the device are around 10^6 and ∼ −17.5 V, respectively. We have selected a cylinder-onplate model [122] to calculate the coupling capacitance between the ZNW and the gate electrode that can be given by

$c_{OX} = \frac{2\pi\varepsilon_0\varepsilon L}{\cos^{-1}\frac{r+t_{OX}}{r}}$,where ε is the dielectric constant of the thermally grown SiO_2 (~3.9), L is the nanowire active channel length (~700 nm), r is the radius of the nanowire, and t_{OX} is the thickness of SiO_2 (~100 nm). The estimated capacitance C_{OX} in this case is ~0.11 fF (~0.15 fF per micrometer length of active channel length). The mobility was calculated with a MOSFET model [123], which can be given by $\mu = \frac{dI_{ds}}{dV_{gs}} \times \frac{L^2}{C_{OX}} \times \frac{1}{V_{ds}}$. Field effect mobility of the ZNW-FET, estimated by this method is ~28 $cm^2/V{\cdot}s$, which is comparable for zinc oxide thin film transistors [124, 125] and zinc oxide nanowire transistors with similar carrier concentration [126, 127].

5.3 Conclusion

In conclusion, an enhanced electrical characteristic of ZNWFETs was achieved by UV irradiation added with annealing and vacuum conditions. The conductance of ZNW increases ~17 times by using this non-destructive surface cleaning process. An improved representative FET device shows the highest mobility of ~28 $cm^2/V{\cdot}s$ and I_{ON}/I_{OFF} ratio of ~10^6. An increased conductance can be attributed to desorption of various oxygen species (O^- and O^{2-}) from the surface in addition to the photoelectron generation. Further optimization of surface passivation by local doping and surface modification can improve its electrical properties. The suggested nondestructive surface cleaning process for ZNW-FET makes it promising for further application in transparent nanoscale devices and high frequency integrated electronics.

CHAPTER 6

HYSTERESIS PHENOMENON IN ZINC OXIDE NANOWIRE FIELD EFFECT TRANSISTORS

6.1 Introduction

Semiconducting nanowires are promising building blocks for future nanoscale devices. Zinc oxide nanowires, having direct band gap ~3.4 eV and exciton binding energy ~ 60 meV are one of the most sought morphologies for future high temperature and radiation electronics, transparent electronics and laser devices [128, 129]. It is well known that ZnO contains a high density of surface defects and dangling bonds which act as absorption sites for gaseous molecules, mainly oxygen species present in the ambient [130, 131]. Due to high surface to volume ratio in nanoscale materials these surface defects dominate which affect its electron transport properties. In case of ZnO nanowire field effect transistors these surface defects defoliate the device performance by trapping and de-trapping the mobile charge carriers and surface adsorbents [132, 133]. Successful incorporation of ZnO nanowires in these devices need better understanding of charge transport properties and role of the surface states present on the nanowire.

From a real device application point of view hysteresis phenomenon in ZNW-FETs is not desirable and it should be controlled or removed completely. This report investigates on origin of hysteresis phenomenon and charge transport characteristics in bottom gated ZNW-FETs by studying the transfer characteristics of the devices. We have analyzed the detailed mechanism of hysteresis phenomenon by performing the systematic

measurement of transfer characteristics of the device in different ambient conditions. A simple method of surface cleaning of ZNW by annealing under vacuum and UV irradiation was adopted to reduce the hysteresis in FETs. Hysteresis effect due to absorbed gaseous and water molecules entrapped between the NW and gate insulator was discussed.

6.2 Results and discussion

6.2.1 Experiment

For studying the electrical hysteresis phenomenon in ZNW FETs device were fabricated on 100 nm Si/SiO_2 susbtrate as detailed in previous chapter. Electrical measurement of the ZNW-FETs for studying their gate sweep transfer characteristics was performed using a four-probe station equipped with semiconductor parameter analyzer (Agilent 4156C). To understand the effect of various ambient on hysteresis properties, devices were treated in various ambient conditions of vacuum (air pressure ~ 4.0×10^{-4} Torr), elevated temperature (400 K) and ultraviolet irradiation of 340-390 nm wavelength range and 1.4 $mWcm^{-2}$ intensity.

6.2.2 Electrical hysteresis phenomenon in ZNW FET

Figure 30 shows the AFM image of a ZNW-FET, where a ZnO nanowire of ~60 nm diameter and ~2 μm length is contacted at the ends with Ti/Au electrodes. Figure 31 shows the double sweep transfer characteristics of as fabricated FETs at different V_{DS}. For all V_{DS} values, as fabricated device shows clear hysteresis phenomenon in their transfer characteristics. A quantitative measure of hysteresis effect can be estimated by

magnitude of difference between threshold voltage of forward and reverse sweep ($\Delta V_{HY}=|V_{TH,F}- V_{TH,R}|$) [134]. In case of as fabricated device the ΔV_{HY} is ~ 8.0V for all V_{DS} values. This indicates that hysteresis phenomenon is independent of V_{DS} values or amount of current across the nanowire.

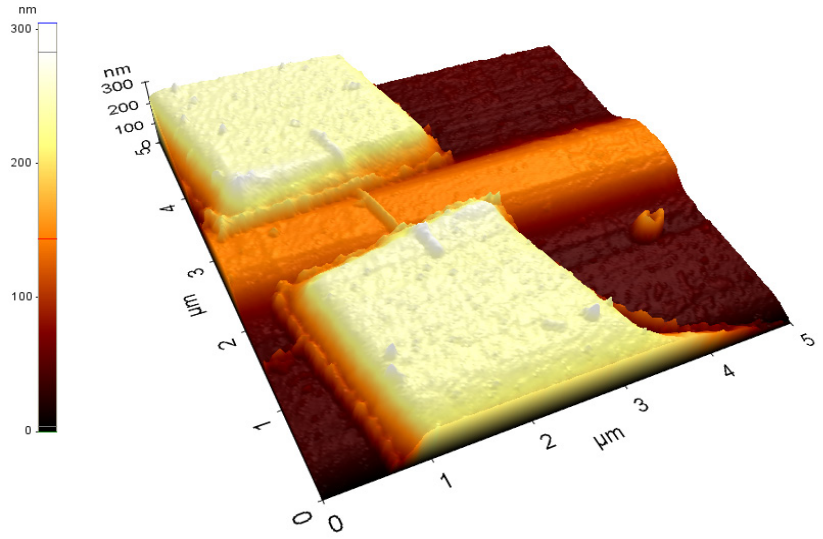

Figure 30. AFM image of single ZNW FET device showing single zinc oxide nanowire trapped at ends by Ti/Au metal electrodes.

This hysteresis phenomenon can be attributed to charging and discharging of states generated by SiO_2/ZNW interface defects and absorbed chemical species on the nanowires. A large number of trap sites are expected to be present at SiO_2/Si interface as we place the nanowire physically on the SiO_2 gate insulator and therefore there is almost no lattice matching is present between the active layer and gate oxide. But the role of these trap sites are limited due to very low contact area between nanowire and SiO_2 gate

insulator due to their different geometry (nanowire is cylinder and gate oxide is a plate) at the interface [135]. With this cylinder-on-plate model [122] the calculated coupling capacitance between ZNW and gate electrode can be given by $C_{OX} = [(2\pi\varepsilon_0\varepsilon L)/\cosh^{-1}((r+t_{OX})/r)]$, where ε is dielectric constant of the thermally grown SiO_2 (~3.9), L is nanowire active channel length (~700 nm), r is radius of nanowire and t_{OX} is thickness of SiO_2 (~100 nm). The calculated capacitance C_{OX} (assuming no Schottky barrier between ZNW and Ti/Au electrodes) in this case is ~0.11 fF (~0.15 fF per micron length of active channel length), while the measured minimum capacitance in a C-V_{gs} sweep was ~ 1 nF. This can be justified by adding the other capacitance due to interface traps and absorbed chemical species between ZNW and SiO_2 gate insulator.

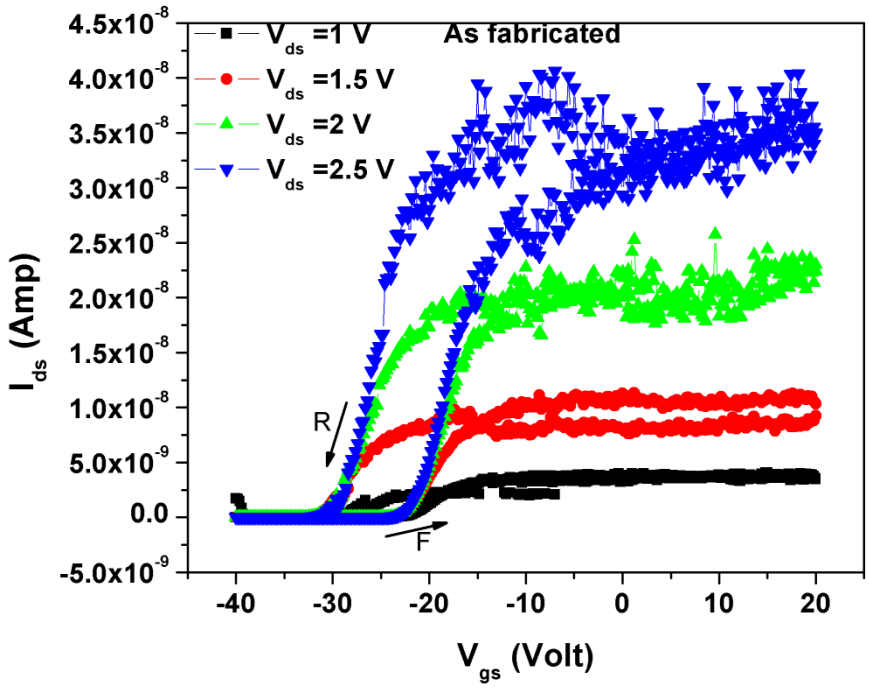

Figure 31. Double sweep Ids-Vgs curves for as fabricated zinc oxide nanowire FET at different Vds.

Figure 32 represents a simple model of cross section of FET and absorbed chemical species on the ZNW and between the ZNW/ SiO_2 interface. In general, ZNWs absorb oxygen molecules from atmosphere to form O^- and O_2^- at high temperature (>450 K) and O^{2-} at room temperature by capturing electrons from the conduction band [94]. Due to high surface-to-volume ratio, ZNWs contain large number of surface oxygen sites, on the order of 10^{20} surface oxygen sites per cm^3 of the material [115]. Absorption of these oxygen molecules on surface of ZNW depletes the surface electron states forming trap sites for charge carriers [31, 136]. Also absorption of water molecules (from humidity and our wet processing of device fabrication) on SiO_2 forms a silanol group (≡SiOH) which may influence the magnitude of the hysteresis in nanotube FETs [137].

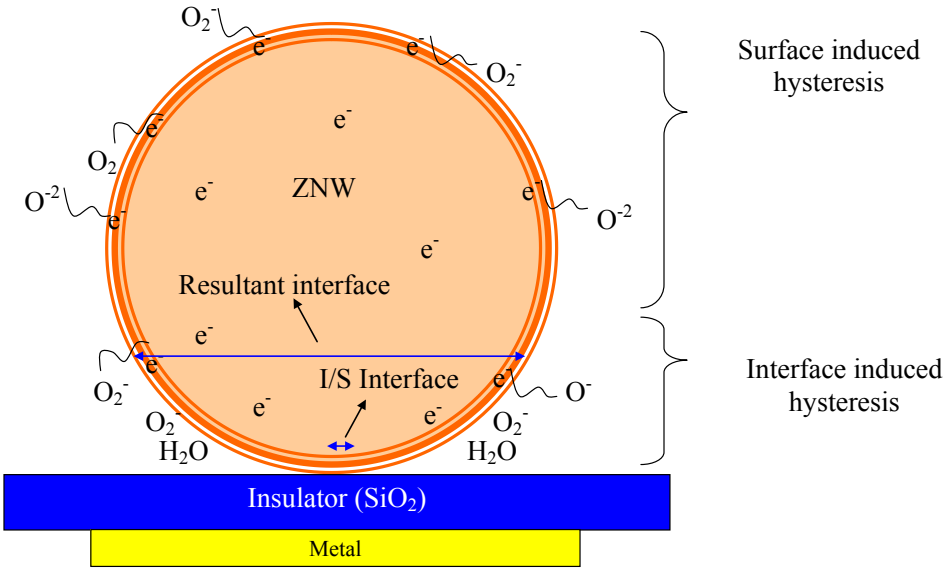

Figure 32. A schematic of cross section of ZNW-FET and hysteresis model represented by adsorbed chemical species on the surface of nanowire and gate oxide.

The transfer characteristics of FETs were also investigated under vacuum after annealing and UV irradiation to understand the effect of absorbed chemical species on the hysteresis phenomenon (Figure 33). As-fabricated devices show a large hysteresis of voltage ~5.6 V. The magnitude of hysteresis decreased to ~2.0 V when the devices were placed and measured in a vacuum of ~4.0 × 10^{-4} Torr. An interesting phenomenon of change in cycle direction in hysteresis loop was observed before and under the vacuum condition. A further decrease in hysteresis (~1.6 V) was achieved by annealing the devices at 400 K under the vacuum. The lowest hysteresis (~1 V) was achieved after irradiating the devices by UV light of 1.4 mW cm^{-2} at 400 K and ~4.0 × 10^{-4} Torr pressure for 30 min.

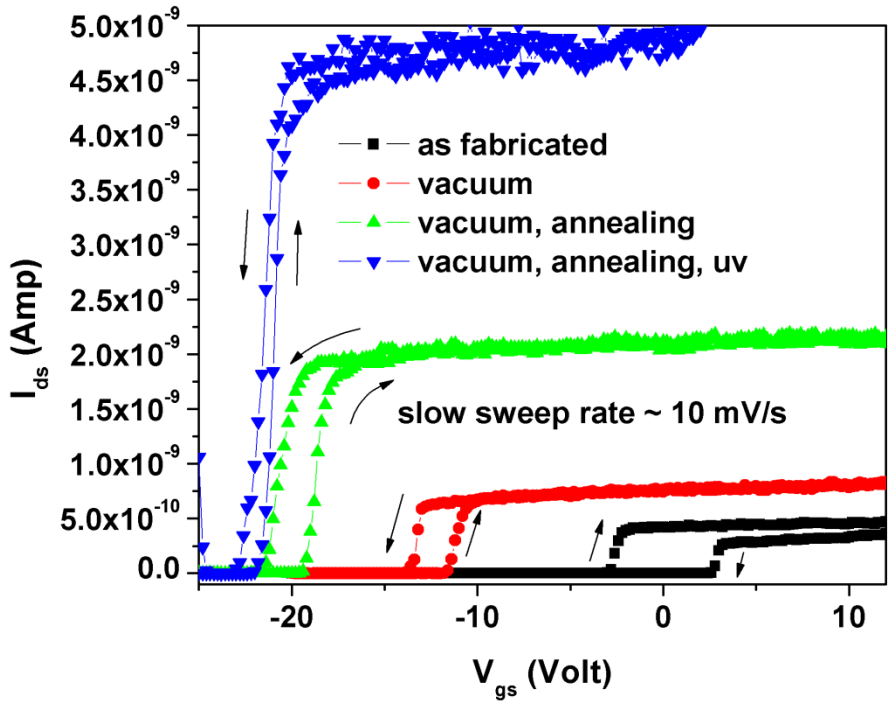

Figure 33. Double sweep I_{ds}-V_{gs} curves for zinc oxide nanowire FET after different surface treatments.

It has to be noted that all the measurements were performed at room temperature and dark environment after each surface treatments stated above. This practice was adopted to avoid the effect of any thermally generated or photo-generated charge carriers in the measurements. A large hysteresis in as-fabricated devices can be attributed to combined effect of absorbed oxygen species (O^-, O_2^- and O^{-2}), interface defects between the nanowire and gate oxide and silanol group (≡ SiOH) attached to the SiO_2 [138]. These unwanted chemical molecules form a complex and unstable interface between the nanowire and gate insulator resulting a hysteresis in double gate sweep transfer characteristics of ZNW-FETs. With successive surface treatments the threshold voltages (in forward and reverse bias) in transfer characteristics shifted towards more negative bias. As fabricated device shows $V_{TH,F}$ and $V_{TH,R}$ of 2 V and 3V. The threshold voltages shifted to -2 V and -3 V after treating the devices in vacuum. A further decrease in threshold voltage was observed when the devices were annealed at 400 K in vacuum conditions. In as-fabricated devices during initial up-sweep mode drove the electrons to the ZNW/SiO_2 interface. A large number of electrons available at this interface facilitate the bonding between gaseous molecules and zinc oxide surface. During down gate sweep these immobile charges carriers result in low current compared to current value at same gate voltage during up-gate sweep. Removal of physiosorbed gaseous molecules by keeping the device in vacuum chamber makes the surface-depletion layer thinner in ZNW and causes hysteresis to decrease. A high temperature treatment under vacuum condition helps to remove adsorbed gaseous species from the ZNW surface as well as water molecules from SiO_2 gate oxide. UV irradiation at high temperature and under vacuum condition can easily break the bond between chemisorbed oxygen species and zinc oxide

surface. These gaseous molecules escape from the vacuum chamber which helps in decreasing the magnitude of hysteresis significantly in ZNW-FET.

6.3 Conclusion

In summary, ZNW-FETs were fabricated on Si/SiO_2 substrate in bottom gated geometry. Effect of surface treatment on the hysteresis phenomenon and intrinsic charge transport mechanism in the nanowire and in the ZNW-FETs were investigated. Hysteresis in ZNW-FETs can be attributed to absorbed gaseous molecules on the zinc oxide surface and water molecules at the SiO_2 substrate. Treating the devices under vacuum, high temperature and UV radiation reduces the hysteresis behavior in ZNW-FETs. The nature of opposite hysteresis cycle direction before and after vacuum treatment and effect of passivation layer on NW to discourage any chemical reaction on the surface are all questions that require further study.

CHAPTER 7

NITRIC OXIDE GAS SENSING AT ROOM TEMPERATURE BY FUNCTIONALIZED SINGLE ZINC OXIDE NANOWIRE

7.1 Introduction

Detection of NO gas at low concentration is of paramount importance for real time monitoring of environment and lower airways inflammatory diseases [139, 140]. NO is an atmospheric pollutant, which plays an important role in formation of smog [141]. Also, detection of NO concentration in exhaled gases has become standard medical practice for monitoring chronic obstructive pulmonary disease (COPD) [142]. The most common techniques available for monitoring exhaled NO are based on chemi-luminescence and photochemical methods which involve huge system and expertise [143, 144]. Though one portable NO analyzer, based on electrochemical technique has already been developed by Hemmingsson et. al. [145], the demand for a very inexpensive and hand held analyzer is still to be realized.

Zinc oxide nanowire is one of the most promising materials systems for semiconducting gas sensors, owing their easy functionality and specific combination of physico-chemical properties [146]. Large surface to volume ratio and quasi-one dimensional functionality of ZNW make their conductivity highly sensitive towards surface chemical reactions [147]. Moreover, relatively large surface defects and favorable gas adsorption/desorption parameters [148, 149], give ZNW edge over other nanowires and nanotubes for NO gas detection. There have been many reports on ZNW based gas sensors for the detection of ethanol, CO, NH_3, H_2, O_2, NO, H_2S and NO_2 [24, 31, 35, 147,

150-152]. However, these sensors need to be operated at high temperature to achieve improved gas-semiconductor surface reaction and high signal to noise ratio [147, 150]. In their study, Fan *et. al.* [153] have demonstrated a strategy for NO_2 gas sensing at room temperature by gate refreshable ZNW field effect transistors. Kaur *et. al.* [154] and Ramgir *et. al.* [155] have detected nitric oxide gas (concentration >40 ppm) at room temperature by bare zinc oxide nanostructures and Ru doped ZNW, respectively. Despite multiple reports on gas sensing by ZNW, detection of low concentration level of NO gas at room temperature remains a challenge.

Metal particles are well-known as effective catalysts, due to their ability to control the redox reactions of the gas molecule at the sensor surface [156]. At nanoscale, metal particles show superior catalytic properties due to their high surface to volume ratio and chemical potential [157]. Functionalization by catalyst nanoparticles is one of the most important strategies for enhancing sensitivity and selectivity of metal oxide gas sensors. However very few literatures are available which explore sensing application of catalyst supported single metal oxide nanowire sensor [33].

Direct detection of NO gas at low-ppm level using metal nanoparticles decorated single ZNW sensor, which can operate at room temperature and low power is discussed in this chapter. Compared to bare ZNW, a Cr functionalized ZNW can detect lower concentration NO gas at room temperature. More importantly, combination of ZNW and the catalytic property of metal nanoparticles can exhibit selectivity at room temperature for low concentrations of gases. This ZNW sensor with unique functionality can provide efficient detection and real time monitoring of exhaled NO gases. Further-more, this single ZNW based sensor can provide clear understanding of surface chemistry occurring

at nanoscale devices which is almost averaged and unclear when using large number of nanowires in single sensor device.

7.2 Results and discussions

7.2.1 Experimental details

For fabricating chemiresitive gas sensor ZNWs were synthesized via chemical vapor deposition method [95] as described in chapter 3. Single ZNW sensor devices were fabricated on Si/SiO_2 (500nm) substrate using standard photolithography, electron beam lithography process, metal deposition and lift-off process. Once again electron beam lithography process was use to open a window over ZNW for catalyst deposition. Cr nanoparticles (2-5 nm) were deposited on ZNW by a 4 sec of metal deposition by RF sputtering system, operating at 75 Watt power and 5 mTorr of Ar gas pressure. Characterization of Cr nanoparticles on ZNW was done by high resolution transmission electron microscopy (Hitachi H9000NAR) and atomic force microscopy (Vecco; Nanoscope IIIa ADC 5). AFM was operated in non-contact mode with super sharp antimony doped silicon tip (Vecco; TESP-SS) having cantilever constant K = 20-80 N/m. ZNW devices were mounted on a multi-pin metal sensor head and connected to two pins of the sensor head by wire bonding (Figure 34 inset). An ultraviolet (UV) light source of 2 mW power and of 375 nm wavelength was installed over the sensor device.

Figure 34 shows gas sensing measurement set up developed in our lab. Sensor device was loaded inside a small custom-built gas flow chamber with low dead volume. Flow of gases into the chamber was controlled by gas mixing system (Environics 4000), connected to NO (10 ppm), N_2 (100%), CO (500 ppm) and CO_2 (50%) gas cylinders.

Electrical measurement was performed using semiconductor parameter analyzer (Agilent 4156C). During each test sensor was flushed with nitrogen gas for one hour before injecting series of interest gases and UV irradiation. Current response of NW at constant bias voltage (2 V) was measured for 200 sccm of different gas pulses. A 20 sec of UV irradiation was applied between gas pulses to remove adsorbed gas molecules from the ZNW surface.

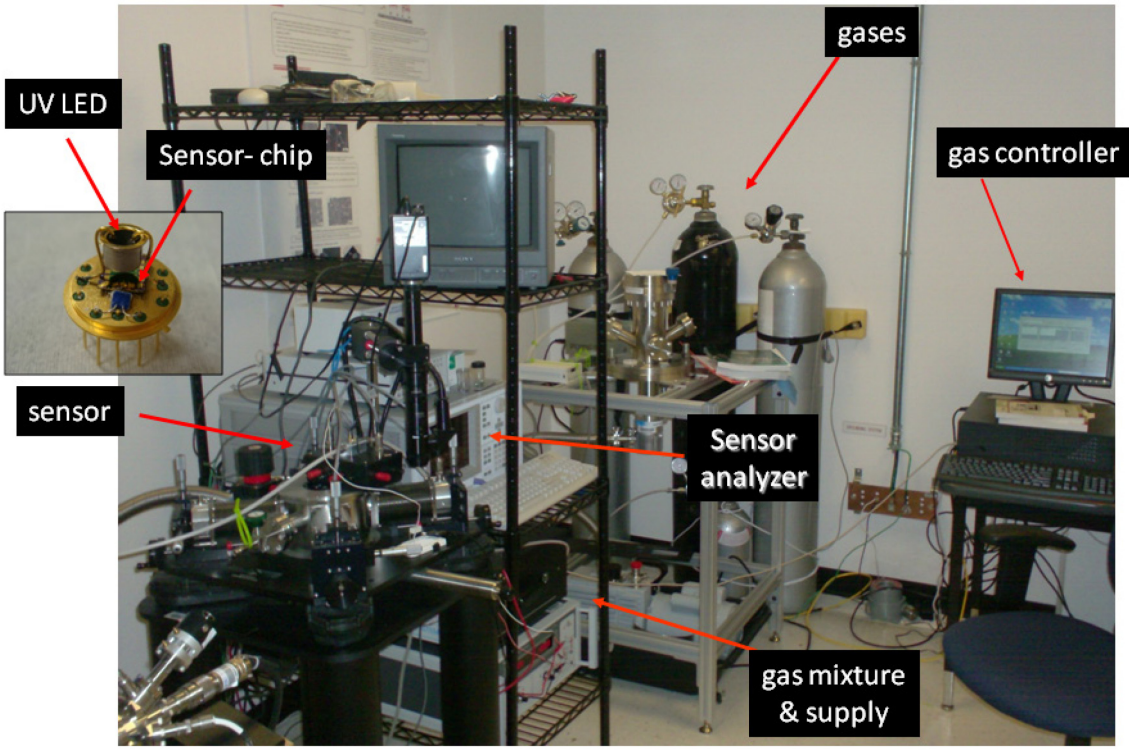

Figure 34. Gas sensor set-up developed in our lab. Inset shows the ZNW sensor device with UV LED mounted on transistor head.

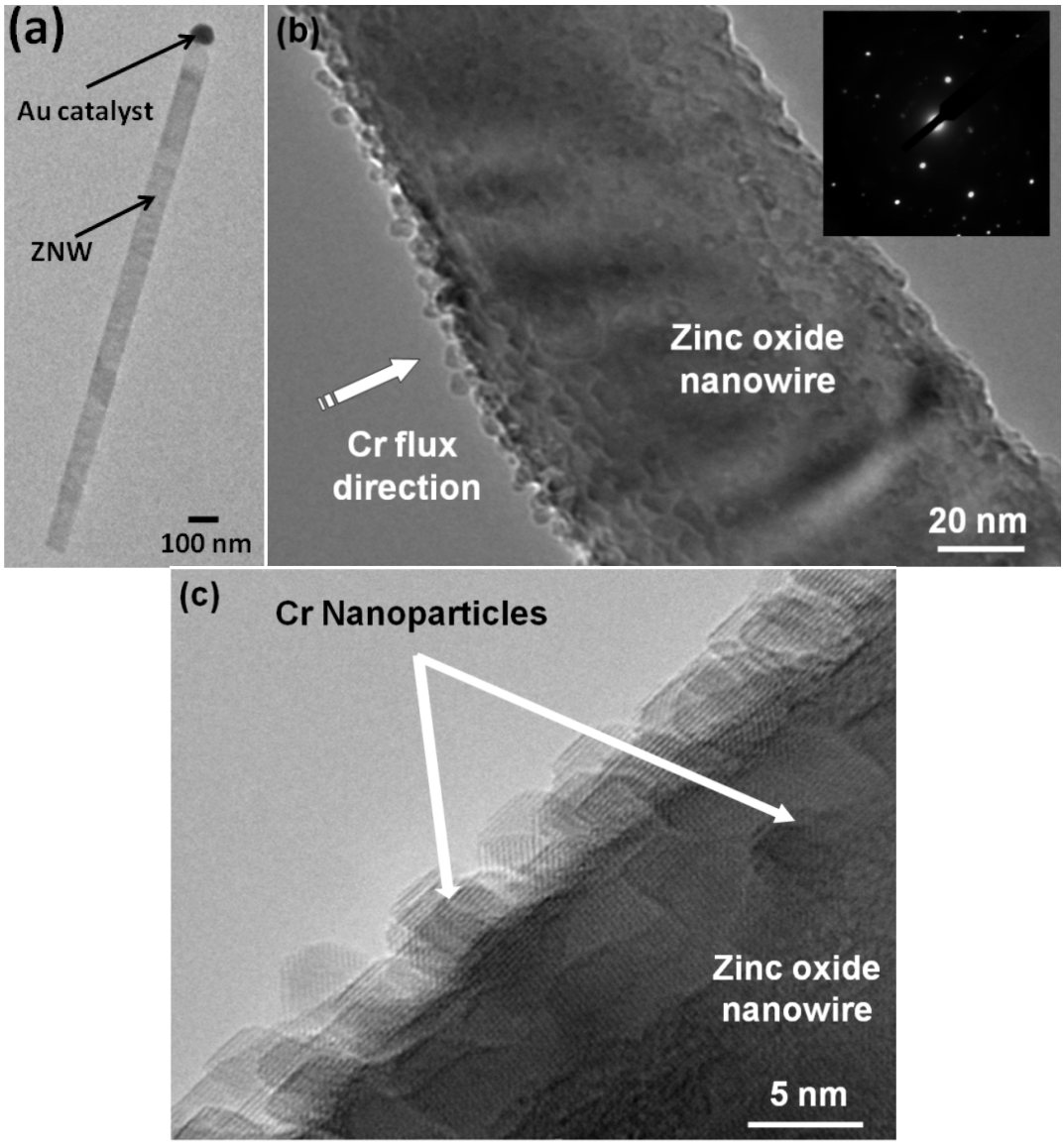

Figure 35. TEM image of Cr nanoparticle decorated ZNWs. (a) Low magnification single ZNW with Au catalyst at the tip. (b) Dense Cr nanoparticles were deposited on the side of nanowire. Inset shows a SAD pattern of Cr-ZNW hybrid structure. (c) Lattice resolved image shows that average size of catalyst nanoparticles is around 5 nm.

7.2.2 ZNW gas sensor device and operation

Morphology of Cr nanoparticles decorated zinc oxide nanowire was investigated by HRTEM operating at 300 kV under bright field condition (Figure 35). Figure 35a shows a tip grown single ZNW decorated with Cr nanoparticles at the surface. A dense structure of nanoparticles was observed at the surface of nanowire, facing the metal flux during sputtering (Figure 35b). Inset shows corresponding selected area diffraction pattern of Cr-ZNW hybrid structure. Particle structure of Cr metal on ZNW, during 4 sec of metal deposition by RF-magnetron sputtering, was generated following the Volmer-Weber growth mode [158]. Figure 35c shows the lattice resolved images of nanoparticles, with some of them in faceted shape, on the ZNW. Figure 36a shows the FE-SEM image of single ZNW sensor device fabricated on Si/SiO_2 substrate. A NW of length ~7.5 μm and diameter ~150 nm was connected by Ti (150 nm)/Au (300 nm) electrodes at both the ends by e-beam lithography and metal deposition, as explained in the experimental process. Figure 36b shows AFM image of Cr nanoparticles decorated on ZNW and Si/SiO_2 substrate. Particle size measurement (inset of Figure 36b) shows that Cr nanoparticles had an average size of ~5 nm.

Figure 37 shows a comparative sensing behavior between bare ZNW and Cr functionalized ZNW, towards NO gas. It is clearly shown that, decoration Cr catalyst nanoparticles over ZNW enhanced its sensitivity for NO gas. Since under dark condition NO gas gets permanently absorbed at ZNW surface (Figure 38a), whereas under continuous UV illumination condition it does not show any interaction with nanowire (Figure 37b), we have used an UV pulse technique [159] for surface cleaning and NO gas sensing by ZNW device. In this sensing technique, before introduction of N_2 gas, a UV

radiation pulse for 20s was applied for regenerating the sensor by desorption of oxygen species and NO_2 gas molecules from the ZNW surface. Figure 39a shows the repeatable sensing performance of a functionalized ZNW at room temperature towards the successive pulses of pure nitrogen gas and 10 ppm of nitric oxide gas. At normal conditions under exposure to air, these surface defects are passivated by various oxygen species (O^-, O^{2-}, O_2^-) formed by dissociation of oxygen molecules over the surface defects [94]. Due to high surface-to-volume ratio, ZNWs contain large number of surface oxygen sites, on the order of 10^{20} sites per cm^3 of the material [115]. The surface cleaning by UV radiation maximizes reaction area between interest gas and active sites present at NW surface. A high current peak is observed during UV irradiation. UV irradiation has dual effects; first, it decreases the depletion layer by removing parasitic gaseous molecules and secondly, it generates electron hole pairs in the NW. A high energy UV radiation (>3.2 eV) can easily break the O_2 and NO_2 bonds on the ZNW surface as the dissociation of physisorbed O_2 is barrier-less and chemisorbed NO_2 over the ZnO surface has very low activation barrier of 0.49 eV [160]. Just after the UV irradiation, a 5 min of N_2 flow was maintained over the sensor. During this 5 min of N_2 flow, electrons and holes which were photo- generated by UV radiation get recombined [114, 161]. Five minutes of N_2 flow time was carefully optimized as longer time of N_2 flow only leads to saturation of current.

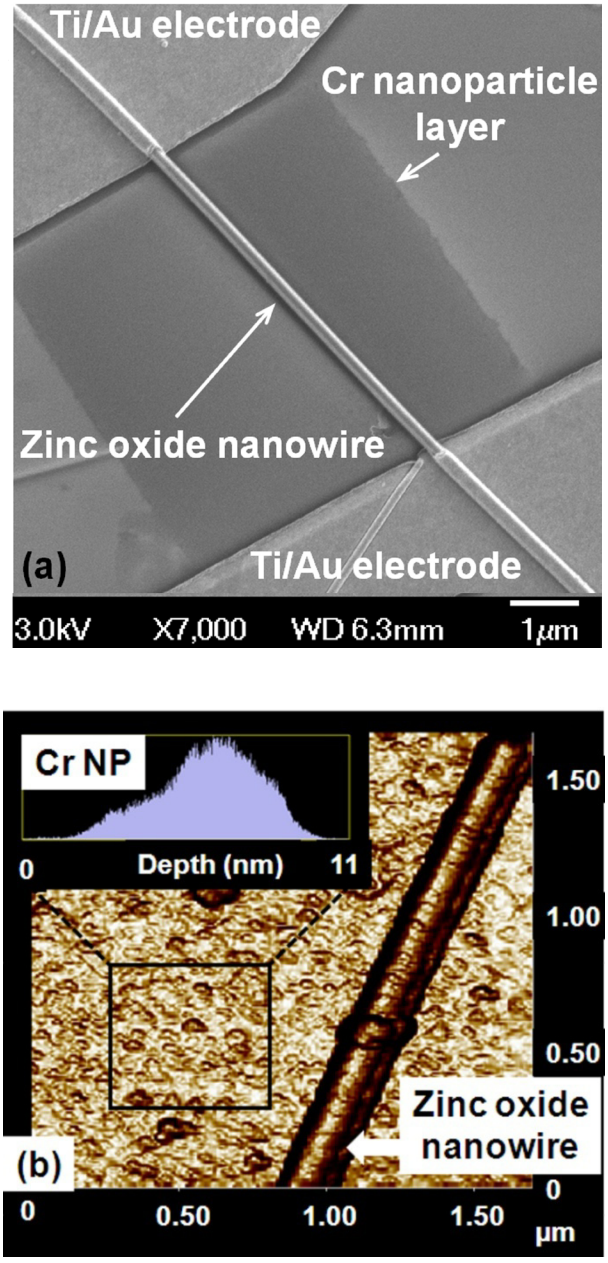

Figure 36. (a). SEM micrograph of a zinc oxide nanowire sensor device fabricated on Si/SiO_2 substrate. A Cr nanoparticle thin film was deposited over ZNW. (b) AFM image of Cr nanoparticles deposited on single zinc oxide nanowire. Inset shows that the average size of Cr nanoparticles was ~5 nm.

After N_2 flow, at base point a 5 min pulse of 200 sccm of NO gas was introduced over the clean NW surface. We believe that this NO gas was oxidized to NO_2 gas in presence of Cr catalyst nanoparticles decorated at NW surface. A similar mechanism for catalytic oxidation of NO to NO_2 over Cr/TiO_2 particle has been demonstrated by Shiba *et. al.* [162]. The results from their study indicate that Cr component in Cr/TiO_2 particle act as active site for the oxidation of NO. In our case, conversion of NO into NO_2 at room temperature can be attributed to lowering of activation energy and improved dynamics by nanoscale catalyst [163]. Also, we suspect that presence of very small of O_2 in diluting gas (N_2) and leaked-air into the test chamber can generate a favorable oxidative atmosphere over the NW. Catalyst nanoparticles deposited over large surface area of SiO_2 substrate along with nanowire may help an efficient conversion of NO into NO_2 over the ZNW surface. NO_2 molecules, possessing strong electron withdrawal nature, easily react with active sites present on the ZNW surface and form depletion layer. This results in decrease in current through NW at a constant bias voltage of 2V. After NO gas exposure, a 20 sec of UV irradiation was applied to refresh the NW for next gas pulse detection. Average percentage sensitivity was calculated from equation $S=100\times[|I_N-I_{NO}|/I_N]$, where I_N and I_{NO} is current values before and after NO gas pulse and was found to be ~46 % for 10 ppm of NO gas.

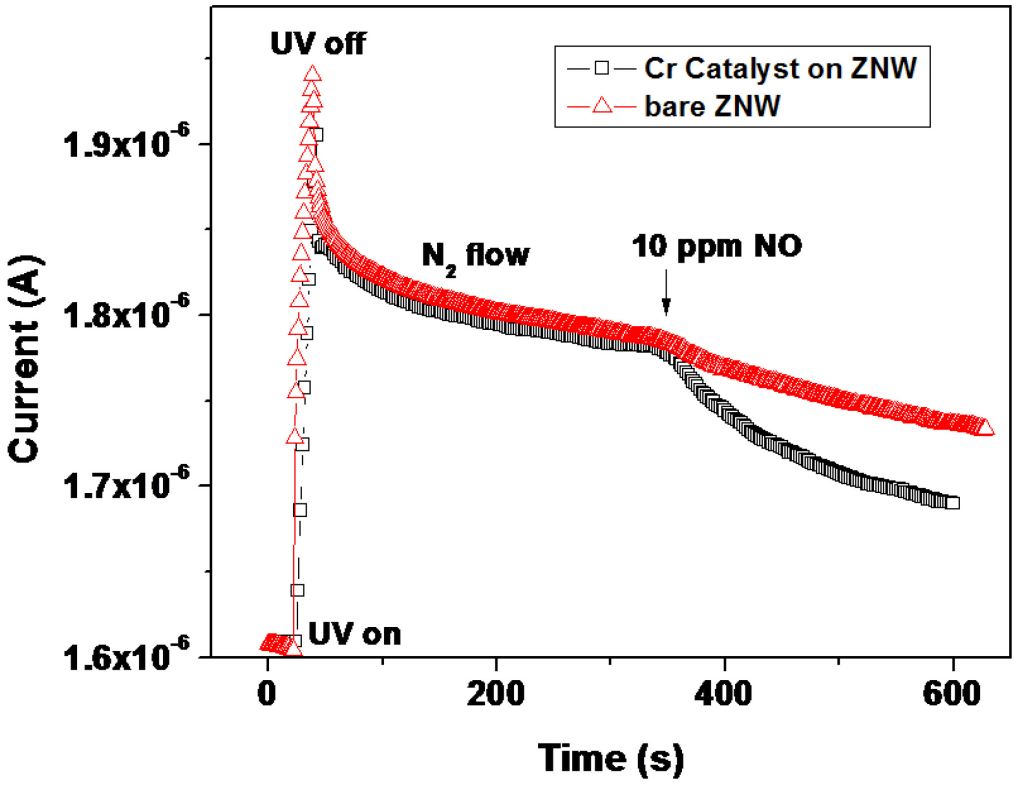

Figure 37. Sensing behavior of zinc oxide nanowire devices with Cr (-□-) and without Cr (-Δ-) nanoparticles decorated on it.

Figure 39b shows the ZNW sensor response for NO gas ranging concentration from 10 ppm to 1.5 ppm in N_2 environment. Inconsistence current values in consecutive cycles of sensing can be related to sensor drift which is the major unsolved problem of the metal oxide chemical sensors [164]. Both reversible and irreversible processes occurring at the metal oxide surface can cause the sensor drift. One of the examples is change in stoichiometry of surface by oxidation-reduction [165]. Also a vigorous dynamic condition of absorption and desorption of NO on ZNW surface and

recombination of electron-hole pairs in zinc oxide during recovery can cause difference in signals [166, 167]. A calibration curve with error bars in Figure 39b shows that the current drop during NO flow decreases with decrease in concentration of the gas. A lowest detection limit of sensor was ~1.5 ppm for NO gas which is lowest in value compared to other reported metal oxide chemi-resistive NO sensors [168, 169].

Figure 40a shows the response of ZNW sensor in 10 ppm of NO and other common interfering gases (N_2, CO and CO_2). It may be pointed that even when the interest gases were passed over the sensor after 20 sec of UV irradiation and 5 min of N_2 flow, noticeable change in current was obtained only during NO gas flow. This demonstrates that Cr nanoparticle decorated ZNW sensor had distinct selectivity towards NO gas. The selectivity of sensor towards NO gas can be attributed to selective oxidation of NO by Cr nanoparticles, and strong interaction between ZnO surface and NO_2 compared to other gases used in this experiment. Figure 40b shows the suggestive schematic of single ZNW sensor device and NO gas sensing mechanism. A single ZNW decorated with Cr nanoparticles was used as semiconducting resistor for gas sensing. The first step for the sensing is the successful conversion of NO into NO_2 in presence of Cr catalyst nanoparticles acting as converter [162]. Detection of NO_2 over NO was selected due to strong withdrawing capability of NO_2 compared to weak electron donating nature of NO [170].

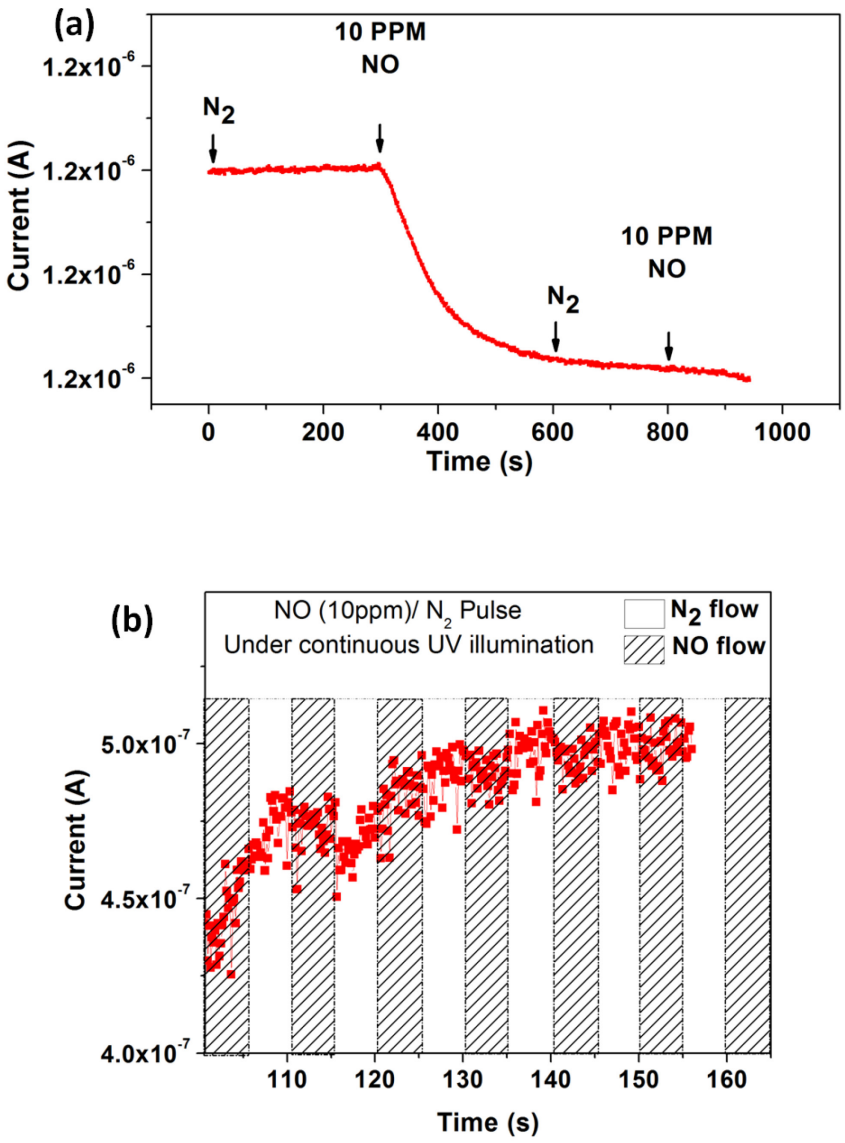

Figure 38. (a) Sensing behavior of ZNW sensor devices for NO and N_2 gas flow, under dark environment. (b) Sensing behavior of devices under continuous UV illumination of 2mW power and 375 nm wavelength.

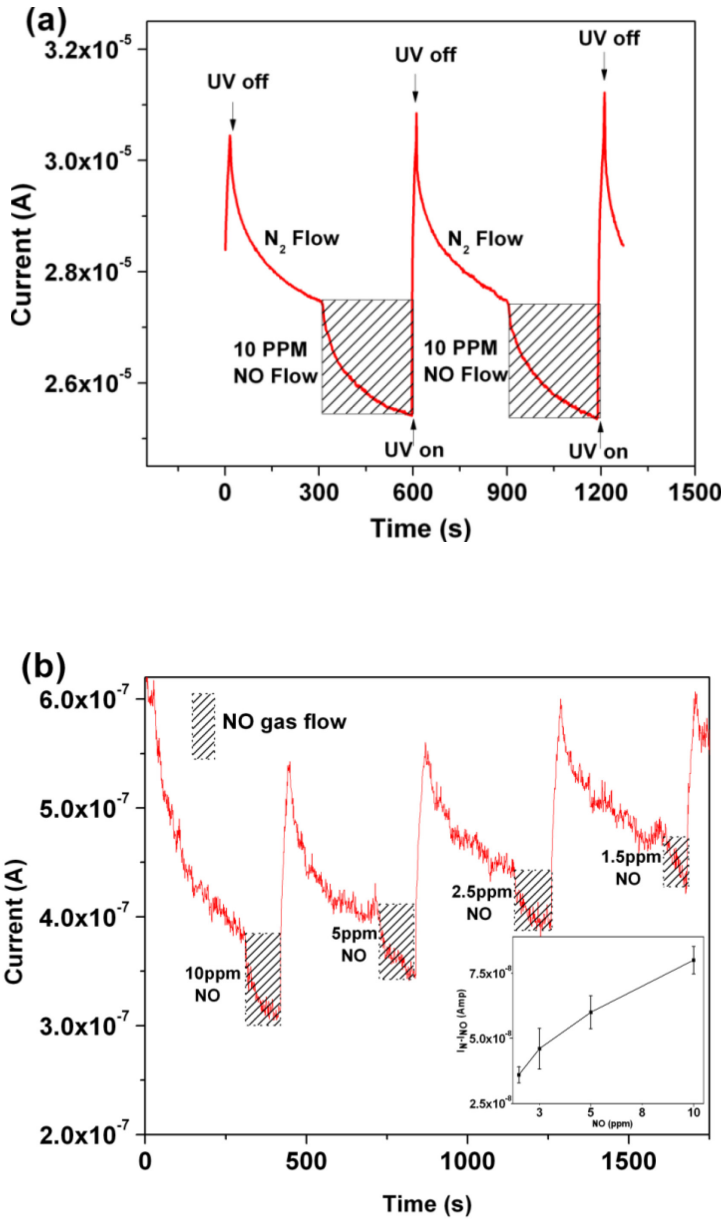

Figure 39. (a). Current versus time dependence of ZNW sensor exposed to two pulses of 10 ppm of NO gas. The base point shows the time at which NO gas was introduce into the chamber. (b) Current versus time dependence of ZNW sensor exposed to NO gas with concentration range of 10 ppm to 1.5 ppm. Inset shows calibration curve for ZNW sensor with error bars.

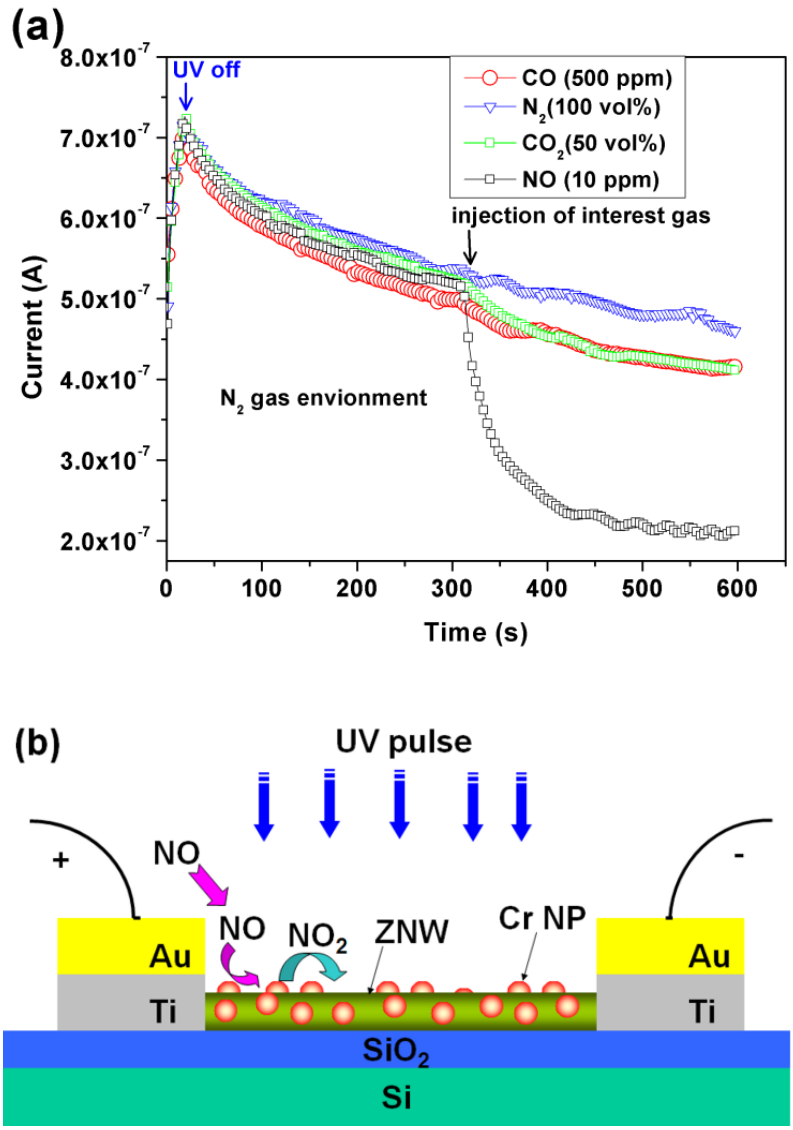

Figure 40. (a) Current versus time response of ZNW sensor for NO, CO, CO_2 and N_2 gases. A sharp decrease in current during NO gas flow shows selectivity of sensor device. (b) Schematic of ZNW FET sensor device. A single ZNW was decorated with Cr nanoparticles which help in formation of NO_2 gas from NO gas over the NW surface.

NO_2 molecules shows a high partial charge transfer of -0.28e when molecularly absorbed on zinc oxide surface [171]. Interaction of NO_2 with zinc oxide surface follow the Fermi energy control mechanism in which electron transfer takes place from a higher chemical potential of ZNW to a lower chemical potential of NO_2, until the Fermi level equilibrium is reached. This phenomenon causes formation of depletion region and decrease in conductivity of ZNW. We have built and tested eight sensor devices. Percent sensitivity of these eight ZNW sensor devices for 10 ppm of NO gas varies from ~11% to 62% which is acceptable for their successful technological applications. Difference in the sensitivity of the eight devices can be attributed to different physical size of nanowires as reported by Fan et. al. [147]. When stored for long time the current value through ZNW at constant voltage decreases significantly because of adsorption of oxygen species and humidity at the surface [136]. In this study the surface refreshing strategy by UV irradiation works well, and was able to restore electronic and sensing properties of devices even after 10 days.

7.3 Conclusions

In summary, Cr nanoparticle deposited ZNW is demonstrated as an efficient material for detecting low-ppm level NO gas at room temperature. The sensor showed a selective behavior towards NO gas, in presence of other common interfering gases, with average sensitivity of ~46% towards 10 ppm NO mixed with N_2. The lowest detection limit of sensor is ~1.5 ppm for NO gas. Desorption of NO_2 gas molecule from the ZNW surface was achieved by UV irradiation. This study opens a starting point for the

application of single nanostructure devices for detection of chemical species at low concentration level. Furthermore, the development of single ZNW sensor is an economical solution for portable or energy efficient high sensitive NO detection.

CHAPTER 8

LARGE-AREA GRAPHENE ON POLYMER FILM FOR FLEXIBLE AND TRANSPARENT ANODE IN FIELD EMISSION DEVICE

8.1 Introduction

Graphene is a two-dimensional carbon material having unique band structure and outstanding thermal, mechanical and electrical properties [172-174]. Some of the potential applications of graphene are for sensors, transistors, super-capacitors, solar cells and flexible displays [175-179]. It is well known that graphene has high mechanical strength with flexibility, high transmittance and high electron mobility [179, 180]. These properties make graphene an emerging alternate for transparent conductive metal oxides electrodes, in particular indium tin oxide which contains indium as a costly and scarce element.

In order to make a transparent conductive graphene film, most of the researchers have used liquid solution of graphene flakes (obtained by reducing graphene oxide flakes) for deposition of transparent conductive film [181, 182]. Recently, Yamaguchi *et. al.* [183] has deposited chemically derived graphene solution on flexible substrate for large area transparent flexible electrode which contains 2 to 30 layers of graphene. Successful incorporation of graphene in flexible electronics will need synthesis of continuous graphene film on substrates and transfer it to polymeric substrate in large scale. Li *et. al.* [184] has first demonstrated high quality, predominately monolayer graphene films grown on copper foils by CVD method. Kim *et. al.* [185] have

demonstrated two different techniques (stamping and scooping) for transferring graphene from nickel substrate to other arbitrary substrates. These techniques are not effective for industrial application which will require low cost, high quality and large area production of graphene flexible electrodes.

This study present a direct and effective method for synthesis of large graphene film on copper foils and transferring it to polyethylene terephthalate (PET) flexible substrate by hot press lamination process. This method provides an effective way to handle large area of graphene film with minimal physical damage to it. The resulting graphene polymer film is flexible and remains conductive under high tensile strains. The application of this graphene film as flexible transparent conductive anode has been demonstrated in carbon nanotube (CNT) field emission devices (FED).

8.2 Results and discussions

8.2.1 Experimental details

Graphene film was synthesized by chemical vapor deposition (CVD) of hydrocarbon on copper foil. Commercially available, cold rolled Cu foil of 50 μm to 200 μm thickness and large area (6 cm width and 15 cm length) was first annealed at 1000 °C for 1 hr under Ar atmosphere. After annealing, Cu foil was acid-treated for 10 min using 1 M acetic acid at 60 °C. This acid treatment helps in removing oxide layer generated at the Cu foil surface during annealing process. Copper foils were thoroughly washed with de-ionized water and dried at the ambient conditions. Graphene films were grown on copper foils in a similar way to the previously reported CVD process [184]. In short, graphene on the Cu foil was synthesized at 1000 °C and 1 atm pressure, using a 5 min

flow of CH_4 and H_2 gases in 1:4 ratios. After graphene growth, the foil was cooled down to room temperature before being taken out from the furnace.

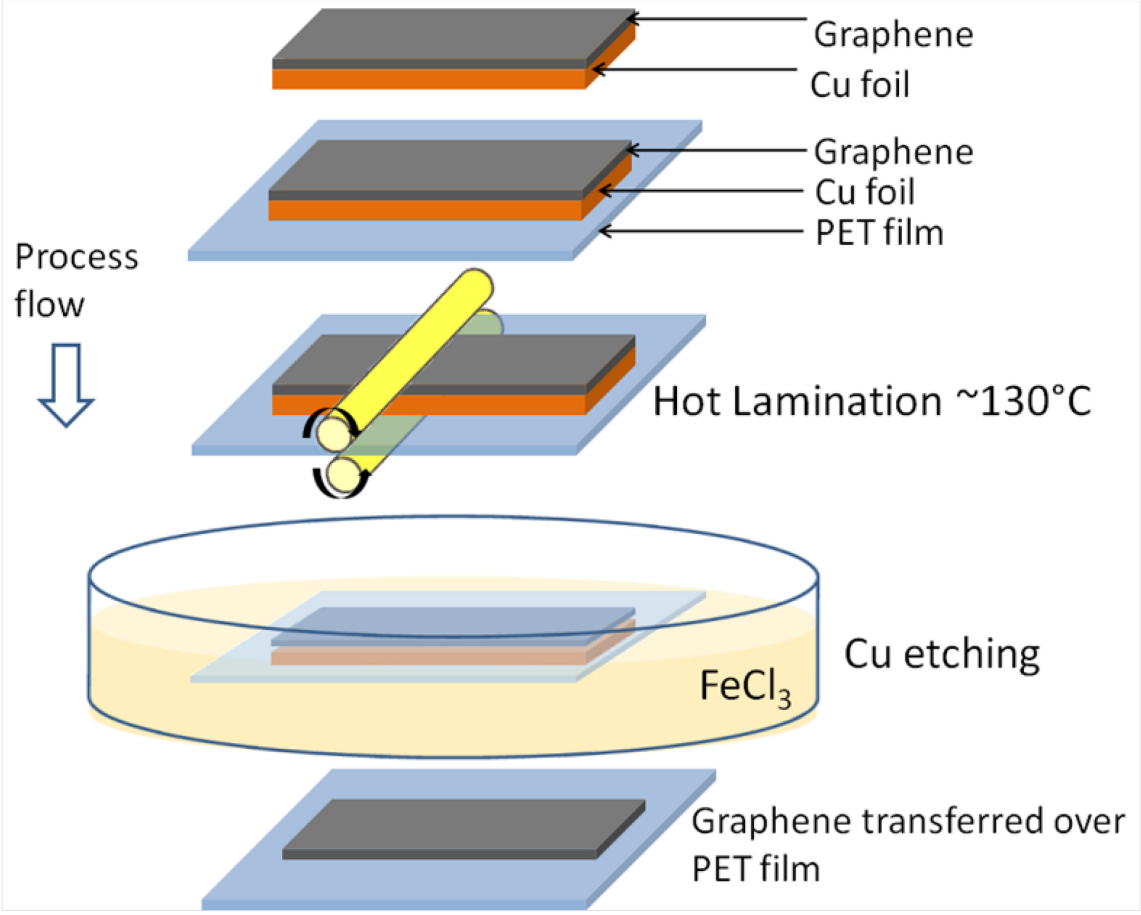

Figure 41. Process flow for graphene transfer from Cu foil to PET substrate. Hot press lamination and chemical etching processes were used in this method.

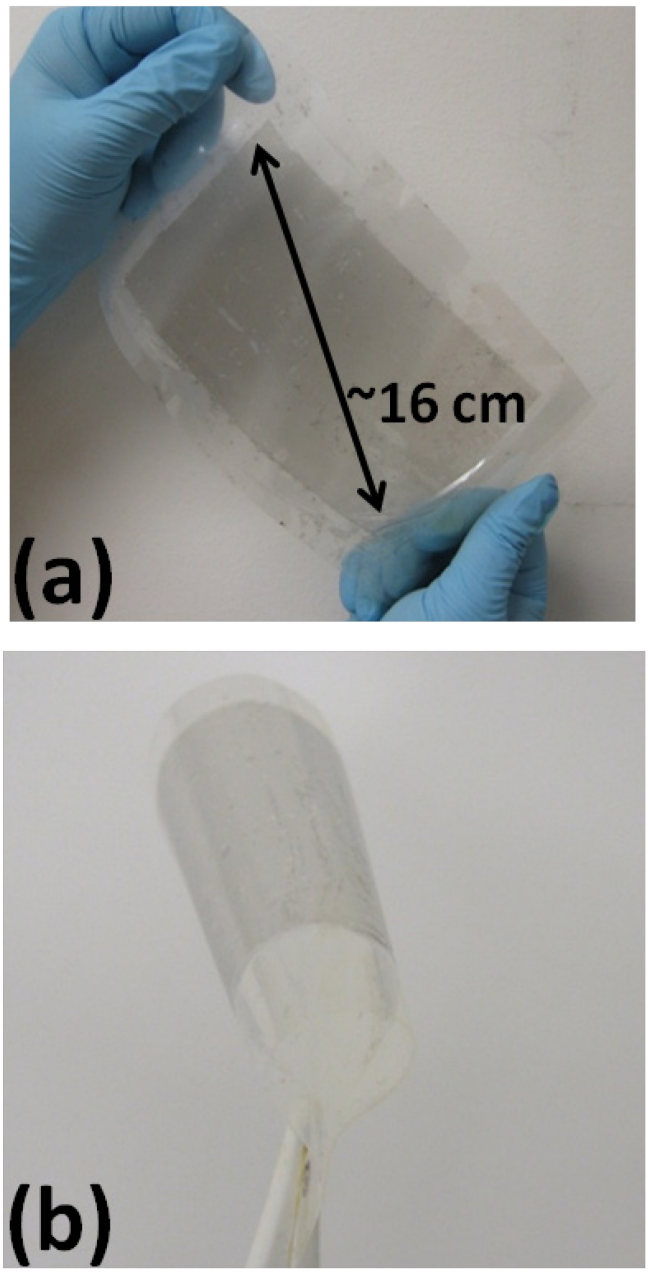

Figure 42. (a) Large area graphene film transferred over PET substrate. (c) Flexibility of graphene/PET film.

We have used hot press lamination and chemical etching process for transferring graphene grown over the Cu foils to the transparent flexible substrates. Figure 41 shows flow diagram of graphene transfer technique. Cu foils with graphene were hot press rolled with a transparent flexible PET film having thickness ~50 μm. For complete removal of Cu from the graphene and laminated film, we have used concentrated $FeCl_3$ solution. Laminated polymer film with graphene and Cu foil underneath was floated over the $FeCl_3$ acid bath at room temperature. After 40 min of etching process Cu was completely dissolved into the solution leaving graphene film with the PET substrate. This transparent flexible film was then thoroughly washed with de-ionized water and dried in air at room temperature. Figure 42a demonstrates a flexible, transparent graphene film with diagonal length of ~ 16 cm. This hot press lamination process provides a very adherent graphene film on the flexible substrate which can be deformed easily into various geometries (Figure 42b) without damaging the film.

8.2.2 Characterization of flexible graphene/PET Film

Characterization of graphene over Cu and flexible substrate were done by Raman spectroscopy. The Raman spectrum of graphene film on Cu foil and PET film are shown in Figure 43a. A symmetric and sharp 2D-band indicates monolayer of graphene film over Cu foil. The I_G/I_{2D} ratio for graphene on Cu foil was 0.4, conforming monolayer graphene film [184]. A high quality of graphene film over Cu foil was in compliance with a small D peak [186]. Successful transfer of graphene film on PET substrate was evident from Raman spectrum, showing characteristic G and 2D bands.

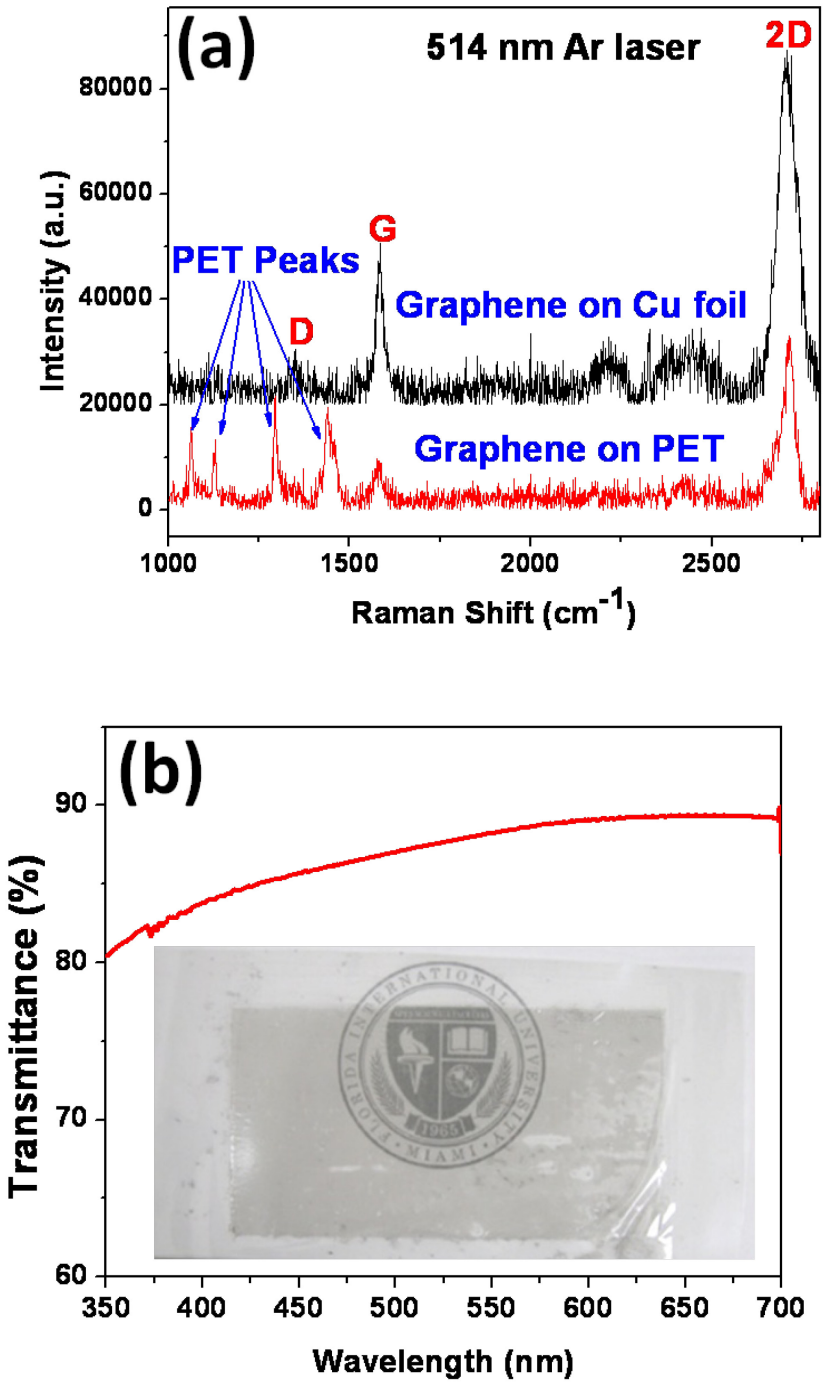

Figure 43. (a) Raman spectra from graphene on copper foil and PET substrates. (b) Transmittance of graphene film over PET substrate. Inset shows large area transparent graphene/PET film.

Optical transmission spectroscopy measurement was performed using Scinco, SD-1000 UV-Visible spectrophotometer. Figure 43b shows the transmittance of the graphene film with optical range of wavelengths. Percent transmission of graphene film on PET substrate is 88.80 at 550 nm wavelength. The graphene film shows higher transmittance compared to carbon nanotube[187] and ITO films [188]. Sheet resistance of the graphene film measured by four-point probe method was ~1.1742 kΩ/sq which is comparable to other reported graphene films [179, 189]. Graphene has an advantage over ITO, as it shows superior electrical-mechanical properties. To investigate the electro-mechanical properties of graphene/PET film, bending and stretching tests was performed. Graphene/PET film (dimension 1cm×1cm) was mounted on the lower jaws of a Vernier caliper which helps in bending and stretching the film in desired amount. The linear resistance of the film was measured at two edges across the film. Figure 44a shows the resistance of graphene/PET film with tensile strain ranging from 0 to 60%. Surprisingly, graphene/PET film remains conductive and shows only one order of magnitude change by ~60% stretching. Foldability of graphene/PET film was evaluated by measuring resistance with respect to bending radii (Figure 44b).

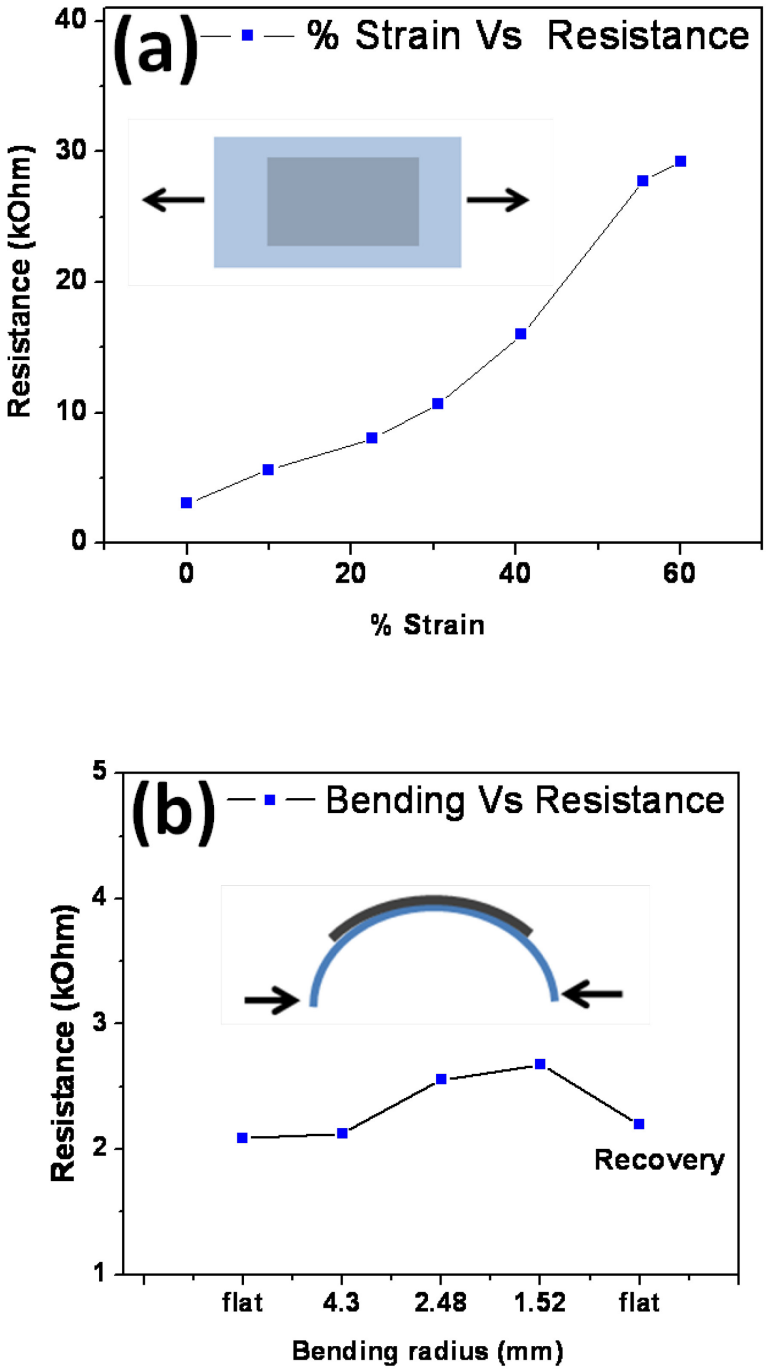

Figure 44. (a) Variation in resistance of graphene/PET film uniaxial stretched by 60%. (b) Resistance of graphene/PET film with different bending radii. Insets show schematic of stress modes applied to graphene/PET film.

The synthesized graphene is only few nanometers thick and PET thickness (~50 μm) alone is used in tensile strain calculation. Bending the film upto a radius of curvature of 1.52 mm (approximate tensile strain of 6.5%) changes the resistance of graphene from 2.09 kΩ to 2.68 kΩ, which was recovered completely after un-bending the graphene/PET film. These stretching and bending tests shows that graphene film has superior mechanical and electrical properties compared to brittle ITO electrode, which generate micro-cracks inside the film under mechanical stress[190]. The excellent mechanical properties of graphene film can be attributed to atomically perfect lattice of hexagonally arranged strong carbon-carbon bonds[191].

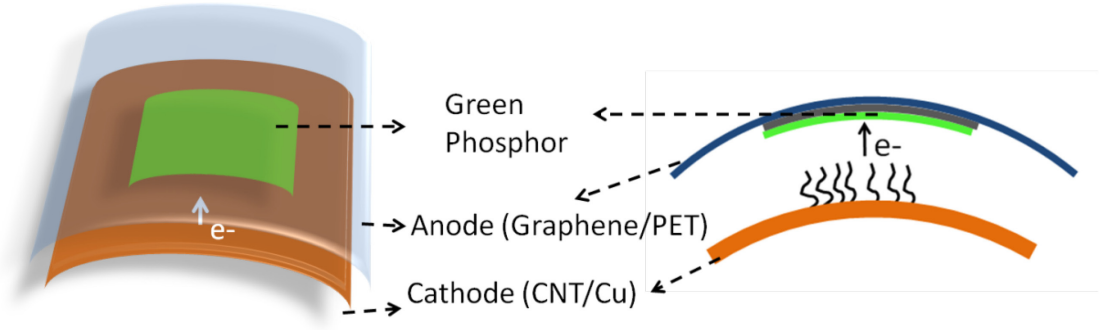

Figure 45. Schematic of CNT field emission device consisting flexible graphene anode. Multiwall CNT grown on Cu substrate was used as cathode and graphene/PET film was used as anode. Green phosphor deposited over graphene was used to show the illumination from flexible anode.

8.2.3 Graphene/PET Film for flexible anode

This transparent and conductive graphene film was characterized for its possible application in field emission devices, where graphene/PET film was used as a flexible anode. Green phosphor (Phosphor Tech; DPG01) material was deposited on the graphene/PET flexible substrate by dip coating process. This graphene/PET anode was assembled over bent (radius of curvature ~13.65 mm) CNT field emitters grown on copper foil (Figure 45). Details of synthesis and field emission properties of CNT field emitters are discussed in our past publication [192]. The inter-electrode distance was kept constant at 600 μm and the device was tested for its performance and stability under DC bias and high vacuum (~1×10^{-7} torr) condition. Figure 46 shows the field emission response of the device in bent configuration. The emission current behavior of the device was analyzed using Fowler-Nordheim (F-N) equation $I = (aA\beta^2E^2/\Phi)\exp(-b\Phi^{3/2}/\beta E)$, where $a = 1.54\times10^{-6}$ A eV V^{-2} and $b = 6.83\times10^{7}$ $eV^{3/2}$ V cm^{-1}, respectively, *A* is the emission area, β is the field enhancement factor, *E* is the applied electric field in V cm^{-1}, and Φ is the work function in eV [193]. Inset in Figure 46a shows the corresponding F-N plot. Straight line nature of the F-N plot indicates that the emission current was due to field emission. Turn-on field for the device was found to be 1.75 V/μm and field enhancement factor (β), as calculated from the slope of F-N plot, was approximately 1000. Figure 46b presents the stability of the field emitter device for more than 3 hours, at an average current level of 7.5 μA. It can be clearly observed from the figure that the device could produce a stable emission for the stipulated time period, indicating the stability of the graphene anode for long period of operation.

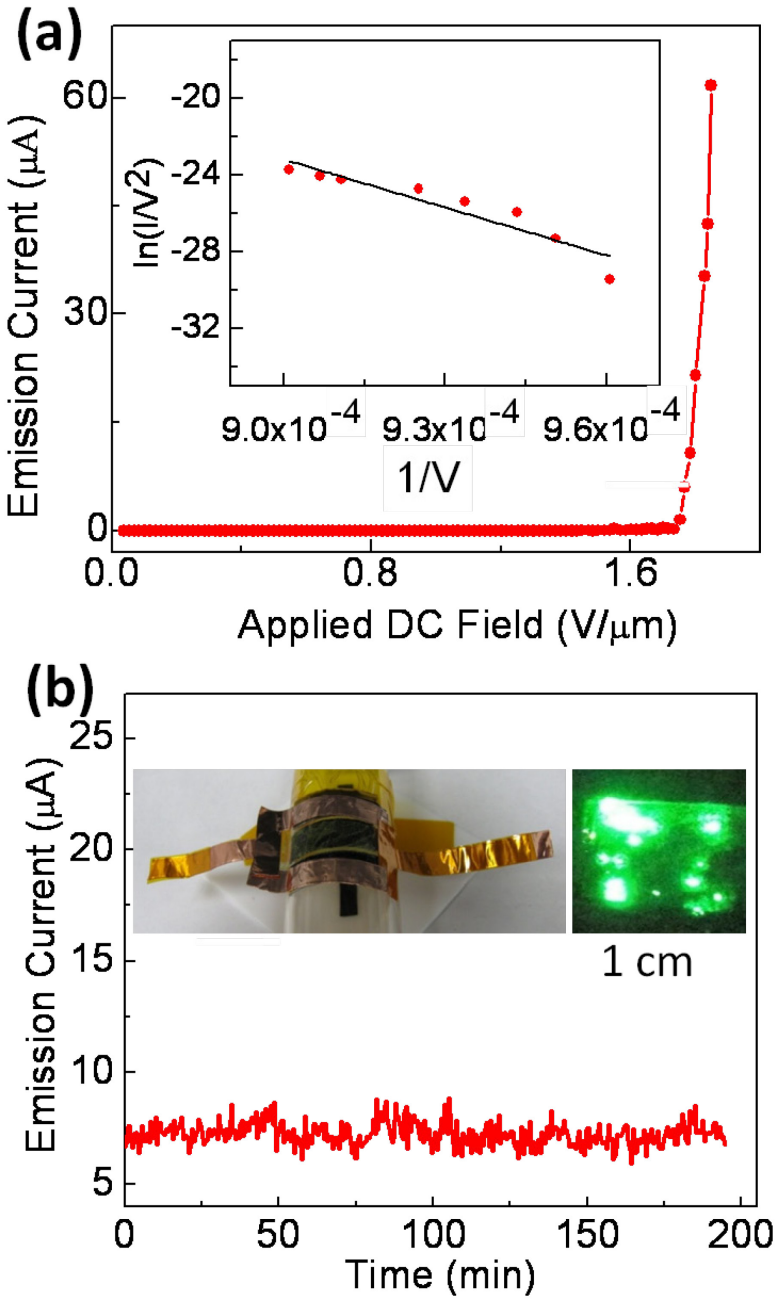

Figure 46. (a) Emission current-voltage characteristics of field emission device. Inset shows corresponding FN plot. (b) Emission current stability for >3 hrs. Inset shows bent field emission device and green illumination from graphene flexible electrode.

Inset of Figure 46b shows the bent field emission device and corresponding emission image, captured by using a thin layer of green phosphor on the graphene anode. The image clearly shows presence of emission from multiple sites of the field emitter device. The performance of the transparent, flexible graphene shows its potential in low-current, flexible field emission applications. Although, there have been published reports about flexible (and non-transparent) field emission devices (FED) [194, 195], our demonstration of graphene as the transparent, flexible anode of FEDs opens up a new factor of transparency to the FEDs and shows possibility for future transparent, flexible FEDs. Graphene anodes could act as a possible replacement for toxic and expensive ITO coatings.

8.3 Conclusions

In conclusion, we have synthesized large area graphene film and transferred it to PET flexible substrate by using hot press lamination technique. Graphene film on PET substrate shows high transmittance (>88%) and conductivity with mechanical stability. Also we have demonstrated application of this graphene/PET film as a flexible transparent anode in FED. The flexible FED with CNT emitter and graphene anode shows turn-on field of 1.75 V/μm and β values of ~1000 with good field emission stability. The proposed techniques can be tailored for any flexible substrate and large scale production at low-cost, which could open up exciting applications in foldable electronics and electro-mechanical devices.

CHAPTER 9

SUMMARY AND FUTURE WORK

9.1 Summary

Zinc oxide nano structures (thin film and nanowire) were synthesized by rf-magnetron sputtering and chemical vapor deposition techniques. Application of the ZnO nanostructures has been shown into electronic and sensing devices. This dissertation also include synthesize and study of large area graphene films.

ZnO and Ga doped ZnO thin film transistors were fabricated on Si/SiO_2 and flexible substrates. Structural characteristics of thin film were investigated by various techniques such as x-ray diffraction, AFM and optical spectroscopy. Gallium is proved to be better n-type doping element for ZnO as GZO TFTs shows and an enhanced device performance compared to ZnO TFTs. Reliability and stability of device were studied at elevated temperature and under high vacuum conditions.

ZNW were grown by chemical vapor deposition method at low pressure. NW FETs were fabricated by standard photolithography and electron beam lithography techniques. An enhanced conductance in ZNW FETs was achieved by non-destructive surface cleaning process which includes high vacuum annealing and UV irradiation. Further electrical hysteresis phenomenon in ZNW FETs was investigated. It was demonstrated that nondestructive surface cleaning process developed in our lab can help to remove unwanted hysteresis from the FET device. Furthermore, the novel application of ZNW was demonstrated by designing single nanowire gas sensors. Functinalization of

nanowire by Cr nanoparticles were done for achieving sensitivity and selectivity in the sensor device. In this study, successful detection of low ppm level of nitric oxide gas in presence of other common interfering gases was also conducted. A strategy was developed for refreshing the sensor device by UV radiation.

Large area of graphene film was synthesized by CVD method on Cu foils. A unique hot-press-lamination process to transfer the graphene film from metal substrate to PET material was also developed in this research. Graphene on PET substrate shows high flexibility and transparency, making it ideal candidate for electrode material in foldable electronics and devices. Application of this graphene/PET flexible film as anode in carbon nanotube field emission devices has been demonstrated.

9.2 Future scope of this work

Zinc oxide nanostructures have potential in future electronics, opto-electronics, sensor, solar cells and supercapacitors. Clear understanding of their physical and chemical properties at nanoscale is yet to be established for their successful integration in real devices. It was found that the electronic and chemical properties of ZnO thin films and nanowires are very unstable which challenges stability and reliability of the devices made from them. The surface properties of ZnO nanostructures are highly volatile due large number of defects (dangling bonds and oxygen species) present at the surface. For the successful adoption of ZnO nanostructures in the electronics devices, it is very important to eliminate or control these surface defects without losing the intrinsic properties of material. Implementing various passivation techniques and doping of suitable elements in ZnO thin films and nanowires without losing their transparency and

conductivity can be one area to investigate. An economical and efficient way to synthesis high quality ZnO thin films at large scale is paramount important for its successful commercialization. A control growth of high quality of zinc oxide nanowire and its integration in flexible electronics is very much sought for future optoelectronic devices.

Because of their high surface to volume ratio and specific physio-chemical properties ZNW have huge potential in chemical and biological sensors. Functionalization of nanowire with various catalyst nanoparticles and their integration in single devices can lead to development of smart artificial olfaction system-electronic nose.

Graphene is relatively new material which has created great interest because of its distinctive band structure, physical properties and potential in future devices. In this dissertation research CVD technique was used to synthesize large area graphene on Cu foil and to show its application in transparent flexible electrode. CVD method provides easy growth conditions for large area graphene on metal foils, but for electronic devices (transistors, inverter etc.), graphene has to be transfer to the Si wafer, which is still a challenging task. An efficient way for this will be direct growth of graphene over dielectric substrates. Also synthesizing graphene film with controlled number of layers and high crystalline is very much required for successful commercialization of its devices. Although graphene shows very remarkable properties intrinsically, such as high mobility and zero band gap, its properties get affected by strong interaction with substrate material. Also it is hard to imagine graphene without substrate in device design or architecture. A detailed study is needed for understanding the charge transport behavior in graphene on various substrate and environmental conditions.

LIST OF REFERENCES

[1] U.Ozgur, Y.I.Alivov, C.Liu, A.Teke, M.A.Reshchikov, S.Dogan, V.Avrutin, S.J.Cho, H.Morkoc, *J. Appl. Phys.* **2005**, *98*, 041301.

[2] C.W.Bunn, *Proceedings of the Physical Society* **1935**, *47*, 835.

[3] W.Tjhen, T.Tamagawa, C.P.Ye, C.C.Hsueh, P.Schiller, D.L.Polla, "Properties of piezoelectric thin films for micromechanical devices and systems", presented at Micro Electro Mechanical Systems, 1991, MEMS 91.

[4] C.Klingshirn, *Chemphyschem* **2007**, *8*, 782.

[5] T.Minami, H.Sato, H.Nanto, S.Takata, *Japanese Journal of Applied Physics Part 2-Letters* **1985**, *24*, L781-L784.

[6] S.J.Pearton, D.P.Norton, K.Ip, Y.W.Heo, T.Steiner, *Superlattices and Microstructures* **2007**, *34*, 3.

[7] G.J.Exarhos, X.D.Zhou, *Thin Solid Films* **2007**, *515*, 7025.

[8] B.X.Lin, Z.X.Fu, Y.B.Jia, *Appl. Phys. Lett.* **2001**, *79*, 943.

[9] R.L.Hoffman, B.J.Norris, J.F.Wager, *Appl. Phys. Lett.* **2003**, *82*, 733.

[10] K.Nomura, H.Ohta, A.Takagi, T.Kamiya, M.Hirano, H.Hosono, *Nature* **2004**, *432*, 488.

[11] H.Q.Chiang, J.F.Wager, R.L.Hoffman, J.Jeong, D.A.Keszler, *Appl. Phys. Lett.* **2005**, *86*.

[12] B.J.Norris, J.Anderson, J.F.Wager, D.A.Keszler, *Journal of Physics D-Applied Physics* **2003**, *36*, L105-L107.

[13] S.Masuda, K.Kitamura, Y.Okumura, S.Miyatake, H.Tabata, T.Kawai, *J. Appl. Phys.* **2003**, *93*, 1624.

[14] H.Yabuta, M.Sano, K.Abe, T.Aiba, T.Den, H.Kumomi, K.Nomura, T.Kamiya, H.Hosono, *Appl. Phys. Lett.* **2006**, *89*.

[15] D.C.Paine, B.Yaglioglu, Z.Beiley, S.Lee, *Thin Solid Films* **2008**, *516*, 5894.

[16] J.Goldberger, D.J.Sirbuly, M.Law, P.Yang, *J. Phys. Chem. B* **2005**, *109*, 9.

[17] H.T.Ng, J.Han, T.Yamada, P.Nguyen, Y.P.Chen, M.Meyyappan, *Nano Lett.* **2004**, *4*, 1247.

[18] S.H.Ju, K.Lee, D.B.Janes, *Nano Lett.* **2005**, *5*, 2281.

[19] S.Ju, K.Lee, M.H.Yoon, A.Facchetti, T.J.Marks, D.B.Janes, *Nanotechnology* **2007**, *18*, 155201.

[20] J.Goldberger, D.J.Sirbuly, M.Law, P.Yang, *J. Phys. Chem. B* **2005**, *109*, 9.

[21] Y.W.Heo, L.C.Tien, Y.Kwon, D.P.Norton, S.J.Pearton, B.S.Kang, F.Ren, *Appl. Phys. Lett.* **2004**, *85*, 2274.

[22] P.C.Chang, Z.Fan, C.J.Chien, D.Stichtenoth, C.Ronning, J.G.Lu, *Appl. Phys. Lett.* **2006**, *89*, 133113.

[23] K.Keem, D.Y.Jeong, S.Kim, M.S.Lee, I.S.Yeo, U.I.Chung, J.T.Moon, *Nano Lett.* **2006**, *6*, 1454.

[24] Q.Wan, Q.H.Li, Y.J.Chen, T.H.Wang, X.L.He, J.P.Li, C.L.Lin, *Appl. Phys. Lett.* **2004**, *84*, 3654.

[25] Z.Y.Fan, J.G.Lu, *Ieee Transactions on Nanotechnology* **2006**, *5*, 393.

[26] H.T.Wang, B.S.Kang, F.Ren, L.C.Tien, P.W.Sadik, D.P.Norton, S.J.Pearton, J.Lin, *Appl. Phys. Lett.* **2005**, *86*, 243503.

[27] C.H.Wang, X.F.Chu, M.W.Wu, *Sensors and Actuators B-Chemical* **2006**, *113*, 320.

[28] Z.Yang, L.M.Li, Q.Wan, Q.H.Liu, T.H.Wang, *Sensors and Actuators B-Chemical* **2008**, *135*, 57.

[29] Y.L.Cao, P.F.Hu, W.Y.Pan, Y.D.Huang, D.Z.Jia, *Sensors and Actuators B-Chemical* **2008**, *134*, 462.

[30] O.Lupan, G.Chai, L.Chow, *Microelectronic Engineering* **2008**, *85*, 2220.

[31] Z.Y.Fan, D.W.Wang, P.C.Chang, W.Y.Tseng, J.G.Lu, *Appl. Phys. Lett.* **2004**, *85*, 5923.

[32] N.S.Ramgir, I.S.Mulla, K.P.Vijayamohanan, *Sensors and Actuators B: Chemical* **2005**, *107*, 708.

[33] A.Kolmakov, D.O.Klenov, Y.Lilach, S.Stemmer, M.Moskovits, *Nano Lett.* **2005**, *5*, 667.

[34] D.S.Vlachos, C.A.Papadopoulos, J.N.Avaritsiotis, *Sensors and Actuators B: Chemical* **1997**, *44*, 458.

[35] L.C.Tien, P.W.Sadik, D.P.Norton, L.F.Voss, S.J.Pearton, H.T.Wang, B.S.Kang, F.Ren, J.Jun, J.Lin, *Appl. Phys. Lett.* **2005**, *87*, 222106.

[36] S.J.Chang, T.J.Hsueh, I.C.Chen, S.F.Hsieh, S.P.Chang, C.L.Hsu, Y.R.Lin, B.R.Huang, *Ieee Transactions on Nanotechnology* **2008**, *7*, 754.

[37] T.J.Hsueh, S.J.Chang, C.L.Hsu, Y.R.Lin, I.C.Chen, *Appl. Phys. Lett.* **2007**, *91*.

[38] S.J.Chang, T.J.Hsueh, I.C.Chen, B.R.Huang, *Nanotechnology* **2008**, *19*, 175502.

[39] J.Hass, W.A.de Heer, E.H.Conrad, *Journal of Physics-Condensed Matter* **2008**, *20*, 323202.

[40] A.K.Geim, K.S.Novoselov, *Nat Mater* **2007**, *6*, 183.

[41] K.I.Bolotin, K.J.Sikes, Z.Jiang, M.Klima, G.Fudenberg, J.Hone, P.Kim, H.L.Stormer, *Solid State Communications* **2008**, *146*, 351.

[42] K.I.Bolotin, K.J.Sikes, J.Hone, H.L.Stormer, P.Kim, *Phys. Rev. Lett.* **2008**, *101*, 096802.

[43] K.S.Novoselov, A.K.Geim, S.V.Morozov, D.Jiang, Y.Zhang, S.V.Dubonos, I.V.Grigorieva, A.A.Firsov, *Science* **2004**, *306*, 666.

[44] T.Ando, *NPG Asia Mater.* **2009**, *1*, 17.

[45] P.R.Wallace, *Phys. Rev.* **1947**, *71*, 622.

[46] R.R.Nair, P.Blake, A.N.Grigorenko, K.S.Novoselov, T.J.Booth, T.Stauber, N.M.R.Peres, A.K.Geim, *Science* **2008**, *320*, 1308.

[47] J.Liu, A.R.Wright, C.Zhang, Z.Ma, *Appl. Phys. Lett.* **2008**, *93*, 041106.

[48] C.Lee, X.Wei, J.W.Kysar, J.Hone, *Science* **2008**, *321*, 385.

[49] K.S.Kim, Y.Zhao, H.Jang, S.Y.Lee, J.M.Kim, K.S.Kim, J.H.Ahn, P.Kim, J.Y.Choi, B.H.Hong, *Nature* **2009**, *457*, 706.

[50] X.Wang, L.J.Zhi, K.Mullen, *Nano Lett.* **2008**, *8*, 323.

[51] D.Choi, D.Choi, M.Choi, W.Choi, H.Shin, H.Park, J.Seo, J.Park, S.Yoon, S.Chae, H.Young, S.Kim, J.Choi, S.Lee, J.Kim, *Advanced Materials* **2010**, *22*, 2187.

[52] J.B.Wu, M.Agrawal, H.A.Becerril, Z.N.Bao, Z.F.Liu, Y.S.Chen, P.Peumans, *ACS Nano* **2010**, *4*, 43.

[53] G.Jo, M.Choe, C.Y.Cho, J.H.Kim, W.Park, S.Lee, W.K.Hong, T.W.Kim, S.J.Park, B.H.Hong, Y.H.Kahng, T.Lee, *Nanotechnology* **2010**, *21*, 175201.

[54] J.Wu, H.A.Becerril, Z.Bao, Z.Liu, Y.Chen, P.Peumans, *Appl. Phys. Lett.* **2008**, *92*, 263302.

[55] X.Li, Y.Zhu, W.Cai, M.Borysiak, B.Han, D.Chen, R.D.Piner, L.Colombo, R.S.Ruoff, *Nano Lett.* **2009**, *9*, 4359.

[56] X.Wang, L.Zhi, K.Mullen, *Nano Lett.* **2007**, *8*, 323.

[57] X.Y.Kong, Y.Ding, Z.L.Wang, *The Journal of Physical Chemistry B* **2003**, *108*, 570.

[58] Y.R.Ryu, T.S.Lee, H.W.White, *Journal of Crystal Growth* **2004**, *261*, 502.

[59] P.J.Kelly, R.D.Arnell, *Vacuum* **2000**, *56*, 159.

[60] A.Sugunan, H.C.Warad, M.Boman, J.Dutta, *Journal of Sol-Gel Science and Technology* **2006**, *39*, 49.

[61] Z.L.Wang, *Journal of Physics-Condensed Matter* **2004**, *16*, R829-R858.

[62] A.C.Ferrari, J.C.Meyer, V.Scardaci, C.Casiraghi, M.Lazzeri, F.Mauri, S.Piscanec, D.Jiang, K.S.Novoselov, S.Roth, A.K.Geim, *Phys. Rev. Lett.* **2006**, *97*, 187401.

[63] DasA., PisanaS., ChakrabortyB., PiscanecS., SahaS.K., WaghmareU.V., NovoselovK.S., KrishnamurthyH.R., GeimA.K., FerrariA.C., SoodA.K., *Nat Nano* **2008**, *3*, 210.

[64] I.Calizo, W.Bao, F.Miao, C.N.Lau, A.A.Balandin, *Appl. Phys. Lett.* **2007**, *91*, 201904.

[65] Y.y.Wang, Z.h.Ni, T.Yu, Z.X.Shen, H.m.Wang, Y.h.Wu, W.Chen, A.T.Shen Wee, *The Journal of Physical Chemistry C* **2008**, *112*, 10637.

[66] Y.J.Li, Y.W.Kwon, M.Jones, Y.W.Heo, J.Zhou, S.C.Luo, P.H.Holloway, E.Douglas, D.P.Norton, Z.Park, S.Li, *Semiconductor Science and Technology* **2005**, *20*, 720.

[67] C.Bundesmann, N.Ashkenov, M.Schubert, D.Spemann, T.Butz, E.M.Kaidashev, M.Lorenz, M.Grundmann, *Appl. Phys. Lett.* **2003**, *83*, 1974.

[68] B.H.Choi, H.B.Im, J.S.Song, K.H.Yoon, *Thin Solid Films* **1990**, *193*, 712.

[69] E.J.Egerton, A.K.Sood, R.Singh, Y.R.Puri, R.F.Davis, J.Pierce, D.C.Look, T.Steiner, *Journal of Electronic Materials* **2005**, *34*, 949.

[70] J.H.Hu, R.G.Gordon, *Solar Cells* **1991**, *30*, 437.

[71] H.J.Ko, Y.F.Chen, S.K.Hong, H.Wenisch, T.Yao, D.C.Look, *Appl. Phys. Lett.* **2000**, *77*, 3761.

[72] E.M.C.Fortunato, P.M.C.Barquinha, A.C.M.B.Pimentel, A.M.F.Goncalves, A.J.S.Marques, R.F.P.Martins, L.M.N.Pereira, *Appl. Phys. Lett.* **2004**, *85*, 2541.

[73] K.Y.Cheong, N.Muti, S.R.Ramanan, *Thin Solid Films* **2002**, *410*, 142.

[74] G.A.Hirata, J.McKittrick, T.Cheeks, J.M.Siqueiros, J.A.Diaz, O.Contreras, O.A.Lopez, *Thin Solid Films* **1996**, *288*, 29.

[75] H.Kato, M.Sano, K.Miyamoto, T.Yao, *Journal of Crystal Growth* **2002**, *237*, 538.

[76] N.R.Aghamalyan, E.A.Kafadaryan, R.K.Hovsepyan, S.I.Petrosyan, *Semiconductor Science and Technology* **2005**, *20*, 80.

[77] B.T.Lee, T.H.Kim, S.H.Jeong, *Journal of Physics D-Applied Physics* **2006**, *39*, 957.

[78] T.Makino, Y.Segawa, S.Yoshida, A.Tsukazaki, A.Ohtomo, M.Kawasaki, *Appl. Phys. Lett.* **2004**, *85*, 759.

[79] F.K.Shan, Z.F.Liu, G.X.Liu, W.J.Lee, G.H.Lee, I.S.Kim, B.C.Shin, Y.S.Yu, *Journal of Electroceramics* **2004**, *13*, 195.

[80] "Powder Diffraction File, International Centre for Diffraction, Data", Newton Square,PA, **2000**.

[81] S.H.Jeong, I.S.Kim, S.S.Kim, J.K.Kim, B.T.Lee, *Journal of Crystal Growth* **2004**, *264*, 110.

[82] S.L.Cho, J.Ma, Y.K.Kim, Y.Sun, G.K.L.Wong, J.B.Ketterson, *Appl. Phys. Lett.* **1999**, *75*, 2761.

[83] S.Shirakata, T.Sakemi, K.Awai, T.Yamamoto, *Thin Solid Films* **2003**, *445*, 278.

[84] P.F.Carcia, R.S.Mclean, M.H.Reilly, G.Nunes, *Appl. Phys. Lett.* **2003**, *82*, 1117.

[85] C.D.Dimitrakopoulos, D.J.Mascaro, *Ibm Journal of Research and Development* **2001**, *45*, 11.

[86] I.Yagi, K.Tsukagoshi, Y.Aoyagi, *Appl. Phys. Lett.* **2005**, *86*, 103502.

[87] I.D.Kim, Y.W.Choi, H.L.Tuller, *Appl. Phys. Lett.* **2005**, *87*, 043509.

[88] A.Janotti, C.G.Van de Walle, *Journal of Crystal Growth* **2006**, *287*, 58.

[89] S.H.Jeong, B.S.Kim, B.T.Lee, *Appl. Phys. Lett.* **2003**, *82*, 2625.

[90] B.X.Lin, Z.X.Fu, Y.B.Jia, *Appl. Phys. Lett.* **2001**, *79*, 943.

[91] F.K.Shan, G.X.Liu, W.J.Lee, G.H.Lee, I.S.Kim, B.C.Shin, *Appl. Phys. Lett.* **2005**, *86*.

[92] S.R.Morrison, *Sensors and Actuators* **1987**, *11*, 283.

[93] W.Gopel, *Progress in Surface Science* **1985**, *20*, 9.

[94] J.Lagowski, E.S.Sproles, H.C.Gatos, *J. Appl. Phys.* **1977**, *48*, 3566.

[95] M.H.Huang, Y.Y.Wu, H.Feick, N.Tran, E.Weber, P.D.Yang, *Advanced Materials* **2001**, *13*, 113.

[96] S.Shirakata, T.Sakemi, K.Awai, T.Yamamoto, *Thin Solid Films* **2003**, *445*, 278.

[97] Z.L.Wang, *Journal of Physics-Condensed Matter* **2004**, *16*, R829-R858.

[98] P.X.Gao, Y.Ding, I.L.Wang, *Nano Lett.* **2003**, *3*, 1315.

[99] M.S.Arnold, P.Avouris, Z.W.Pan, Z.L.Wang, *J. Phys. Chem. B* **2003**, *107*, 659.

[100] H.T.Ng, J.Han, T.Yamada, P.Nguyen, Y.P.Chen, M.Meyyappan, *Nano Lett.* **2004**, *4*, 1247.

[101] F.Zhiyong, J.G.Lu, *Nanotechnology, IEEE Transactions on* **2006**, *5*, 393.

[102] T.M.Borseth, B.G.Svensson, A.Y.Kuznetsov, P.Klason, Q.X.Zhao, M.Willander, *Appl. Phys. Lett.* **2006**, *89*, 262112.

[103] W.R.Murphy, T.F.Veerkamp, T.W.Leland, *Journal of Catalysis* **1976**, *43*, 304.

[104] S.R.Morrison, *Sensors and Actuators* **1987**, *11*, 283.

[105] S.A.Dayeh, D.P.R.Aplin, X.T.Zhou, P.K.L.Yu, E.T.Yu, D.L.Wang, *Small* **2007**, *3*, 326.

[106] S.A.Dayeh, C.Soci, P.K.L.Yu, E.T.Yu, D.Wang, *Appl. Phys. Lett.* **2007**, *90*, 162112.

[107] J.Goldberger, D.J.Sirbuly, M.Law, P.Yang, *J. Phys. Chem. B* **2005**, *109*, 9.

[108] S.Ju, S.Kim, S.Mohammadi, D.B.Janes, Y.G.Ha, A.Facchetti, T.J.Marks, *Appl. Phys. Lett.* **2008**, *92*, 022104.

[109] M.C.Jeong, B.Y.Oh, M.H.Ham, J.M.Myoung, *Appl. Phys. Lett.* **2006**, *88*, 202105.

[110] W.I.Park, J.S.Kim, G.C.Yi, M.H.Bae, H.J.Lee, *Appl. Phys. Lett.* **2004**, *85*, 5052.

[111] K.Keem, D.Y.Jeong, S.Kim, M.S.Lee, I.S.Yeo, U.I.Chung, J.T.Moon, *Nano Lett.* **2006**, *6*, 1454.

[112] Y.Dai, Y.Zhang, Y.Q.Bai, Z.L.Wang, *Chemical Physics Letters* **2003**, *375*, 96.

[113] Q.H.Li, T.Gao, Y.G.Wang, T.H.Wang, *Appl. Phys. Lett.* **2005**, *86*, 123117.

[114] C.Soci, A.Zhang, B.Xiang, S.A.Dayeh, D.P.R.Aplin, J.Park, X.Y.Bao, Y.H.Lo, D.Wang, *Nano Lett.* **2007**, *7*, 1003.

[115] J.Mizusaki, H.Koinuma, J.I.Shimoyama, M.Kawasaki, K.Fueki, *Journal of Solid State Chemistry* **1990**, *88*, 443.

[116] Z.Fan, D.Wang, P.C.Chang, W.Y.Tseng, J.G.Lu, *Appl. Phys. Lett.* **2004**, *85*, 5923.

[117] Q.H.Li, T.Gao, Y.G.Wang, T.H.Wang, *Appl. Phys. Lett.* **2005**, *86*, 123117.

[118] T.H.Moon, M.C.Jeong, B.Y.Oh, M.H.Ham, M.H.Jeun, W.Y.Lee, J.M.Myoung, *Nanotechnology* **2006**, *17*, 2116.

[119] T.I.Barry, F.S.Stone, "The Reactions of Oxygen at Dark and Irradiated Zinc Oxide Surface".

[120] N.Asakuma, H.Hirashima, H.Imai, T.Fukui, A.Maruta, M.Toki, K.Awazu, *J. Appl. Phys.* **2002**, *92*, 5707.

[121] Q.H.Li, T.Gao, Y.G.Wang, T.H.Wang, *Appl. Phys. Lett.* **2005**, *86*, 123117.

[122] S.Ramo, J.R.Whinnery, T.V.Duzer, *Fields and Waves in Communication Electronics*, Wiley, New York, **1994**.

[123] S.M.Sze, *Physics of Semiconductor Devices*, Wiley, New York, **1981**.

[124] Y.Kwon, Y.Li, Y.W.Heo, M.Jones, P.H.Holloway, D.P.Norton, Z.V.Park, S.Li, *Appl. Phys. Lett.* **2004**, *84*, 2685.

[125] V.P.Verma, D.H.Kim, H.Jeon, M.Jeon, W.Choi, *Thin Solid Films* **2008**, *516*, 8736.

[126] Q.H.Li, Q.Wan, Y.X.Liang, T.H.Wang, *Appl. Phys. Lett.* **2004**, *84*, 4556.

[127] Y.W.Heo, L.C.Tien, Y.Kwon, D.P.Norton, S.J.Pearton, B.S.Kang, F.Ren, *Appl. Phys. Lett.* **2004**, *85*, 2274.

[128] M.H.Huang, S.Mao, H.Feick, H.Yan, Y.Wu, H.Kind, E.Weber, R.Russo, P.Yang, *Science* **2001**, *292*, 1897.

[129] S.Ju, S.Kim, S.Mohammadi, D.B.Janes, Y.G.Ha, A.Facchetti, T.J.Marks, *Appl. Phys. Lett.* **2008**, *92*, 022104.

[130] T.M.Borseth, B.G.Svensson, A.Y.Kuznetsov, P.Klason, Q.X.Zhao, M.Willander, *Appl. Phys. Lett.* **2006**, *89*, 262112.

[131] W.R.Murphy, T.F.Veerkamp, T.W.Leland, *Journal of Catalysis* **1976**, *43*, 304.

[132] S.A.Dayeh, C.Soci, P.K.L.Yu, E.T.Yu, D.Wang, *Appl. Phys. Lett.* **2007**, *90*, 162112.

[133] S.Ju, S.Kim, S.Mohammadi, D.B.Janes, Y.G.Ha, A.Facchetti, T.J.Marks, *Appl. Phys. Lett.* **2008**, *92*, 022104.

[134] R.A.B.Devine, G.V.Herrera, *Phys. Rev. B* **2001**, *63*, 233406.

[135] O.Wunnicke, *Appl. Phys. Lett.* **2006**, *89*, 083102.

[136] V.P.Verma, H.Jeon, S.Hwang, M.Jeon, W.Choi, *Nanotechnology, IEEE Transactions on* **2008**, *7*, 782.

[137] J.S.Lee, S.Ryu, K.Yoo, I.S.Choi, W.S.Yun, J.Kim, *The Journal of Physical Chemistry C* **2007**, *111*, 12504.

[138] J.S.Lee, S.Ryu, K.Yoo, I.S.Choi, W.S.Yun, J.Kim, *The Journal of Physical Chemistry C* **2007**, *111*, 12504.

[139] K.Alving, E.Weitzberg, J.M.Lundberg, *European Respiratory Journal* **1993**, *6*, 1368.

[140] S.A.Kharitonov, D.Yates, R.A.Robbins, R.Logansinclair, E.A.Shinebourne, P.J.Barnes, *Lancet* **1994**, *343*, 133.

[141] G.S.Thomas, William M.Stigliani, *Environmental Science in Perspective*, SUNY Press, **1985**.

[142] P.Montuschi, S.A.Kharitonov, P.J.Barnes, *Chest* **2001**, *120*, 496.

[143] J.Harper, M.J.Sailor, *Anal. Chem.* **1996**, *68*, 3713.

[144] K.Kikuchi, T.Nagano, H.Hayakawa, Y.Hirata, M.Hirobe, *Anal. Chem.* **1993**, *65*, 1794.

[145] T.Hemmingsson, D.Linnarsson, R.Gambert, *Journal of Clinical Monitoring and Computing* **2004**, *18*, 379.

[146] G.Korotcenkov, *Materials Science and Engineering: B* **2007**, *139*, 1.

[147] Z.Y.Fan, J.G.Lu, *Ieee Transactions on Nanotechnology* **2006**, *5*, 393.

[148] V.Brinzari, G.Korotcenkov, V.Golovanov, *Thin Solid Films* **2001**, *391*, 167.

[149] S.R.Morrison, *Sensors and Actuators* **1987**, *11*, 283.

[150] K.Jong-Won, O.Eu-Gene, C.Geon-Young, J.Soo-Hwan, H.Jeung-Soo, "NO sensing characteristics of ZnO nanorod prepared by ultrasound radiation method", presented at Sensors, 2006. 5th IEEE Conference on.

[151] N.Zhang, K.Yu, Q.Li, Z.Q.Zhu, Q.Wan, *J. Appl. Phys.* **2008**, *103*, 104305.

[152] E.K.Kim, H.Y.Lee, S.E.Moon, J.Park, S.J.Park, J.H.Kwak, S.Maeng, K.H.Park, J.Kim, S.W.Kim, H.J.Ji, G.T.Kim, *Journal of Nanoscience and Nanotechnology* **2008**, *8*, 4698.

[153] Z.Fan, J.G.Lu, *Appl. Phys. Lett.* **2005**, *86*, 123510.

[154] M.Kaur, S.V.S.Chauhan, S.Sinha, M.Bharti, R.Mohan, S.K.Gupta, J.V.Yakhmi, *Journal of Nanoscience and Nanotechnology* **2009**, *9*, 5293.

[155] N.S.Ramgir, I.S.Mulla, K.P.Vijayamohanan, *Sensors and Actuators B: Chemical* **2005**, *107*, 708.

[156] D.S.Vlachos, C.A.Papadopoulos, J.N.Avaritsiotis, *Sensors and Actuators B: Chemical* **1997**, *44*, 458.

[157] X.Zhou, W.Xu, G.Liu, D.Panda, P.Chen, *Journal of the American Chemical Society* **2009**, *132*, 138.

[158] G.E.Poirier, R.E.Cavicchi, S.Semancik, "Particle growth of palladium on epitaxial tin oxide thin films".

[159] J.D.Prades, R.Jimenez-Diaz, F.Hernandez-Ramirez, S.Barth, A.Cirera, A.Romano-Rodriguez, S.Mathur, J.R.Monante, *Sensors and Actuators B-Chemical* **2009**, *140*, 337.

[160] W.An, X.Wu, X.C.Zeng, *J. Phys. Chem. C* **2008**, *112*, 5747.

[161] L.Lei, B.D.Sosnowchik, L.Liwei, "UV-enhanced oxygen sensing of zinc oxide nanowires", presented at Micro Electro Mechanical Systems, 2008. MEMS 2008. IEEE 21st International Conference on.

[162] K.Shiba, H.Hinode, M.Wakihara, *Reaction Kinetics and Catalysis Letters* **1996**, *58*, 133.

[163] X.Zhou, W.Xu, G.Liu, D.Panda, P.Chen, *Journal of the American Chemical Society* **2009**, *132*, 138.

[164] J.R.Stetter, W.R.Penrose, "Artificial chemical sensing, oflaction and the electronic nose", presented at International Symposium on Olfaction and the Electronic Nose (8th 2001 Washington, D.C.), March 25, 2001.

[165] T.Seiyama, *Chemical sensor technology*, Kodansha . Elsevier, Tokyo, **1988**.

[166] H.Kind, H.Q.Yan, B.Messer, M.Law, P.D.Yang, *Advanced Materials* **2002**, *14*, 158-+.

[167] J.D.Prades, F.Hernandez-Ramirez, R.Jimenez-Diaz, M.Manzanares, T.Andreu, A.Cirera, A.Romano-Rodriguez, J.R.Morante, *Nanotechnology* **2008**, *19*, 465501.

[168] Y.B.Li, Z.W.Huang, S.Q.Rong, *Sensors and Materials* **2006**, *18*, 241.

[169] N.S.Ramgir, I.S.Mulla, K.P.Vijayamohanan, *Sensors and Actuators B: Chemical* **2005**, *107*, 708.

[170] H.Chang, J.D.Lee, S.M.Lee, Y.H.Lee, *Appl. Phys. Lett.* **2001**, *79*, 3863.

[171] W.An, X.Wu, X.C.Zeng, *J. Phys. Chem. C* **2008**, *112*, 5747.

[172] S.Ghosh, D.L.Nika, E.P.Pokatilov, A.A.Balandin, *New Journal of Physics* **2009**, *11*, 095012.

[173] K.S.Novoselov, A.K.Geim, S.V.Morozov, D.Jiang, M.I.Katsnelson, I.V.Grigorieva, S.V.Dubonos, A.A.Firsov, *Nature* **2005**, *438*, 197.

[174] S.Stankovich, D.A.Dikin, G.H.B.Dommett, K.M.Kohlhaas, E.J.Zimney, E.A.Stach, R.D.Piner, S.T.Nguyen, R.S.Ruoff, *Nature* **2006**, *442*, 282.

[175] F.Schedin, A.K.Geim, S.V.Morozov, E.W.Hill, P.Blake, M.I.Katsnelson, K.S.Novoselov, *Nature Materials* **2007**, *6*, 652.

[176] Y.M.Lin, K.A.Jenkins, A.Valdes-Garcia, J.P.Small, D.B.Farmer, P.Avouris, *Nano Letters* **2009**, *9*, 422.

[177] M.D.Stoller, S.J.Park, Y.W.Zhu, J.H.An, R.S.Ruoff, *Nano Letters* **2008**, *8*, 3498.

[178] X.Wang, L.J.Zhi, K.Mullen, *Nano Letters* **2008**, *8*, 323.

[179] K.S.Kim, Y.Zhao, H.Jang, S.Y.Lee, J.M.Kim, K.S.Kim, J.H.Ahn, P.Kim, J.Y.Choi, B.H.Hong, *Nature* **2009**, *457*, 706.

[180] E.H.Hwang, S.Das Sarma, *Phys. Rev. B* **2008**, *77*, 115449.

[181] J.Wu, H.A.Becerril, Z.Bao, Z.Liu, Y.Chen, P.Peumans, *Applied Physics Letters* **2008**, *92*, 263302.

[182] X.Wang, L.Zhi, K.Mullen, *Nano Letters* **2007**, *8*, 323.

[183] H.Yamaguchi, G.Eda, C.Mattevi, H.Kim, M.Chhowalla, *ACS Nano* **2010**, *4*, 524.

[184] X.S.Li, W.W.Cai, J.H.An, S.Kim, J.Nah, D.X.Yang, R.Piner, A.Velamakanni, I.Jung, E.Tutuc, S.K.Banerjee, L.Colombo, R.S.Ruoff, *Science* **2009**, *324*, 1312.

[185] K.S.Kim, Y.Zhao, H.Jang, S.Y.Lee, J.M.Kim, K.S.Kim, J.H.Ahn, P.Kim, J.Y.Choi, B.H.Hong, *Nature* **2009**, *457*, 706.

[186] A.C.Ferrari, J.C.Meyer, V.Scardaci, C.Casiraghi, M.Lazzeri, F.Mauri, S.Piscanec, D.Jiang, K.S.Novoselov, S.Roth, A.K.Geim, *Phys. Rev. Lett.* **2006**, *97*, 187401.

[187] Z.C.Wu, Z.H.Chen, X.Du, J.M.Logan, J.Sippel, M.Nikolou, K.Kamaras, J.R.Reynolds, D.B.Tanner, A.F.Hebard, A.G.Rinzler, *Science* **2004**, *305*, 1273.

[188] T.Kawashima, H.Matsui, N.Tanabe, *Thin Solid Films* **2003**, *445*, 241.

[189] X.Li, Y.Zhu, W.Cai, M.Borysiak, B.Han, D.Chen, R.D.Piner, L.Colombo, R.S.Ruoff, *Nano Letters* **2009**, *9*, 4359.

[190] J.S.Oh, Y.R.Cho, K.E.Cheon, M.A.Karim, S.J.Jung, *Solid State Phenomena* **2007**, *124-126*, 411.

[191] C.Lee, X.D.Wei, J.W.Kysar, J.Hone, *Science* **2008**, *321*, 385.

[192] I.Lahiri, R.Seelaboyina, J.Y.Hwang, R.Banerjee, W.Choi, *Carbon* **2010**, *48*, 1531.

[193] R.Seelaboyina, J.Huang, W.B.Choi, *Applied Physics Letters* **2006**, *88*, 194104.

[194] H.S.Sim, S.P.Lau, H.Y.Yang, L.K.Ang, M.Tanemura, K.Yamaguchi, *Applied Physics Letters* **2007**, *90*, 143103.

[195] C.Y.Wang, T.H.Chen, S.C.Chang, T.S.Chin, S.Y.Cheng, *Applied Physics Letters* **2007**, *90*, 103111.

APPENDIX

Mater. Res. Soc. Symp. Proc. Vol. 963 © 2007 Materials Research Society 0963-Q12-01

Fabrication and Characteristics of Low Doped Gallium-Zinc Oxide Thin Film Transistor

Ved Prakash Verma[1], Dohyun Kim[1], Minhyon Jeon[2], and Wonbong Choi[1]
[1]Mechanical Engineering, Florida International University, 10555, West Flagler Street, miami, FL, 33174
[2]School of Nanoengineering, Inje University, Gimhae, 621-749, Korea, Republic of

ABSTRACT

We report on fabrication and electrical characteristics of transparent thin film transistor (TFT) based on low Ga-doped zinc oxide (GZO). Low Ga (1 wt%) doped ZnO thin film is deposited as an active channel by rf-magnetron sputtering at room temperature. The devices show a mobility of 5.7 cm^2/Vs at low operation voltage of <5V and a low turn-on voltage of 0.5 V with a sub-threshold swing of 85 mV/decade. The TFT device performance is significantly affected by vacuum-level and annealing treatment, which is attributed to the chemisorption/ desoption of oxygen from the surface of active channel. Low doped GZO is a new class of TFT channel material that has the potential of high performance, multi-functionality and easy-process.

INTRODUCTION

Zinc oxide (ZnO) is a transparent and wide band gap (3.36 eV) semiconducting material that has been extensively studied due to its multi-functionality such as optoelectronic, piezoelectric and pyroelectric with high exciton binding energy of ~60 meV [1,2,3]. The potential applications include ultraviolet lasers, light emitting devices, transparent conductors and thin film transistors. The intrinsic oxygen defects and Zn interstitials enable good electrical conductivity of ZnO thin films. However, the conductivity of ZnO can be further improved by doping with several elements such as As, In, Ga, Fe, Sb, Al and Li. The minimal resistivity of ZnO achieved by doping was about 10^{-4} Ωcm [4,5,21,22]. Of all the elements considered Ga is the best n-type doping element because of its good lattice match with ZnO lattice; the bond lengths of Ga-O and Zn-O are 2.92 Å and 2.97 Å respectively [6]. Also the Ga atom replaces the zinc ions and acts as substitutional impurity, releasing a free electron in the conduction band at room temperature. High doped GZO material has been used for contact electrodes in transparent oxide TFTs due to its high conductivity and transparency [7]. Recently, ZnO films with low resistance and high transparency have been obtained with Ga doping concentration range of 2.0–4.0 at% [18,19]. ZnO with different concentration of gallium has been studied for high mobility and crystalline thin films. Carrier concentration of Ga doped ZnO increases linearly with increase in Ga concentration [16]. An improved high carrier concentration of ~10^{21} /cm^3 can be achieved by Ga doping compared to un-doped zinc oxide thin film which has typical carrier concentration of ~10^{17}/cm^3 [16,17,20]. Recent reports have demonstrated that low Ga-doped ZnO down to ~1wt% can be grown in single crystal by rf-magnetron sputtering [8]. This material has potential in optoelectronic devices because it can be grown as a transparent single crystal thin film at room temperature and has a wide band gap of ~3.76 eV [23,32].

Since the electrical properties of ZnO surface are affected by gaseous molecules present in the ambient, many researches have studied the effect of annealing treatment on ZnO film at different ambient conditions [8,10]. However, the choice of annealing atmosphere, temperature

Thin Solid Films 516 (2008) 8736–8739

Contents lists available at ScienceDirect

Thin Solid Films

journal homepage: www.elsevier.com/locate/tsf

Characteristics of low doped gallium-zinc oxide thin film transistors and effect of annealing under high vacuum

Ved Prakash Verma [a], Do-Hyun Kim [a,b], Hoonha Jeon [b], Minhyon Jeon [b], Wonbong Choi [a,*]

[a] Nanomaterials and Devices Laboratory, Mechanical and Materials Engineering, Florida International University, Miami, FL 33174, USA
[b] School of Nanoengineering, Inje University, Gimhae, 621-749, South Korea

ARTICLE INFO

Article history:
Received 6 August 2007
Received in revised form 30 May 2008
Accepted 10 June 2008
Available online 22 June 2008

Keywords:
Zinc oxide
Zinc oxide:metal
Thin film transistor
X-ray diffraction
Electrical measurements and properties

ABSTRACT

We report on the fabrication and electrical characteristics of thin film transistors (TFTs) based on low Ga-doped zinc oxide (GZO). Low Ga-doped (1 wt.%) ZnO thin films deposited as an active channel by radio frequency magnetron sputtering at room temperature exhibit a high transmittance (>80%). The devices show a mobility of ~5.7 cm^2/Vs at low operation voltage of <5 V and a low turn-on voltage of ~0.5 V with a subthreshold swing of ~85 mV/decade. The TFT device performance is significantly affected by vacuum-level and annealing treatment, which is attributed to the chemisorption/desorption of oxygen from the surface of active channel. Low doped GZO is a type of TFT channel material that has potential for high performance, multi-functionality and easy-process.

1. Introduction

Zinc oxide (ZnO) is a transparent and wide band gap (~3.36 eV) semiconducting material that has been extensively studied due to its multi-functionality such as optoelectronic, piezoelectric and pyroelectric with high exciton binding energy of ~60 meV [1–3]. The potential applications include ultraviolet lasers, light emitting devices, transparent conductors and thin film transistors. The intrinsic oxygen defects and Zn interstitials enable good electrical conductivity of ZnO thin films. However, the conductivity of ZnO can be further improved by doping with several elements such as As, In, Ga, Fe, Sb, Al and Li. The minimal resistivity of ZnO achieved by doping was about 10^{-4} Ωcm [4–7]. Of all the elements considered Ga is the best n-type doping element because of its good lattice match with ZnO lattice; the bond lengths of Ga–O and Zn–O are 1.92 Å and 1.97 Å, respectively [8]. Also the Ga atom replaces the zinc ions and acts as substitutional impurity, releasing a free electron in the conduction band at room temperature. High gallium doped zinc oxide (GZO) material has been used for contact electrodes in transparent oxide thin film transistors (TFTs) due to its high conductivity and transparency [9]. Recently, ZnO films with low resistance and high transparency have been obtained with Ga doping concentration range of 2.0–4.0 at.% [10,11]. ZnO with different concentration of gallium has been studied for high mobility and crystalline thin films. Carrier concentration of Ga-doped ZnO increases linearly with increase in Ga concentration [12]. An improved high carrier concentration of ~$10^{21}/cm^3$ can be achieved by Ga doping compared to un-doped zinc oxide thin film which has typical carrier concentration of ~$10^{17}/cm^3$ [12–14]. Recent reports demonstrated that low Ga-doped ZnO down to ~1 wt.% can be grown in single crystal by radio frequency (rf) magnetron sputtering [15]. This material has potential in optoelectronic devices because it can be grown as a transparent single crystal thin film at room temperature and has a wide band gap of ~3.76 eV [16,17].

Since the electrical properties of ZnO surface are affected by gaseous molecules present in the ambient, many researchers have studied the effect of annealing on ZnO film at different ambient conditions [15,18]. However, the choice of annealing atmosphere, temperature and pressure still remains controversial. There is also lack of information about the environmental effects on ZnO thin film grown by rf-magnetron sputtering.

Here we present electrical characteristics of low Ga-doped (1 wt.%) ZnO thin film transistor fabricated at room temperature. Device characteristics with different ambient conditions are studied and the corresponding mechanism is discussed. This letter demonstrates our effort to develop a thin film transistor fabricated at room temperature with low Ga-doped (1 wt.%) ZnO, and its environmental effect.

2. Experimental details

GZO-TFTs were fabricated with the use of a thermally grown SiO_2 thin film on Si substrate. The alignment marks and patterns were generated by standard electron beam lithography process. A 35 nm of GZO thin film was deposited with a growth rate of 3.5 nm/min at room temperature by rf-magnetron sputtering system using (1 wt.%)

* Corresponding author. Tel.: +1 305 348 1973; fax: +1 305 348 1932.
E-mail address: choiw@fiu.edu (W. Choi).

0040-6090/$ – see front matter © 2008 Elsevier B.V. All rights reserved.
doi:10.1016/j.tsf.2008.06.054

Enhanced Electrical Conductance of ZnO Nanowire FET by Nondestructive Surface Cleaning

Ved P. Verma, Hoonha Jeon, Sookhyun Hwang, Minhyon Jeon, and Wonbong Choi

***Abstract*—Electrical characteristics of zinc oxide nanowire (ZNW) FETs are investigated by nondestructive surface cleaning, ultraviolet irradiation treatment at high temperature and vacuum. UV-light-stimulated oxygen desorption from the active channel improves the device performance of ZNW-FETs. Results show that charge transport in single ZNW strongly depends on its surface environmental conditions and can be explained by formation of depletion layer at the surface by various surface states present on it. The nondestructive surface cleaning removes these absorbed surface states from the nanowire and the current values increase upto $\sim$7 μA from $\sim$0.4 μA at a bias voltage of 3 V. ZNW-FETs fabricated in this study exhibit mobility of $\sim$28 cm^2/V·s and a high $I_{ON} \neq I_{OFF}$ ratio of $\sim 10^6$.**

***Index Terms*—Nanotechnology, surface treatment, ultraviolet (UV) radiation effect.**

I. Introduction

SEMICONDUCTING zinc oxide nanowires (ZNWs) are very promising materials for high-power/high-temperature electronics due to their remarkable physical properties like wide band gap of $\sim$3.4 eV and high exciton binding energy of $\sim$60 meV [1]–[4]. FETs with ZNW as an active channel may enable promising applications for flexible and transparent electronics and chemical sensors [5]–[7]. It is well known that zinc oxide contains a high density of surface defects and dangling bonds that act as absorption sites for gaseous molecules, mainly oxygen species present in the ambient [8], [9]. The surface state model presented by Morrison [10] treats the oxygen interaction with semiconductor surface as a two-step process. Initially, rapid physisorption of oxygen takes place on the surface leading to weakly bonded molecules, which then capture the electrons from material and form into strongly bonded chemisorbed species. Due to high surface to volume ratio in nanoscale materials, these surface states dominate which affects their electron transport properties and catalytic reactions occurring at the surface [11]. In case of metal oxide nanostructures, these surface states defoliate the electronic properties of the materials by scattering and trapping of charge carriers that significantly hinders their application to the high-density and high-speed nanoelectronic circuits [12]–[14]. Several efforts have been made to passivate these surface states and improve the electrical performance of ZNWs and thin films [15]. Park *et al.* reported the fabrication of high-mobility ($\sim$1000 cm^2/V·s) zinc oxide FETs by coating of polyimide layer on the nanorod surface [16]. Also, Keem *et al.* demonstrated omega-shaped-gate ZNW-FETs with Al_2O_3-coated zinc oxide nanowires for high device performance [17]. However, no direct investigation has been done for adsorption and desorption of these gaseous molecules on zinc oxide nanostructures. The aim of the present paper is to study the effect of ultraviolet irradiation at elevated temperature and vacuum conditions on electronic properties of ZNW-FETs. This nondestructive cleaning process removes the surface states present on the ZNW in the form of absorbed oxygen species and enhances the device performance of the FET.

Manuscript received May 27, 2008; revised May 28, 2008. First published September 3, 2008; current version published December 24, 2008. The review of this paper was arranged by Associate Editor G. Ramanath.

V. P. Verma and W. B. Choi are with Florida International University, Miami, FL 33174 USA (e-mail: ved.verma@fiu.edu; choiw@fiu.edu).

H. Jeon, S. Hwang, and M. Jeon are with Inje University, Gimhae 621-749, Korea (e-mail: blacksnow89@naver.com; yellowsu@naver.com, mjeon@inje.ac.kr).

Color versions of one or more of the figures in this paper are available online at http://ieeexplore.ieee.org.

Digital Object Identifier 10.1109/TNANO.2008.2005186

II. Experimental

ZNWs were grown by vapor–liquid–solid process in a high-temperature and low-pressure horizontal chemical-vapor deposition (CVD) system. Catalysts of gold nanoparticles (Sigma Aldrich) (10 nm) suspended in deionized (DI) water were dispersed on quartz substrate. A mixture of pure zinc oxide and graphite powders (Sigma Aldrich) (1:1 wt ratio) was used as the source material. Typical temperature and pressure for ZNW synthesis process were 900 °C and 150 torr, respectively. After 30 min of growth process, a thin layer of ZnWs was deposited on the quartz substrate. In order to make ZNW-FET, the ZNWs were stripped from the substrate and dispersed in isopropanol solution by ultrasonication. ZNWs dissolved in solution were randomly dispersed on a heavily doped p-Si/SiO_2 substrate that had patterned metal electrodes and align marks fabricated by photolithography. Source and drain electrode patterning at the edges of single nanowires was done by electron beam lithography followed by Ti (80 nm)/Au (150 nm) metal deposition. Thermally grown SiO_2 (100 nm) and heavily doped Si (p^+) substrate under the nanowire were used as gate oxide and back gate electrode, respectively. Electrical characterization of the ZNW-FETs was done at room temperature and in dark environment using a four-probe station equipped with a semiconductor parameter analyzer (Agilent 4156 C). Devices were treated in various ambient conditions of vacuum (air pressure $\sim 4.0 \times 10^{-4}$ torr), elevated temperature (400 K), and ultraviolet (UV) irradiation at 340–390-nm wavelength range and 1.4 mWcm^{-2} intensity.

III. Results and Discussion

Fig. 1(a) shows the scanning electron microscopy (SEM) image of ZNWs grown on quartz substrate. Typical length and diameter of the nanowires were 2–3 μm and 20–50 nm, respectively. High-resolution transmission electron microscopy

Materials Science and Engineering B 171 (2010) 45–49

Contents lists available at ScienceDirect

Materials Science and Engineering B

journal homepage: www.elsevier.com/locate/mseb

Nitric oxide gas sensing at room temperature by functionalized single zinc oxide nanowire

Ved Prakash Verma [a], Santanu Das [a], Sookhyun Hwang [b], Hyonkwang Choi [b], Minhyon Jeon [b], Wonbong Choi [a,*]

[a] Mechanical and Materials Engineering Department, Florida International University, Miami, FL 33174, USA
[b] Department of Nanosystems Engineering, Inje University, Gimhae 621-749, Republic of Korea

ARTICLE INFO

Article history:
Received 28 September 2009
Received in revised form 2 February 2010
Accepted 27 March 2010

Keywords:
Nanotechnology
Sensor
Zinc oxide
Nanowires
Catalyst

ABSTRACT

We report on room temperature detection of nitric oxide (NO) gas at low-ppm level by Cr nanoparticle decorated single zinc oxide nanowire (ZNW) sensor. In this sensor device Cr nanoparticles, act as catalyst to transform NO into NO_2 and results in change in current value through ZNW, corresponding to NO gas concentration. The sensor exhibits average sensitivity of ~46% for 10 ppm of NO gas. The lowest detection limit of the sensor is ~1.5 ppm for NO gas. Sensor shows selectivity towards NO gas during a cross-sensitivity test with N_2, CO and CO_2 gases. Recovery of the sensor is achieved by ultraviolet light induced desorption of gases from ZNW surface.

1. Introduction

Detection of NO gas at low concentration is of paramount importance for real time monitoring of environment and lower airways inflammatory diseases [1,2]. NO is an atmospheric pollutant, which plays an important role in formation of smog [3]. Also, detection of NO concentration in exhaled gases has become standard medical practice for monitoring chronic obstructive pulmonary disease (COPD) [4]. The most common techniques available for monitoring exhaled NO are based on chemi-luminescence and photochemical methods which involve huge system and expertise [5,6]. Though one portable NO analyzer, based on electrochemical technique has already been developed by Hemmingsson et al. [7], the demand for a very inexpensive and hand held analyzer is still to be realized.

Zinc oxide nanowire (ZNW) is one of the most promising materials systems for semiconducting gas sensors, owing their easy functionality and specific combination of physico-chemical properties [8]. Large surface to volume ratio and quasi-one-dimensional functionality of ZNW make their conductivity highly sensitive towards surface chemical reactions [9]. Moreover, relatively large surface defects and favorable gas adsorption/desorption parameters [10,11], give ZNW edge over other nanowires and nanotubes for NO gas detection. There have been many reports on ZNW based gas sensors for the detection of ethanol, CO, NH_3, H_2, O_2, NO, H_2S and NO_2 [9,12–17]. However, these sensors need to be operated at high temperature to achieve improved gas–semiconductor surface reaction and high signal to noise ratio [9,13]. In their study, Fan and Lu [18] have demonstrated a strategy for NO_2 gas sensing at room temperature by gate refreshable ZNW field effect transistors. Kaur et al. [19] and Ramgir et al. [20] have detected nitric oxide gas (concentration > 40 ppm) at room temperature by bare zinc oxide nanostructures and Ru doped ZNW, respectively. Despite multiple reports on gas sensing by ZNW, detection of low concentration level of nitric oxide (NO) gas at room temperature remains a challenge.

Metal particles are well-known as effective catalysts, due to their ability to control the redox reactions of the gas molecule at the sensor surface [21]. At nanoscale, metal particles show superior catalytic properties due to their high surface to volume ratio and chemical potential [22]. Functionalization by catalyst nanoparticles is one of the most important strategies for enhancing sensitivity and selectivity of metal oxide gas sensors. However very few literatures are available which explore sensing application of catalyst supported single metal oxide nanowire sensor [23].

In this paper, we report direct detection of NO gas at low-ppm level using metal nanoparticles decorated single ZNW sensor, which can operate at room temperature and low power. Compared to bare ZNW, a Cr functionalized ZNW can detect lower concentration NO gas at room temperature (see Electronic Annex 1 in the online version of this article). More importantly, combi-

* Corresponding author at: Mechanical and Materials Engineering Department, Florida International University, 10555 West Flagler Street, EC 3465, Miami, FL 33174, USA. Tel.: +1 3053481973; fax: +1 3053481932.
E-mail address: choiw@fiu.edu (W. Choi).

0921-5107/$ – see front matter © 2010 Elsevier B.V. All rights reserved.
doi:10.1016/j.mseb.2010.03.066

Large-area graphene on polymer film for flexible and transparent anode in field emission device

Ved Prakash Verma, Santanu Das, Indranil Lahiri, and Wonbong Choi[a)]
Department of Mechanical and Materials Engineering, Florida International University, Miami, Florida 33174, USA

(Received 25 March 2010; accepted 28 April 2010; published online 20 May 2010)

We present the fabrication and electrical characterization of large graphene structure on polyethylene terephthalate (PET) flexible substrate. Graphene film was grown on Cu foil by thermal chemical vapor deposition and transferred to PET by using hot press lamination. The graphene/PET film shows high quality, flexible transparent conductive structure with unique electrical-mechanical properties; ~88.80% light transmittance and ~1.1742 kΩ/sq sheet resistance. We demonstrate application of graphene/PET film as flexible and transparent electrode for field emission displays. Our proposed techniques can be tailored for any flexible substrate and large scale production, which could open up exciting device applications in foldable electronics. © *2010 American Institute of Physics*. [doi:10.1063/1.3431630]

Graphene is a two-dimensional (2D) carbon material having unique band structure and outstanding thermal, mechanical, and electrical properties.[1–3] Some of the potential applications of graphene are for sensors, transistors, supercapacitors, solar cells, and flexible displays.[4–8] It is well known that graphene has high mechanical strength with flexibility, high transmittance, and high electron mobility.[8,9] These properties make graphene an emerging alternate for transparent conductive metal oxides electrodes, in particular, indium tin oxide (ITO) which contains indium as a costly and scarce element.

In order to make a transparent conductive graphene film, most of the researchers have used liquid solution of graphene flakes (obtained by reducing graphene oxide flakes) for deposition of transparent conductive film.[7,10] Recently, Yamaguchi *et al.*[11] has deposited chemically derived graphene solution on flexible substrate for large area transparent flexible electrode which contains 2 to 30 layers of graphene. Application of graphene in flexible electronics will need synthesis of continuous graphene film on substrates and transfer it to polymeric substrate in large scale. Li *et al.*[12] has grown high quality, predominately monolayer graphene films on copper foils by chemical vapor deposition (CVD) method. Kim *et al.*[8] have demonstrated two different techniques (stamping and scooping) for transferring graphene from nickel substrate to other arbitrary substrates. These techniques are not effective for industrial application which will require low cost, high quality, and large area production of graphene flexible electrodes.

Here we present a direct and effective method for synthesis of large graphene film on copper foils and transferring it to polyethylene terephthalate (PET) flexible substrate by hot press lamination process. This method provides an effective way to handle large area of graphene film with minimal physical damage to it. The resulting graphene polymer film is flexible and remains conductive under high tensile strains. The application of this graphene film as flexible transparent conductive anode has been demonstrated in carbon nanotube (CNT) field emission devices (FEDs).

Graphene film was synthesized by CVD of hydrocarbon on copper foil. Commercially available, cold rolled Cu foil of 50 to 200 μm thickness and large area (6 cm width and 15 cm length) was first annealed at 1000 °C for 1 h under Ar atmosphere. After annealing, Cu foil was acid-treated for 10 min using 1 M acetic acid at 60 °C. This acid treatment helps in removing oxide layer generated at the Cu foil surface during annealing process. Copper foils were thoroughly washed with de-ionized water and dried at the ambient conditions. Graphene films were grown on copper foils in a similar way to the previously reported CVD process.[12] In short, graphene on the Cu foil was synthesized at 1000 °C and 1 atm pressure, using a 5 min flow of CH_4 and H_2 gases in 1:4 ratios. After graphene growth, the foil was cooled down to room temperature before being taken out from the furnace. Graphene growth on Cu foil has been reported as a surface-catalyzed process which indicates that Cu act as catalyst for CVD of graphene. A detailed discussion about growth mechanism of graphene formation on copper foil has been presented elsewhere.[12]

We have used hot press lamination and chemical etching process for transferring graphene grown over the Cu foils to the transparent flexible substrates. Figure 1(a) shows flow diagram of graphene transfer technique. Cu foils with graphene were hot press rolled with a transparent flexible PET film having thickness ~50 μm. For complete removal of Cu from the graphene and laminated film, we have used concentrated $FeCl_3$ solution. Laminated polymer film with graphene and Cu foil underneath was floated over the $FeCl_3$ acid bath at room temperature. After 40 min of etching process Cu was completely dissolved into the solution leaving graphene film with the PET substrate. This transparent flexible film was then thoroughly washed with de-ionized water and dried in air at room temperature. Figure 1(b) demonstrates a flexible, transparent graphene film with diagonal length of ~16 cm. This hot press lamination process provides a very adherent graphene film on the flexible substrate which can be deformed easily into various geometries [Fig. 1(c)] without damaging the film.

Characterization of graphene over Cu and flexible substrate were done by Raman spectroscopy. The Raman spec-

a)Electronic mail: choiw@fiu.edu.

VITA

VED PRAKASH VERMA

EDUCATION

2003	B.Tech., Metallurgical Engineering Institute of Technology, BHU, INDIA
2005	M. Tech., Materials Science Indian Institute of Technology, INDIA
2010	Doctoral Candidate in Materials Engineering Florida International University, FL

AWARDS AND HONOURS

1. Winner of Best Student Award; TMS 2008 Annual meeting, New Orleans, Nanomaterials symposium
2. Winner of Best Poster presentation; ASM-TMS FIU Chapter-2008
3. Awarded first place in Technical Oral Presentation Competition organized by ASM-TMS FIU Chapter-2008
4. Best Poster presentation; ASM-TMS FIU Chapter-2009
5. Dissertation Year Fellowship (May 2009-April 2010) awarded by Florida International University

PUBLICATIONS CONFERENCE PROCEDINGS AND PATENTS

1. Jeon, H., Verma, V. P., Hwang, S., Noh, K., Lee, S., Park, C., Moon, J., Kim, J., Kim, D.H., Choi, W., and Jeon, M., "Low Voltage Zinc Oxide Thin Film Transistors on a Conventional SiO_2 Gate Insulator Grown by Radio Frequency Magnetron Sputtering at Room Temperature" JKPS, 51, (2007) 1999.
2. Jeon, H., Verma, V. P., Noh, K., Kim, D, H., Choi, W., Jeon; M., "Fabrication and characteristics of ZnO- and Ga doped ZnO thin film transistor using rf-magnetron sputtering at room temperature" JKVS, 16, (2007) 359.
3. Jeon, H., Verma, V. P., Hwang, S., Lee, S., Park, C., Kim, D. H., Choi, W., and Jeon, M., "Characteristics of Gallium-Doped Zinc Oxide Thin-Film Transistors Fabricated at Room Temperature Using Radio Frequency Magnetron Sputtering Method" JJAP, 47, (2008), 87.

4. Kim, D. H., Jeon, H., Leem, J. Y., Jeon, M., Verma, V P., and Choi, W., Lee, S. H., and Moon, J., "Influence of Grain Size and Room-Temperature Sputtering Condition on Optical and Electrical Properties of Undoped and Ga-Doped ZnO Thin Films" JKPS, 51, (2007) 1987.

5. Kim, D. H., Jeon, H., Kim, G., Hwangboe, S., Verma, V. P., Choi, W., Jeon, M., "Comparison of the optical properties of undoped and Ga-doped ZnO thin films deposited using RF magnetron sputtering at room temperature" Optics Communication, 281,(2008) 2120.

6. Verma, V. P., Kim, D. H., Jeon, M., Choi, W., "Fabrication and Characteristics of Low Doped Gallium-Zinc Oxide Thin Film Transistor" Mater. Res. Soc. Symp. Proc., 963, (2007) 0963-Q12-01.

7. Verma, V. P., Kim, D. H., Jeon, H., Jeon, M., Choi, W., "Characteristics of Low doped Gallium-Zinc Oxide Thin Film Transistors and effect of Annealing under High Vacuum" Thin Solid Films, 516, (2008) 8736.

8. Verma, V. P., Jeon, H., Hwang, S., Jeon, M., Choi, W., "Enhanced Electrical Conductance of ZnO Nanowire FET by Non-destructive Surface Cleaning" IEEE-Trans-nano, 7, (2008) 782.

9. Verma, V. P., Das, S., Hwang, S., Choi, H., Jeon, M., Choi, W., "Nitric Oxide gas sensing at room temperature by functionalized single zinc oxide nanowire" Mater. Sci. Eng. B, 171, (2010) 45.

10. Verma, V. P., Das, S., Lahiri, I., and Choi, W., "Large-area graphene on polymer film for flexible and transparent anode in field emission device". Appl. Phys. Lett., 96, (2010) 203108, and Vir. J. Nan. Sci. & Tech. (2010) May.

11. Verma, V. P., Lahiri, I., and Choi, W., Fully transparent and flexible field emission device by graphene and nanotube hybrid structure. (Manuscript under preparation)

12. Choi, W., Verma, V.P., "UV assisted and surface functionalized zinc oxide nanostructure sensor for nitric oxide gas detection at ppb level", Provisional patent submitted to USPTO. Appl.# 61174879.

13. Choi, W., Verma, V. P., "Large-area graphene on polymer film for flexible and transparent electrode" Provisional patent submitted to USPTO. Appl.# 61318547.

Also attended and presented the work at 6 national and international conferences during the dissertation period.